ANL-5853
Physics and Mathematics

ARGONNE NATIONAL LABORATORY
P.O. Box 299
Lemont, Illinois

ON THE PHOTOFISSION CROSS SECTIONS NEAR THRESHOLD OF NUCLEI IN THE REGION OF THE VERY HEAVY ELEMENTS

by
Kenneth M. Clarke

(Thesis)

CHEMISTRY DIVISION

July 1958

Operated by the University of Chicago
under
Contract W-31-109-eng-38

DISCLAIMER

TABLE OF CONTENTS

TABLE OF CONTENTS

LIST OF TABLES

LIST OF FIGURES

LIST OF FIGURES

ON THE PHOTOFISSION CROSS SECTIONS NEAR THRESHOLD OF NUCLEI IN THE REGION OF THE VERY HEAVY ELEMENTS

Kenneth M. Clarke

ABSTRACT*

Variations in the photofission cross section near "threshold" with initial kind of nucleus were investigated for seven spheroidal nuclei in the region of atomic numbers 90, 92, 93. The photofission cross sections at the two discrete energies 6.14 and 7.0 Mev were determined for the following even-even nuclides: Th^{232}, U^{234}, U^{236}, and U^{238}; and also the odd-A nuclides: U^{233}, U^{235}, and Np^{237}. This problem was suggested partly by the qualitative proposals of A. Bohr concerning odd-parity states and low energy photofission and partly by the results of betatron studies at low energies on the very heavy elements.

Nuclear excitation of the target nuclei was achieved via gamma rays from nuclear capture of protons on fluorine. Protons of 1.380- and 3.645-Mev energy impinged on a thick CaF_2 target. The high-energy quanta of 6.14, 6.91, and 7.12 Mev so obtained represent the well-known ground state transitions in O^{16}, whose relative intensities change with bombarding energy of the proton. The fission counting was done in a double-region ionization chamber of 2π geometry. The heavy-element samples were nearly uniform oxide deposits of about one mg/cm^2, on platinum. Employing the known thick target relative gamma-ray intensity ratio, $I(6.91 + 7.12)/I(6.14)$, plus the measured gamma flux and fission counting yield at each of the two above proton energies, the $(\gamma, \text{fission})$ cross sections at 6.14 and 7.0 Mev were calculated.

The $(\gamma, \text{fission})$ cross sections for Th^{232} and U^{238} are greater at 6.0 Mev than at 7.0 Mev, as indicated by earlier betatron results. U^{236} also exhibits a strong resonance at about 6.0 Mev. However, the other even-even uranium isotope investigated, U^{234}, does not show this behavior. Its $(\gamma, \text{fission})$ cross section appears to be increasing monotonically with energy between 6.0 and 7.0 Mev. The odd-A uranium isotopes U^{233} and U^{235} also do not show any unusual behavior in this energy interval. The $(\gamma, \text{fission})$ cross section for U^{234} appears to be essentially constant, which again is a confirmation of earlier betatron studies. For U^{233}, the cross section is increasing with energy. The one odd-proton nuclide examined,

---

*Based on a thesis submitted to the Graduate Faculty of the Pennsylvania State University in partial fulfillment of the requirements for the degree of Doctor of Philosophy.

Np^{237}, appears also to exhibit a resonance behavior at or about 6.0 Mev. These experimental results are correlated with existing information on low-energy photofission and other nuclear data to explain tentatively the small bumps or resonances in the photofission excitation curves.

I. INTRODUCTION

The property of the very heavy nuclei ($Z \geqslant 90$) which probably best characterizes their physical behavior is the ability to undergo fission. Fission(120) may be initiated by impact of a material particle, by absorption of electromagnetic radiation, by capture of a negatively charged meson (π^-), or even by a heavy nucleus remaining in its ground state for a sufficiently long period, as in the case of spontaneous fission. The particular facet of nuclear fission of concern here is nuclear division brought about by the excitation of a heavy nucleus through electromagnetic radiation, or, more simply, photofission. In an effort to elucidate the nature of the photofission process and, perhaps, to provide information on the structure of the fissioning nucleus, the absolute cross sections for photofission, near threshold, were examined for a number of spheroidal nuclei in the region of atomic numbers 90, 92 and 93.

Recently, it has been suggested by A. Bohr(19) that, for even-even nuclei (zero ground state spin(98)), photofission close to the fission threshold should occur predominantly via a single or small number of well-defined, low-lying excited states rather than from a large number of excited states of the compound nucleus at the saddle-point configuration. In the Bohr interpretation, this excitation is an odd-parity (1-) state, similar to observed low-energy excitations of the nuclear ground state, representing a collective mode of excitation(26) associated with asymmetric vibrations in the shape of the nuclear surface.(25,56) By contrast, the intrinsic excitations for odd-A heavy nuclei (non-zero ground state spin(98)) are predicted to be much more closely spaced; hence, many "fission channels" should be available to such nuclei as a result of photon excitation. Such a picture nicely explains the experimentally observed angular distributions for photofissions of Th^{232}, U^{238}, and U^{235} near the fission threshold.(145) From these considerations, the implication is that the cross sections for photofission in even-even nuclei near "threshold" may be significantly correlated with the spin state of the excited nucleus at the saddle point. Further, such a correlation would imply that the level spacing of the (1-) states should be reflected in these cross sections.

The earliest work designed to obtain threshold photofission cross sections for the very heavy elements was reported by two groups of workers(5,66) is early as 1941. In the paper by Haxby, et al.,(66) (γ, fission) cross sections for both natural uranium and thorium using the 6 and 7-Mev gamma rays from the $F^{19}(p,\alpha\gamma)\ O^{16}$ reaction were reported. These investigators employed a fission fragment detector to monitor the fission

yield. More recently, in a thesis by Hartley,[64] (γ, fission) cross sections for the same nuclides and photon source, as obtained from measured neutron yields, were given. Other than these results, no measurements in this energy region have been made at discrete gamma energies. In passing it may be mentioned that all of the above measurements really represent weighted "average" cross sections in the energy interval 6.14 to 7.0 Mev, since the excitation curve was assumed flat in this region and the photon source monochromatic.

The study of the cross sections for photonuclear reactions as a continuous function of photon energy has been possible through the use of the bremsstrahlung beam obtainable from a betatron. Over the past few years, a number of investigators[9,44,58,116,145] have reported cross sections for photofission near threshold using this tool. Values have been obtained for asymmetric and symmetric photofission cross sections[116] as well as total[58,145] (asymmetric plus symmetric) photofission cross sections. The usual technique employed has been the measurement of fission yields as a function of the maximum energy of the X-ray spectrum. With the aid of a theoretical bremsstrahlung spectrum, the yield curves can be analyzed (generally after smoothing) to give excitation curves, i.e., the cross section as a function of gamma-ray energy. The standard photon difference method[84,85] is usually employed in the analysis. Unfortunately, there are large errors inherent in cross sections determined by this procedure. In particular, the measurement of (γ,fission) cross sections at low excitation energies[116] requires the use of a thick-target bremsstrahlung spectrum which precludes the accurate extraction of cross sections from the observed activation functions because the exact shape of the spectrum is unknown. Moreover, since the yields are determined at finite energy increments, averaging over these intervals in effect tends to smooth out any structure in the excitation curve that might otherwise be observed. For this reason only approximate cross sections or relative values have been derived from betatron studies in the threshold region.

Owing to the limitation noted above, the precise form of the excitation curves near threshold is uncertain, and only their general shape has had any significance. In the range of atomic numbers 90 through 94, there have been indications of the occurrence of non-uniform variation of the cross sections with energy at low excitation energies (5 to 7 Mev). The most striking feature is the apparent existence of a small bump or resonance at about 6 Mev for Th^{232} and U^{238}. This bump has been clearly established by a number of workers.[44,58,116,145] These same workers find that no similar bump exists in the excitation curve for U^{235}. It thus appears that the excitation function for certain nuclei shows "structure" at low excitation energies and then rises to a maximum of the giant resonance.[9]

The observations described above may have some correlation with the experiments of Winhold and Halpern on the anisotropy in the angular distribution(145) of the fragments from the photofission of Th^{232}, U^{235}, and U^{238} near "threshold." The angular distributions observed were compatible with the form $a + b \sin^2 \theta$, where the ratio b/a is a measure of the anisotropy. They found that the anisotropy for Th^{232} and U^{238} drops to a small value at photon energies of three Mev or more above the fission "threshold." The anisotropy for Th^{232} was greater than that for U^{238}. On the other hand, no anisotropy at all was observed for U^{235}. It may be noted here that the observation(50) has been made that mass asymmetry and angular anisotropy are related phenomena.

In this investigation a detailed study of the absolute photofission cross sections at two discrete energies, 6.14 and 7.0 Mev, for a number of spheroidal nuclei ($Z \geqslant 90$) is reported.(34) These energies are slightly above the (γ, fission) "thresholds" (approximately 5.3 Mev) in this region of high atomic number. The nuclides studied included the following members of the actinide and transuranium series of elements: Th^{232}, U^{233}, U^{234}, U^{235}, U^{236}, U^{238}, and Np^{237}. Nuclear excitation of the heavy nuclei was achieved through use of the gamma rays available from the F^{19} $(p, \alpha\gamma)O^{16}$ reaction. The high-energy gamma-ray spectrum from this source consists of three intense lines(2,46,107) of 6.14, 6.91, and 7.12 Mev, respectively, whose relative intensities are strongly dependent on the bombarding proton beam energy.(14,137) The 7.0-Mev radiation becomes more intense relative to the 6.14-Mev line as the proton bombarding energy increases. By proper choice of the proton beam energy, it is possible to make either the 6.91 and 7.12-Mev photon group or the 6.14-Mev line the predominant source component.

The present work is an effort to furnish pertinent data to assist in the theoretical interpretation of the fission process. The answer to the question of how the (γ, fission) cross section changes with energy and initial kind of nucleus, when excited by photons of discrete energy, will be examined in terms of its implications for the fission process. The determination of accurate cross sections to uncover possible further "structure" and provide information on the precise form of the excitation curves near the (γ, neutron) thresholds(73) was the general objective of this investigation. In the fission "threshold" region for heavy nuclei, competing processes, i.e., (γ,γ') and (γ, neutron) reactions, are thought to play an important role in determining the overall shape of the excitation curve.(9)

II. THEORETICAL CONSIDERATIONS

A. General Remarks

The fissioning nucleus represents a clear case of the creation of a compound system. When a heavy spheroidal nucleus captures a high energy photon, a compound nucleus is formed in which the excitation energy is distributed among a large number of degrees of freedom of the nucleus. The complex state of motion thereby initiated may be described in terms of collective nuclear vibrations and rotations coupled to the motion of the individual nucleons. Such a description is in conformity with the now well-founded collective or unified model of the nucleus. In this model, developed by A. Bohr[20,23,24] and by Hill and Wheeler,[68] the shell model is connected with the idea of collective oscillations of the nucleons.

For fission to occur, considerable energy must be put into potential energy of deformation so that the nucleus can pass over the saddle point. In the liquid drop model,[26,54] this is the point on the path of deformation at which the potential energy attains its largest value. Since the effect of shell structure on the activation energy for fission is such that the energy goes down after a closed shell,[82,90] only those nuclides for which Z^2/A is large ($Z \geqslant 90$) and the activation energy for fission correspondingly low will be considered. For nuclei of this description, the type of fission that occurs may well depend upon the nuclear dynamics that prevail after the system has passed over the saddle point.[140] In nuclei having a large value of the fissionability parameter, Z^2/A, the activation energy for fission is found experimentally to be about 5.3 Mev.[30,90] This value is lower than the energy predicted by the liquid drop model.[53] For purposes of future discussion it is worth noting that the notion of a "threshold" for photofission, which implies the existence of an energy selection rule, is not a perfectly precise one. The "classical threshold" for photofission is in principle equal to the height of the potential barrier which opposes the division of a nucleus into two fragments. Both theory and experiment, however, indicate a smooth variation of fission probability over the barrier due to barrier penetration. Further, it is a well-known fact that nuclear fission is an exothermic process. Therefore the experimental "threshold" values henceforth referred to might be best thought of as activation energies which closely approximate the classical barrier heights.

B. Competing Reactions in the Compound Nucleus

The lifetime of the compound or transition state nucleus is relatively long compared to the fundamental nuclear periods.[138] Hence, nuclei excited with gamma rays within about 2 Mev or so of photofission threshold can de-excite by re-emission of one or a cascade of gamma rays, by neutron emission, or by fission. For the latter process to occur a

sufficient amount of energy must be concentrated in the potential energy of deformation to enable the nucleus to pass over the saddle point at which the repulsive Coulomb forces balance the cohesive nuclear interactions.

For fission to compete to a measurable extent, it must take place in nuclear times comparable to those involved in gamma and neutron emission. In the region of low excitation energies, the process of photon absorption results in an excited nucleus which can be described by the statistical theory of the compound nucleus. The states or energy levels of the compound nucleus are typically sharp, with a width (finite spread in excitation energy) much less than the separation of the levels.[71] In the Bohr theory of the compound nucleus, the mode of de-excitation depends only on the energy, angular momentum, and probably parity of the compound system and is further independent of the means of formation. According to this picture, one may represent the total photon capture cross section, $\sigma_c(\gamma)$, near threshold by

$$\sigma_c(\gamma) = \sigma_{(\gamma,\gamma')} + \sigma_{(\gamma,n)} + \sigma_{(\gamma,f)} \quad . \tag{1}$$

Other reaction involving the emission of charged particles are omitted owing to their inhibition in the heavy-element region by Coulomb forces and the short times involved. Also, only simple fission and single neutron emission are considered, since only one mode of de-excitation will be likely near threshold.

The fate of the compound nucleus is determined by its branching or level-width ratios which determine the relative probability for decay via a specified mode. In the terminology of references 18 and 100, these are $\overline{\Gamma}_\gamma/\overline{\Gamma} = G_\gamma$ for gamma-ray emission, $\overline{\Gamma}_n/\overline{\Gamma} = G_n$ for neutron emission, and $\overline{\Gamma}_f/\overline{\Gamma} = G_f$ for fission. The "average total width," $\overline{\Gamma} = \Sigma_i \overline{\Gamma}_i$, of a compound nuclear state of given excitation energy is, in principle, a summation taken over all possible de-excitation modes and $\Sigma_i G_i = 1$. Since fission is the most important process occurring within 1 to 2 Mev of the threshold, the branching probability for decay via fission, G_f, will outweigh both G_γ and G_n. The competition in the compound nucleus between fission and other modes of disposition of the excitation energy is governed by the ratio

$$\overline{\Gamma}_f/(\overline{\Gamma}_f + \overline{\Gamma}_n + \overline{\Gamma}_\gamma) \quad .$$

The cross section for photofission can be readily connected with the cross section for photon capture by the relation

$$\begin{aligned} \sigma_{(\gamma,f)} &= \sigma_c(\gamma) \cdot G_f \\ &= \sigma_c(\gamma) \cdot \overline{\Gamma}_f/(\overline{\Gamma}_f + \overline{\Gamma}_n + \overline{\Gamma}_\gamma) \quad . \end{aligned} \tag{2}$$

Below the threshold for (γ, neutron) emission only gamma-ray de-excitation can compete with fission, since $G_n = 0$ and equation (2) takes the form

$$\sigma_{(\gamma,f)} = \sigma_c(\gamma) \cdot \overline{\Gamma}_f/(\overline{\Gamma}_f + \overline{\Gamma}_\gamma) \qquad (3)$$

Below the fission barrier, gamma-ray re-emission is the only mode of de-excitation. As the excitation energy approaches the top of the fission barrier, fission will begin to compete measurably with (γ,γ') reactions. This arises because the probability for fission, G_f, is a small but rapidly increasing function of energy in this region, while that for gamma-ray de-excitation is probably changing quite slowly. The total gamma-ray radiation width shows remarkably little variation both with respect to different nuclei (the exception being a small even-odd effect) and to energy of the compound nuclear level. From the resonance widths for a slow-neutron capture in heavy nuclei, the values of $\overline{\Gamma}_\gamma$ range from 0.023 to 0.043 ev.[126] These widths represent, quite likely the electric dipole transition probability averaged over the many possible final states available.[71] Once the "fission threshold" is exceeded, however, the fission width, $\overline{\Gamma}_f$, becomes much larger than the radiation width, $\overline{\Gamma}_\gamma$, so that gamma emission is no longer a serious competitor.[4,7] From these considerations, for the interval of nuclear excitation energies defined by the "fission threshold" and (γ,neutron) threshold, equation (3) reduces to

$$\sigma_{(\gamma,f)} = \sigma_c(\gamma) \quad . \qquad (3')$$

In this energy interval, then, the observed (γ,fission) cross section should closely approximate the total photon absorption cross section. For energies above the (γ,neutron) threshold equation (2) then reduces to

$$\sigma_{(\gamma,f)} = \sigma_c(\gamma) \cdot \frac{\overline{\Gamma}_f}{\overline{\Gamma}_f + \overline{\Gamma}_n} \quad . \qquad (2')$$

Arguments concerning possible discontinuities in G_f as defined by equation (2') will be developed later in connection with the structure observed in some (γ,fission) excitation curves.

C. Odd-Parity States in Heavy Nuclei

The regions of neutron numbers between 82 and 126 and >126 represent the regions of maximum distortion in the shape of the nuclear surface. Such large nuclear deformations of the ground states are characteristic of nuclei with nucleon configurations far removed from closed shells[23] and reflect the polarizing effect of nucleons outside the closed shells, i.e., Z = 82, N = 126. There is an apparent decrease, however, in the deformation at about neutron number 152, which lends support to the idea for the occurrence of a sub-shell in this region.[61] Nuclei in these regions attain lower energy by taking advantage of the additional collective degrees

of freedom represented by nucleons moving in a spheroidal-well collective potential.[20,23,24,112] The region of neutron numbers >126 is the one of particular interest in fission. Energy levels, spins, and parities here have been the subject of considerable investigation in recent years.

A measure of the nuclear distortion can be obtained from a number of sources: nuclear energy level spacings, gamma-ray transition probabilities as derived from Coulomb excitation cross-section measurements, and quadrupole moments. Relative distortions can be obtained from energy level spacings using a relation derived by assuming that a hydrodynamical model[4] of irrotational flow describes the nucleus. Such a model is of only limited scope, however, as is suggested by the unusually large deformations so derived. As obtained from the classical electrodynamics of an ellipsoid of revolution,[63,119] the nuclear electric quadrupole moment can be interpreted in terms of the nuclear charge distribution. It is zero for a spherical distribution, positive for one that is prolate spheroidal about the spin axis, and negative for one that is oblate spheroidal about the same axis. A low negative quadrupole moment is observed[61] near the double closed shell at N = 126. All other observed moments (for odd Z or N nuclei) beyond this shell are positive, with the exception of that for Ac^{227}, suggesting the predominate occurrence of prolate nuclear shapes.

According to the collective model of Bohr and Mottelson[23] for strongly deformed nuclei, the collective excitations can be described as being either of the rotational or vibrational type. The first represents a collective motion which rotates the nuclear orientation while preserving the shape, and the second corresponds to oscillations about the equilibrium shape for fixed orientation of the nucleus. For even-even nuclei in the ground state nucleon configuration (K = 0), the energy differences in the rotational level structure are given be:

$$\Delta_{E_I} = \frac{\hbar}{2\mathcal{J}} I(I+1) \quad , (4)$$

where I represents the total angular momentum.

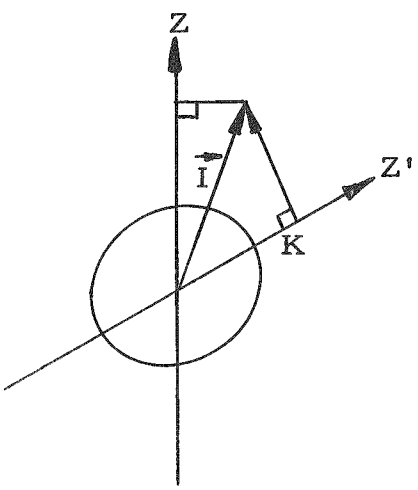

FIGURE II-1.

Coupling Scheme for Deformed Nuclei. I represents the total angular momentum; K, its component along the nuclear symmetry axis Z', represents an intrinsic angular momentum.

$\mathscr{I}$ = an effective moment of inertia

$\hbar/2\mathscr{I} \approx 7$ kev for the ground state of very heavy nuclei

and

$$\mathscr{I} = 3\,B\,\beta^{5}\,, \tag{5}$$

where B = parameter associated with the mass distribution
β = deformation parameter (~0.3 for fissionable nuclei).

Further, if the nucleus is assumed to have ellipsoidal shape, the deformation parameter can be written explicitly in the form:[4]

$$\beta = 4.3\,\left(\frac{\pi}{5}\right)^{\frac{1}{2}} \cdot \frac{\Delta R}{R_o}\,, \tag{6}$$

where R_o = mean nuclear radius
ΔR = the difference between the major and minor semiaxes of the spheroid.

For nuclei possessing reflection symmetry, and K = 0 (see Figure II-1), only rotational levels with even I-values and positive parity are possible. The systematics of such levels are now very well established in deformed nuclei.[22] Since it is likely that at the saddle-point configuration, the nuclear shape in general does not possess reflectional symmetry[19] about a plane perpendicular to the symmetry axis, nuclei in this state may well play a significant role in fission. Moreover, the form or shape of the excited nucleus may determine the actual partition of energy and hence the width for fission.[140] For nuclei possessing this kind of configuration and having K = 0, only rotational levels with odd I-values and negative parity are possible. The systematic occurrence of a number of such odd-parity states for even-even nuclei over a region of at least 18 mass numbers in the actinide region have been observed.[7,8,17,123,124,125] There are indications, too, of the occurrence of similar states in deformed even-even nuclei in the lanthanide region.[102] The known odd-parity states are tabulated in Table II-1.

Since these states of odd parity are known to occur systematically and have relatively low excitation energies, i.e., energies of the order of several hundred kev, which is still below the energy required to unpair nucleons, it has been suggested that these states represent collective oscillations of octupole type.[4,25] This suggestion was first proposed by R. F. Christy to explain the alpha-group transitions to odd-parity states observed for some even-even nuclei. If the surface deformation of the nucleus is given by:

$$R = R_o\,[1 + \beta_2\,Y_{20}\,(\theta) + \beta_3\,Y_{30}\,(\theta) + \ldots.]\,, \tag{7}$$

TABLE II-1

ODD-PARITY STATES IN EVEN-EVEN NUCLEI

Nuclide	N	E(0,1-),* kev	E(0,3-),* kev	E(0,5-),* kev	References
$_{62}Sm^{152}$	90	960			102
$_{88}Ra^{222}$	134	242			123
Ra^{224}	136	217	289		8,123,125
Ra^{226}	138	253	320	445	123,124,125
$_{90}Th^{226}$	136	232			123
Th^{228}	138	328	396		17,123,125
$_{94}Pu^{238}$	144	605			124
Pu^{240}	146	(~600)			7

*(K,Iπ) indicated

where the Y's are Legendre polynomials, then β_2 and β_3 represent the quadrupole and octupole deformations, respectively. The lowest order shape vibration considered is of the quadrupole type, since dipole-type motion does not change the surface deformation.[6] In this interpretation the odd-parity states may be due to a softness toward asymmetric vibration of the type $\beta_3\ Y_{30}\ (\theta)$ in the shape of the nuclear surface. A special case of such a vibration is that of a nucleus which is pear-shaped in equilibrium and which may oscillate between mirror shapes.[21,56]

It has been pointed out that the members of the odd-parity band seem to follow the simple I(I + 1) dependence of equation (4) more closely than the members of the even-parity band of the ground state rotational band.[125] The spacing of these odd-parity levels in a given nucleus is such that the apparent moment of inertia is as much as 40% larger than for the ground-state configuration.[17] The lowest odd-parity state found is of the (1-) type and decays by emission of E1 radiation to the ground state or to the 2+ first rotational state. The transition probability for this decay (or for excitation to the 1- level) depends, quite likely, on the nuclear polarization[25] associated with the vibration since, for a uniformly charged nucleus, the center of mass and center of charge coincide. Such a polarization effect would produce a dipole moment proportional to $\beta_2\beta_3$. For the uranium group nuclei, the collective dipole moment is estimated[128] to be of the order of 0.05 to 0.1 R_o. It may be seen from Table II-1 that, for constant Z, the (1-) energy levels in the actinide region appear to have a minimum value at N = 136.

Also, these levels are generally increasing in spacing above the ground state with increasing Z ($Z \geqslant 90$) and lie lowest in the region of radium and thorium. It should be noted that as yet states of odd parity have not been observed in the isotopes of uranium. This may mean that alpha transitions to these states are highly hindered[124] in uranium or else the states lie very much higher in energy[7] than in neighboring elements of even Z, i.e., uranium nuclei are no longer "soft" to a β_3-type surface deformation.

Two possible interpretations of the octupole (β_3) deformation seem possible.[25] The first would envisage octupole vibrations about an equilibrium shape which itself contains no odd-parity distortion, while the second would imply rotations of a nuclear equilibrium shape possessing a static octupole deformation. The former would seem more probable in that the time average of the nuclear ground state (even-even nuclei) should be symmetric. The second interpretation would lend support to the idea of the existence of stable deformations of this type. The question of stability of pear-shaped deformations has been discussed in the recent literature.[4,97,128,129] Arguments for the correspondence between (1-) states and stable pear-shaped deformations do have some plausibility in that fission probably does proceed by asymmetric passage at the saddle point.

D. Anisotropic Photofission in Heavy Nuclei

The pronounced angular anisotropy in the fragment distributions of Winhold and Halpern[33] for Th^{232} and U^{238} at excitation energies near threshold has already been mentioned. The distributions were observed by counting the total β activity of the fragments caught at various angles with respect to the gamma-ray beam. The amount of anisotropy found increases with decreasing photon energy (approaching unity at energies under 7 Mev), and furthermore in the case of uranium the anisotropy is less than for the photofission of thorium (see Figure II-2). Preliminary results of Brown[29] indicate, moreover, that the anisotropy in Th^{232} probably is very much stronger than in U^{238} under 7 Mev. A b/a value of about 70 at 6.4 Mev has been obtained for Th^{232} from a distribution derived by direct fission counting. The observed distributions described above were compatible with the form $(a + b \sin^2\theta)$, where the second term is suggestive of electric dipole absorption. The angle θ is measured from the direction of the photon beam to the axis of the two fission fragments. The existence of a dipole term in the observed angular distribution can be connnected with the dipole mechanism given by the Goldhaber-Teller model[60] for the giant resonance photon absorption by nuclei. Basically, however, the observed angular anisotropy conflicts with the liquid drop model of the fission process.[16] In this picture, it is assumed that, following photon absorption, a complicated redistribution of the energy occurs before the saddle-point configuration is reached. Thus one would expect no correlation between the direction of incidence of the photon and the direction of emergence of the fragments.

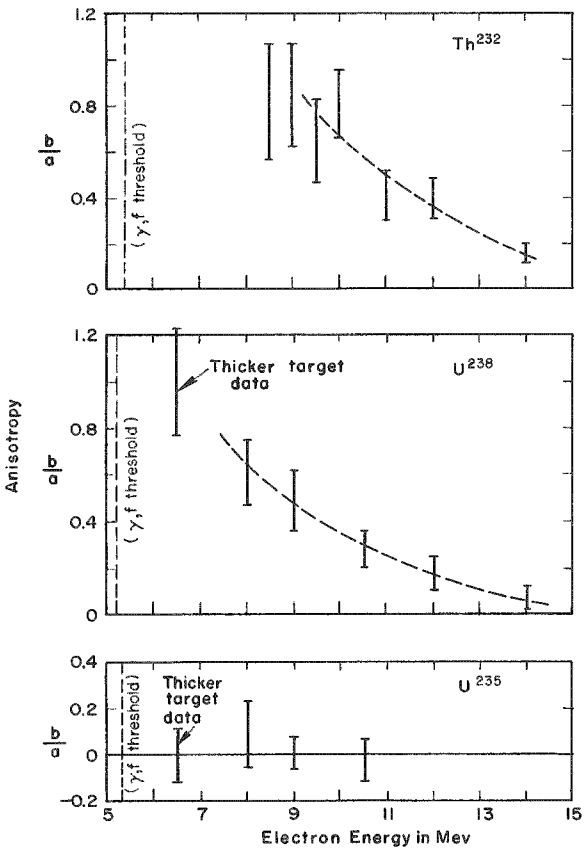

FIGURE II-2

Anisotropy in Photofission. The angular distributions are assumed to be of the form a + b $\sin^2\theta$. Data of Winhold and Halpern, Phys. Rev. 103, 990 (1956).

A qualitative picture of the process, based on the collective model, has been discussed by Bohr[19] and by Hill and Wheeler.[68]

In addition to the isotropic and dipole distributions of fission fragments, there is now an accumulation of evidence that suggests a quadrupole component probably exists as well. In a recent study of the angular distribution of fission fragments from U^{238} excited by 18-Mev betatron bremsstrahlung,[99,114] using nuclear emulsions, a function of the form

$$I(\theta) = a + b \sin^2\theta + C \sin^2 2\theta \qquad (8)$$

was fitted to the data. The quadrupole distribution, $C \sin^2 2\theta$, represents something like 9% relative to the isotropic component. The existence of such a distribution at this energy is in keeping with theoretical estimates[18] and is postulated to result from direct electromagnetic interaction between photons and the nuclear proton distribution under circumstances such that the photon wave lengths are comparable to nuclear dimensions. The idea that quadrupole absorption may take place at still lower energies has been indicated by a similar Russian investigation[11,96] on U^{238} at maximum bremsstrahlung energies of 9.4 and 12 Mev. These results indicate a considerable relative increase of quadrupole absorption at energies less than 10 Mev. It was found that the measured number of fission fragments in the intervals from 30° to 60° and from 60° to 90°, referred to unit solid angle, were identical. Such a distribution cannot conform to a dependence of the type $I(\theta) = a + b \sin^2\theta$. The angular distribution obtained at E_{max} = 9.4 Mev was reported to have the form

$$I(\theta) = a + b \sin^2\theta + c \sin^4\theta \quad , \qquad (9)$$

where $\sin^4\theta = \sin^2\theta - 1/4 \sin^2 2\theta$. It is fair to state, though, that the uncertainty in the data is such that the quadrupole term in the distribution may not be significant.

Theoretical estimates[39,40,89] of the total cross sections for electric quadrupole transitions support the view that such transitions may well occur at low excitation energies. These estimates indicate that the cross section $\sigma_{E2}(E_\gamma)$ has at least two maxima. The first maximum is in the range of energies of the order of 1 Mev and is thought to correspond to the eigenfrequency required for nuclear surface vibrations. The second maximum occurs at considerably higher energies and has a cross-sectional area appreciably larger than the cross-sectional area under the first one. The role of this second maximum is connected with a correspondence to the lowest eigenfrequency of polarization vibrations in nuclear matter.

For nuclei of spheroidal shape the form of nuclear behavior associated with the first quadrupole maximum above may involve the "valence" nucleons[141] of the unfilled surface shells that are responsible for giving the nucleus many of its ground state properties, i.e., spin, parity, and magnetic moment. According to the collective model, a transition (electric quadrupole) to the first state of a surface vibration in the very heavy nuclei should lie around one Mev.[4,61] Recent studies[40] of the levels in the one-Mev region in heavy nuclei of the even-even type have revealed the systematic occurrence of states having many of the expected properties associated with both γ and β-vibrational excitations[4] of the collective model. The form of nuclear behavior associated with the second and larger quadrupole maximum implies, if its assumed nature is correct, that not only the "valence" nucleons are involved, but also those in the core of the nucleus where the greater number is to be found. Such a proposal would find analogy in a recent suggestion[141] that the absorption of El radiation in the closed shells of the nuclear core will give rise to a giant resonance. In this case the quadrupole vibrations might correspond to the β_2 of equation (7) of this section (part C). A recent theoretical estimate[89] of the "center of gravity" of the second maximum cross section for quadrupole transitions in uranium places a lower bound at about 9 Mev. This result is in good agreement with the Russian quadrupole distribution found in U^{238} at 9.4 Mev. One may conclude from this that quadrupole excitation may play an important role in photofission within a few Mev of "threshold." Furthermore, it may well be that the second maximum for quadrupole excitation occurs at energies as low as 6 to 7 Mev in this region of high mass numbers. This circumstance would provide an alternative explanation[19] for the angular anisotropy observed for Th^{232} and U^{238} in this energy region. A further bit of evidence to support these ideas may be taken from photonuclear measurements on light nuclei. Such measurements[36] on C^{13}, typical of behavior observed in a number of light nuclei, indicate that a resonance in the total photon absorption cross section is found at (13.2 $\pm$ 1) Mev as well as the giant resonance at 25 Mev. The lower energy peak is often attributed to quadrupole absorption.[16] If one now assumes the validity of an extrapolation to the heavy mass region, then it seems reasonable to expect quadrupole absorption at about 6 to 7 Mev for the very heavy nuclei whose peak giant resonance cross sections occur at about 13 to 15 Mev.

E. Correlation Between Odd-Parity States and the Existence of Channels for Fission

The photoabsorption by the 0+ ground state of an even-even nucleus at low excitation energies can be pictured[16,139] as occurring predominantly via the electric dipole component of the incident radiation, and secondarily by way of electric quadrupole and magnetic dipole absorption (higher multipole absorption being neglected). The spin and parities of the excited states formed by E1, E2, and M1 absorption are 1-, 2+, and 1+, respectively. In the qualitative proposal of A. Bohr,[19] excitation energies near the fission threshold leave the nucleus in its saddle-point configuration essentially cold, since the major portion of the energy has gone into surface deformation. In this circumstance the low-lying quantum states or channels with K = 0 are expected to form a spectrum similar to the low-energy excitations of the nuclear ground state. Since the barrier height for fission should depend upon both the spin state and nuclear deformation, the (1-) channel may lie perhaps a few tens of kev above 0+ and have practically the same fission threshold.[139] The 1+ channel belonging to a state of intrinsic excitation will be an Mev or more higher. Hence at these energies the great majority of fissioning nuclei would be constrained to pass through one or at least a small number of collective channels of the (1-) type (neglecting quadrupole excitations). The probability for the nuclear symmetry axis to form an angle θ with the photon beam direction is $W(\theta) = b \sin^2\theta$ in this case. As the excitation increases an Mev or more above threshold, other (1-) states (K = 1) corresponding to intrinsic nucleon excitation become available and the level density increases to the extent that the anisotropy "washes out" and the angular distribution becomes $W(\theta) = a + b \sin^2\theta$. Such a picture plausibly explains the anisotropy seen in Th^{232} and U^{238} at low excitation energies. Further, the larger anisotropy seen for Th^{232} over U^{238} may find explanation in relative spacings of the (1-) states involved above the ground state. A correlation [61] of this kind has been shown to exist wherein the degree of fission mass asymmetry increases as the (1-) level moves nearer the ground state.

In odd-A nuclei with unpaired nucleons, the low-lying states are, in general, more dense.[110] For these nuclei, states due to collective modes are superimposed upon each of a number of possible singe particle states, and little correlation exists between spin and parity. In addition, the density of states near the saddle point is probably larger. Therefore, even close to fission "threshold," photofission may proceed through several states, and no pronounced anisotropy is expected.

III. EXPERIMENTAL CONSIDERATIONS

A. Apparatus

1. Gamma-Photon Source

Monoenergetic gamma rays of 6 to 7-Mev energy were obtained from the F^{19} $(p,\alpha\gamma)O^{16}$ reaction. These gamma rays represent the well-known ground state transitions[2,46,107] from excited state in O^{16} shown in Figure III-1. Thick traget gamma yields were obtained using proton bombarding energies of 1.380 (resonant)[33] and 3.645 Mev (non-resonant).[142] At the lower proton energy the predominant gamma component is the 6.14-Mev line, while at the higher bombarding energy the 6.91 and 7.12-Mev gamma groups (unresolved) is in greater abundance. Hereafter the two gamma spectra will be identified as the low (1.380 Mev) and the high (3.645 Mev) energy gamma spectrum. The thick target gamma-ray intensity ratio I(6.91 + 7.12)/I(6.14) as a function of proton energy is plotted in Figure III-2. This graph represents a linear extrapolation of the relative intensities as a function of proton energy as given in references 14, 59, 111, and 137. The details of the experimental equipment employed are shown in Figures III-3 and III-4. Monoenergetic protons were obtained from the Argonne 4-Mev Van de Graaff generator with magnetic beam energy analyzer (energy resolution about 0.1%).

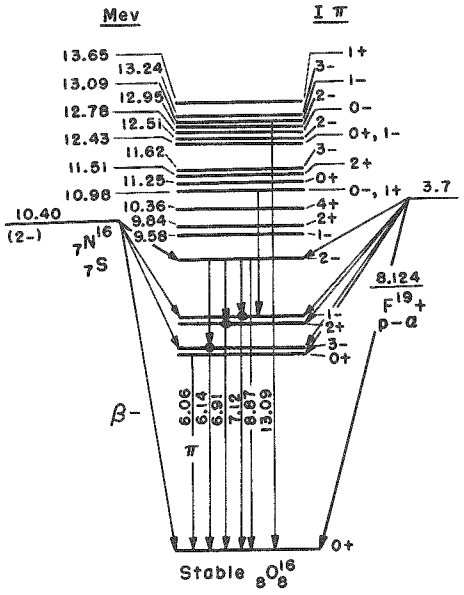

FIGURE III-1

Electromagnetic Transitions in O^{16}.

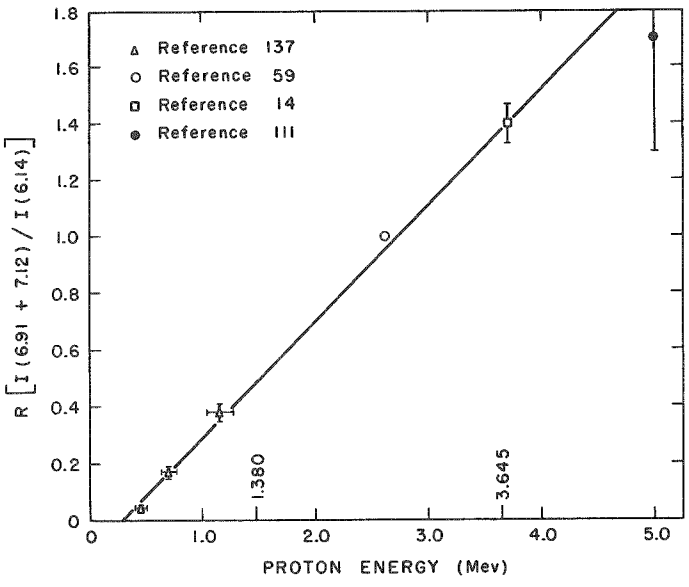

FIGURE III-2

Thick Target Gamma-Ray Intensity Ratio vs. Proton Energy. F^{19} $(p,\alpha\gamma)O^{16}$ Reaction.

Figure III - 3. CaF_2 Target and Target Holder

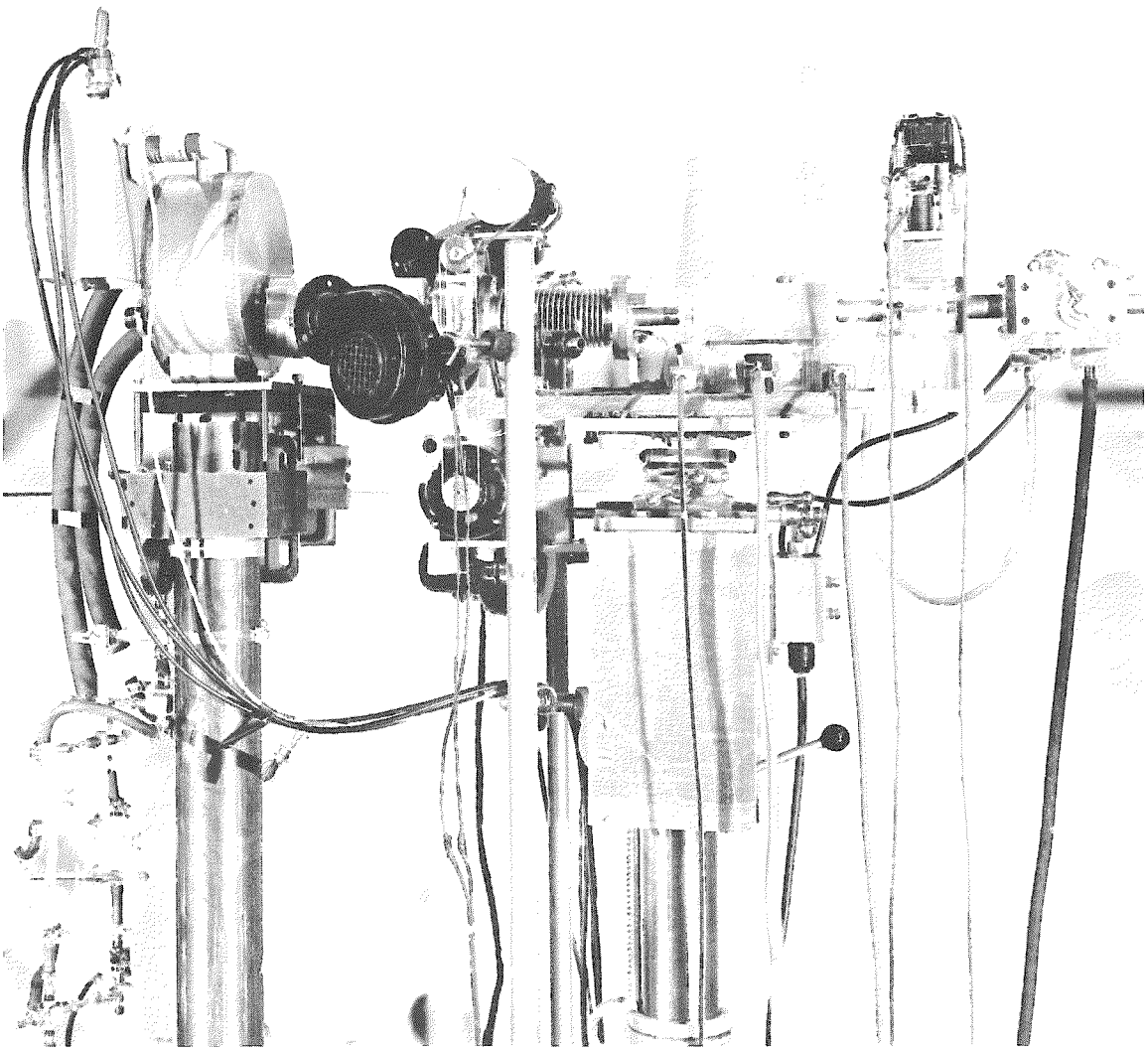

Figure III - 4. Fission Chamber and Rotating CaF_2 - Target Assembly

The fluoride target employed was thicker than the maximum range of the protons at both energies employed in these experiments, i.e., 1.380 and 3.645 Mev. A synthetic CaF_2 crystal(Optovac Company, North Brookfield, Mass.) of dimensions 4.5 cm x 4.5 cm x 1 mm was mounted on a 20-mil tantalum backing. The crystal was held in place by stretching 50 mesh tantalum gauze (3-mil wire) over the crystal and spot-welding it to the heavier tantalum backing. The optical transmission of the gauze was over 50%. Only a cleavage surface of the crystal was exposed to the proton beam. Aside from mechanical support, the gauze served to protect the crystal against the formation of strains caused by the effects of local heating and electrical charging, which might otherwise fracture the crystal. It was essential to this experiment that the fluoride target contain no materials present with low (p, neutron) thresholds. This consideration dictated the choice of a synthetic CaF_2 target. Though calcium is composed of two isotopes (Ca^{46} and Ca^{48}) which have (p, neutron) thresholds below 2 Mev, the abundances of these isotopes are only 0.0033% and 0.185%, respectively. Tantalum was chosen as the supporting material for the crystal because of its high melting point, low gamma yield from proton Coulomb excitation, absence of any (p, neutron) reaction at the proton energies employed, and lastly its relatively high neutron binding energy (7.716 Mev for Ta^{181}).

The mounted fluoride target fitted over the end of an aluminum sleeve (hereafter identified as the target holder) through which the beam traversed. This target and target holder assembly was connected to a drive mechanism which caused the assembly to rotate with a "wobble-motion" superimposed upon it. The rate of this "rotation" was approximately 60 rpm. In effect, then, due to the motion of the target, the beam was caused to trace a circular path upon the CaF_2 surface of about $1\frac{5}{16}$-inch diameter. This innovation in the target arrangement permitted the use of high beam currents and, hence, the realization of high gamma-flux yields without too rapid deterioration of the target. To further minimize heating effects at high beam currents, forced air cooling was employed about the rotating CaF_2-target assembly. Though it was possible to use an uninterrupted proton current as high as 20 μa at 1.380 Mev, actual runs were made with about 14 μa of beam current on the target. As the high-energy gamma flux increases rapidly with proton bombarding energy,[70,131] a beam current of the order of about 1.5 μa was sufficient with 3.645-Mev protons.

The rotating target assembly was also electrically insulated so that the total charge accumulated by the proton beam impinging on the crystal could be found by the use of a current integrator. This feature was employed, however, only in preliminary experiments, since slow disintegration of the CaF_2 target, with a consequent change in the gamma yield, would probably not be discernible in current integration and the results might not be reproducible.[3]

2. Fission Detector

The structural details of the fission chamber are shown in Figure III-5. It is a modified version of a type of fission chamber first used by Baldwin and Klaiber.[10] The chamber is basically a cancellation-type ionization chamber of 2π geometry filled with one atmosphere of methane gas.

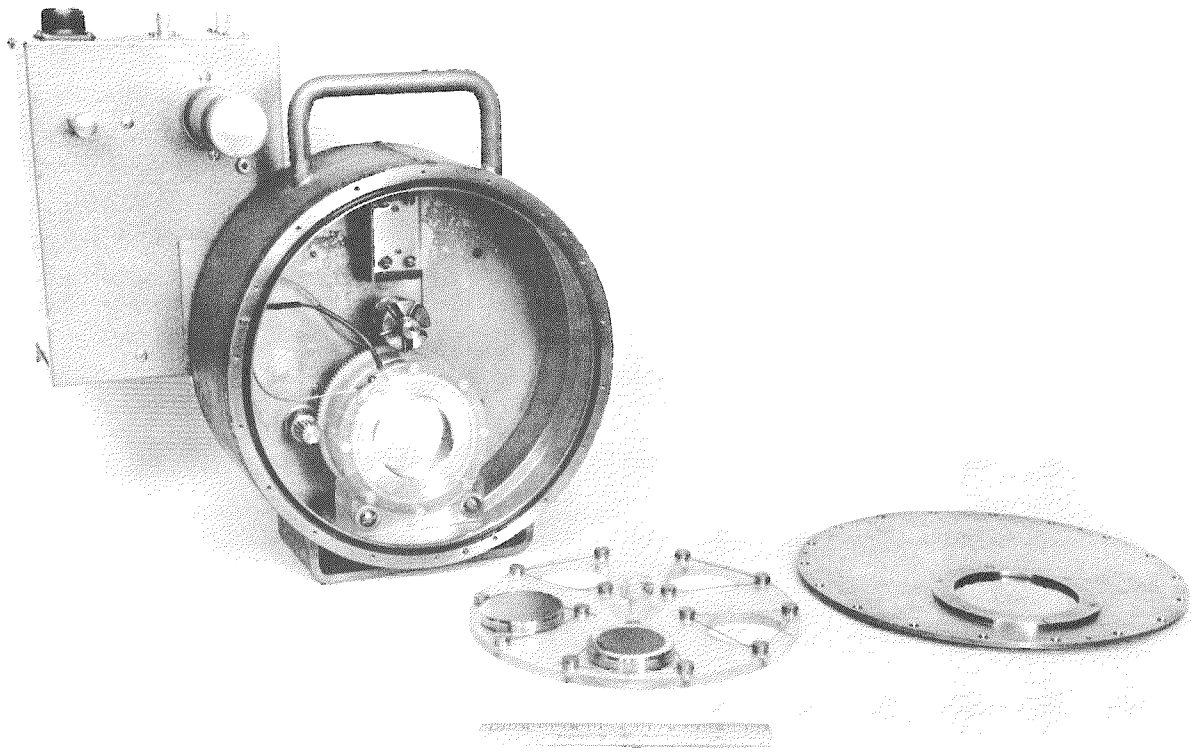

FIGURE III-5

Multiple-Sample Fission Chamber.

As shown in Figure III-6, it consisted of three electrodes - A, B, and C - arranged so as to form two adjacent parallel-plate ionization chambers of approximately equal capacitance. Electrode A was movable so that spacing between electrodes A and B could be varied. The spacing between the electrodes under usual operating conditions was A-B = 0.84 cm and B-C = 0.9 cm. To achieve a positive potential gradient in the beam direction C-B-A, electrode C was operated at ground potential while electrodes B and A were at about +490- and +898 volts, respectively. Electrode B, which served as the signal electrode, was capacitively coupled to the grid of the first tube of a preamplifier. The heavy-element samples were made an integral part of electrode C for fission counting. The sample coated on 0.004-inch platinum by a technique described elsewhere in this treatise was held by a

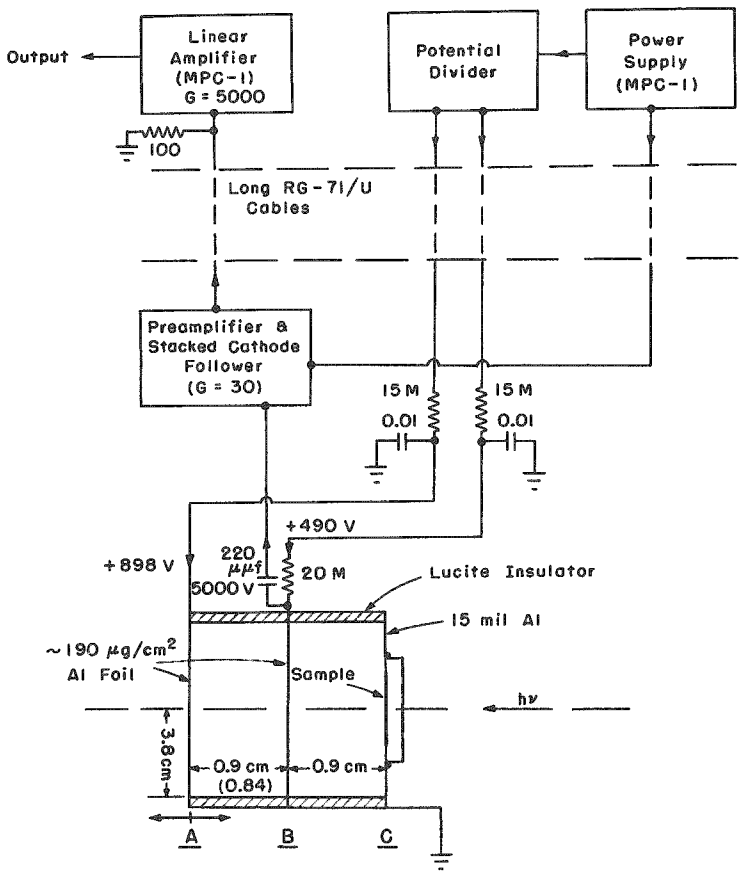

FIGURE III-6

Ionization Chamber and Related Circuitry.

stainless steel holder. This assembly fitted through a precisely defined opening in electrode C such that the platinum backing plate was essentially flush with the back of electrode C. In the interests of efficiency of operation a multiple-sample holder was employed; this held five mounted samples. Each sample could be made an integral part of electrode C by a "rotation" operation which suitably positioned the new sample.

The choice of chamber design for the experiments described herein was made with two purposes in mind: (a) to minimize the background (spurious recoils or secondary electrons) produced by intense gamma radiation; (b) to discriminate effectively between fission and alpha pulses for samples of reasonably high specific activity. The first goal was completely realized while the second was achieved for milligram samples with a specific alpha activity as high as 1.52×10^6 d/m/mg (Np^{237}). In operation, when equal amounts of ionization are produced simultaneously in both region C-B and B-A, i.e., ideally for the case of high-energy gamma quanta passing axially through the chamber, the net signal on electrode B

can in principle be made a very small fraction of the ionization pulse from one region alone.[121] For a collimated source of alpha particles this type of performance would be essentially realized for the reasons: (a) the range of a 4.0-Mev alpha particle (corresponding to Th^{232}, the least energetic heavy-element alpha emitter studied)[109] in CH_4 is about 2.8 cm,[1,55] so that most of the particles would traverse both regions C-B and B-A; (b) an alpha particle ionizes most heavily at the very end of its range.[79] This latter condition requires that the center electrode B be made as thin as possible. For this reason, electrode B was made out of approximately 190-$\mu g/cm^2$ aluminum foil.

In practice the alpha samples were uncollimated, which made for imperfect cancellation. This was due to alpha particles which were emitted at grazing angles and hence did not traverse both regions C-B and B-A or else were seriously degraded in energy by virtue of their having spent a significant fraction of their range (estimate[1,55,109] about 8.3 mg/cm^2 for a 4.4-Mev alpha particle) in the thick sample. The requirement of a thick sample was imposed by two considerations: the low (γ,fission) cross sections of the order of a few millibarns[64,66] and the relatively low photon intensities[14,33] obtainable. No collimation of the sample was attempted, as this would have seriously reduced the observed (γ,fission) counting rate. The alpha noise, however, did not prove to be a serious problem until specific alpha activities of the order of 1-2 x 10^7 d/m/mg(U^{234} and U^{233}) were inserted into the chamber. It appears that this is the maximum specific activity level which can be tolerated in a fission detection system of this design.

The degree of cancellation could be adjusted by either varying the high voltage placed upon electrode A or by changing the inter-electrode distance A-B. The former step affected the saturation in the region A-B, while the latter changed the capacitance of A-B. The optimum conditions for "best" cancellation of the pulses caused by the sample of highest specific alpha-activity is shown in Figure III-6.

The basis for selective detection of fission fragments originates from the fact that both the total ionization and specific ionization from a fission fragment in methane is about 2.0 to 3.0 cm (estimate),[55,83] the ionization produced does not cancel for the reason that a fission fragment ionizes most heavily at the beginning of its path,[79] so that fragments that manage to get into region B-A would be severely degraded in energy and hence ionize much less extensively.

The output signal from electrode B was amplified by a combination preamplifier (theoretical gain of 30) and stacked cathode-follower amplifier (gain of 1) mounted directly behind the chamber and completely shielded by a metal shell. The measured rise time of the output pulse was about 0.12 μsec. After traversing 50 feet of RG-59/U coaxial cable, properly

terminated to eliminate humming and standing waves and with an output-pulse time constant of 2 μsec, the pulse went to a linear amplifier (ANL Model MPC-1, Beckman Instruments, Inc.,Richmond, California) which had a theoretical gain of 5000. The amplified pulse was then fed into a discriminator (ANL Model D 20) where it was used to trigger an enabling trigger-pair(univibrator)[47] which produced an approximately square, negative pulse about 10 μsec long. The negative pulse from the enabling trigger-pair was then distributed into ten level-discriminator circuits of the type shown in Figure F-4. The bias levels of these discriminators were such that each individual discriminator was kept at a level higher than the one preceding. The spacing in bias level between pairs of discriminators or channels was variable. The output pulse from each channel went to a scalar (ANL Model S-9A). For calibration and performance check purposes, the output from a precision exponential pulse generator (ANL Model PG-9B) could be coupled to feed artificial pulses through the grid of the first tube of the preamplifier. In this manner the discriminator output could be checked directly in terms of the input to the grid of the preamplifier.

As a result of the imperfect cancellation of alpha pulses in the double-region ionization chamber, the probability of a multiple superposition of small unwanted pulses simulating a large wanted pulse, i.e., alpha pile-up at a very high alpha-particle rate interfering with the counting of fission fragments, was of serious concern. In the fission detection system employed, pile-up could occur at the following locations: (a) the fission chamber itself, because of the time required to collect the electrons created by an ionizing event (passage of a fission fragment, alpha particle, or gamma-induced electrons produced within a very short time interval through the ionization chamber), and (b) the second stage of amplification (linear amplifier) if the band width is not sufficient to preserve the rise time of pulses from the fission chamber. Pile-up in the discriminator and scalars was neglected as these stages principally affected the resolution loss which was very small for the fission counting rates encountered (about 3 to 60 c/m). The low-level trigger circuit of the discriminator (Figure F-4) which controlled the enabling trigger-pair had a 30-μsec on time. This was the controlling factor in any resolution loss in the discriminator and scalars.

To minimize the alpha-pulse pile-up and hence enhance the resolving power of the fission chamber, the latter was operated as an electron-pulse chamber.[115] The narrowness of the pulses from the counter operated in this manner enabled the toleration of large amounts of alpha activity. In operation, the decay-time constant (2 μsec) for the signal from the ionization chamber after one stage of amplification was large compared to the time for collection of the electrons ($\sim$0.1 μsec), but small compared with the time for collection of positive ions ($\sim$milliseconds). As the chamber operated under these conditions responded only to the fast part of the pulse, i.e., to that part of the pulse due to the motion of electrons, it was able to handle high counting rates. The chamber-filling gas used was unpurified methane (Phillips, 99 mol % minimum), a free-electron gas, which has the very fast

electron collection time of 10.0 cm/μsec at saturation,[27,49] i.e., the collection of all electrons produced in the gas filling by the ionization processes. This gas had the further advantage of having a relatively low saturation voltage, i.e., 1.0 volt/cm/mm Hg.

The possibility for the occurrence of pile-up in the last amplification stage can be evaluated from the band width of the amplifier. A rough estimate of the upper frequency cut-off (approximated by the band-width) can be obtained from the expression[63] $3\ t_r f = 1$, where t_r is the rise time or electron "collection time" in the ionization chamber and f is the band-width of the amplifying system. For a collection time of about 0.1 μsec, $f \cong 3.3$ Mc/sec. Since the amplifier (ANL Model MPC-1) had a rise time, t_r, of 0.17 μsec, its upper cut-off frequency was approximately 1.9 Mc/sec. Though this narrower band-width would in effect work to cause alpha pile-up at this stage, the amplifier had sufficient gain to minimize, in part, if not completely, this defect.

3. Gamma-Ray Scintillation Spectrometer

A sodium iodide scintillation spectrometer, which combines the desirable feature of good detection efficiency with fair resolution,[13] was used as the means of monitoring the high-energy gamma flux from the $F^{19}(p,\alpha\gamma)O^{16}$ reaction. The crystal detector was a thallium-activated sodium iodide crystal, 4 inches in diameter by 4 inches long (Harshaw Chemical Corporation). This crystal was the largest size that was readily available and was so chosen because of the improved energy resolution[52] obtainable for gamma quanta exceeding the threshold for pair production. The crystal had ground surfaces and was "canned" in an hermitically sealed aluminum container of approximately 10-mil wall thickness. The internal reflector was MgO. The effective thickness of the Al + MgO was 165 mg/cm^2 to 22.5-kev Ag X rays.[48] The multiplier phototube was a DuMont 6364 type whose characteristics have been described in the literature.[101] It was mounted in an aluminum can with a concentric Mμ metal shield and with a short Lucite light pipe in the manner prescribed by Swank and Moenich.[130] The "canned" crystal was optically connected to the multiplier phototube with a high viscosity silicone oil. The energy resolution of the detector for Cs^{137} 662-kev gamma rays was about 10% full width at half-maximum.

A preamplifier consisting of a simple cathode-follower amplifier (ANL Model A-70) was employed to receive the pulses directly from the DuMont phototube. After traversing 50 feet of RG-71/U coaxial cable, the output of the preamplifier underwent further amplification in a linear amplifier (ANL Model A-61 A) of good linearity and stability. The pulses from the amplifier were fed into a fast single-channel pulse-height analyzer (ANL Model D-17 A) whose average dead time for counts over the window, i.e., applicable to integral counting, was about 5 μsec. The output from the analyzer in turn went to a scalar (ANL Model S-13 C) whose dead time was

also about 5 μsec. The gamma counting rates (about 250 to 650 c/s) were such that the resolution loss was small. A 256-channel analyzer (RCL Mark 20 - Model 2603) was also employed intermittently by running it in parallel to the single-channel analyzer.

The effects of nonlinearities and slow drifts in gain of the electronic equipment were eliminated with the aid of a precision exponential pulse generator.(67) Test signals could be fed into the input of the preamplifier in parallel with the multiplier phototube by means of a 5-μμf capacitor connected to the input grid such that the pulses at the amplifier output were of the same size as those occurring at any location in the pulse-height distribution being recorded. This feature was principally employed to check the location of the bias level for integral counting.

Since the gamma intensities were high, it was possible to use a collimated geometry arrangement with the 4-inch x 4-inch crystal in preference to an open geometry for the high-energy measurements. This step served to reduce the background, made use of the greater detection efficiency of the large crystal, and improved the energy resolution.(52) Since loss of energy out of the sides and end of the spectrometer crystal determine the energy resolution above 2 Mev, collimation of the incident radiation is a straightforward means of getting around this effect. Hence, when the gamma rays are limited to a fine pencil on the axis of the crystal, the first annihilation escape peak would be reduced as well as the width of the principal photopeak because of improvement in energy resolution. The collimator-crystal detector axis was at an angle of zero degrees with respect to the direction of the incident proton beam. Since the photon yield from the F^{19} $(p\alpha\gamma)O^{16}$ reaction is essentially isotropic,(42) the choice of angle was arbitrary. A 3/4-inch diameter aperture in an 8-inch lead wall, located just in front of the crystal, permitted the irradiation of a cylinder of small diameter on the axis of the spectrometer crystal. This amount of lead was sufficient to reduce the intensity of normally incident 6.14-Mev gamma rays to under 0.1%. Further, the source-to-crystal distance was large, so that, because of distance and angle considerations, the amount of secondary radiation (Compton scattered and annihilation radiation) reaching the detector was small. The scintillation detector was also mounted within a shield having 1/4-inch thick lead walls. This served to screen out very low-energy gamma quanta. The schematic plan view of the single-channel gamma-ray scintillation spectrometer as well as the electronic circuits are shown in Figure III-7.

B. Experimental Methods

1. Heavy-Element Samples

Excepting Th^{232}, the samples employed consisted of separated isotopes. The isotopic composition of the samples is indicated in

Table III-8. Of the separated isotopes, U^{233}, U^{234}, and U^{236} were subjected to radiochemical purification via ether extraction.(77) The thorium was initially in the form $Th(NO_3)_4 \cdot 4H_2O$ (C. P. Baker's Analyzed) and was used without further purification.

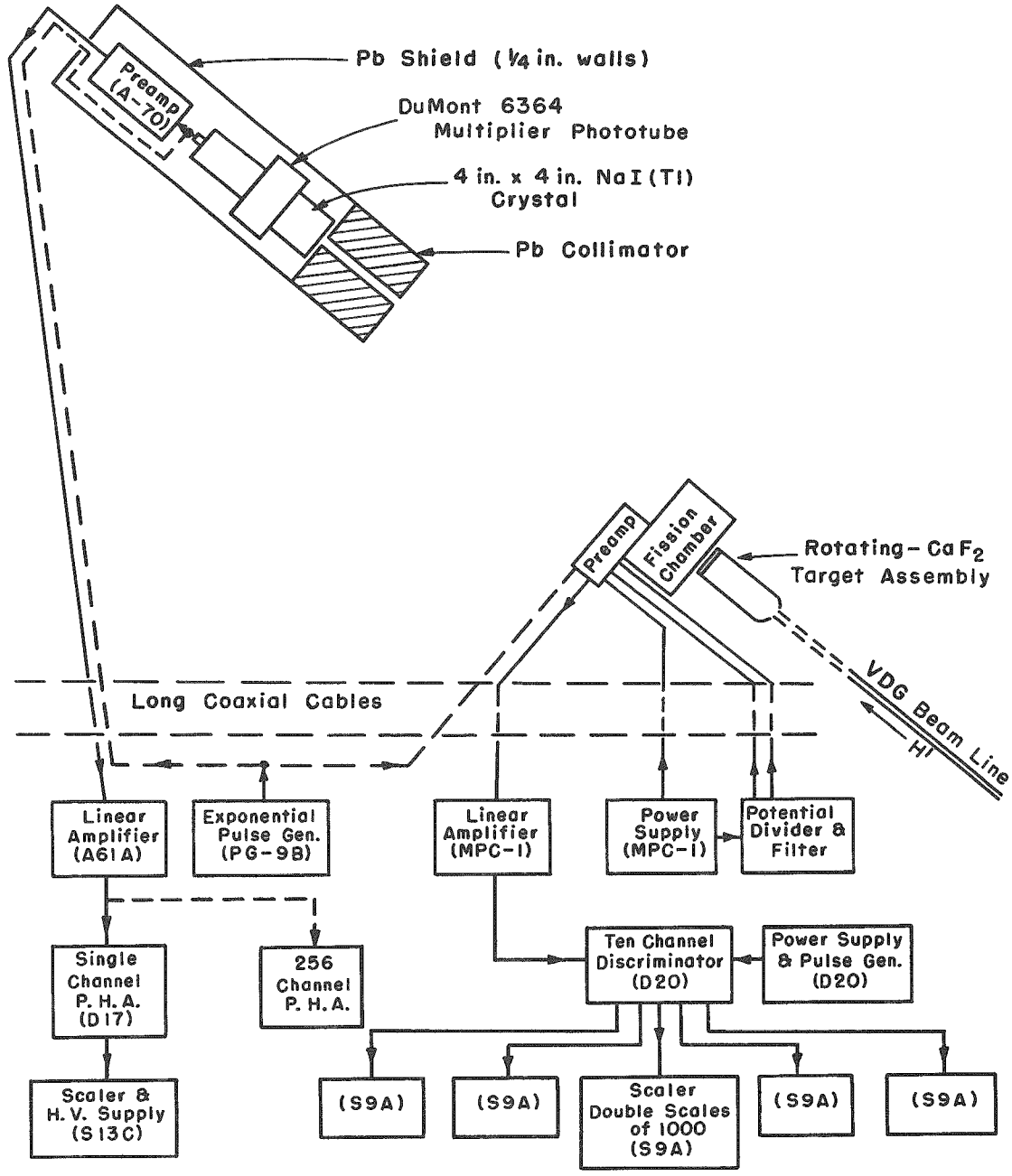

FIGURE III-7

Schematic Diagram of the Experimental Arrangement.

The thick-sample preparation[28,43,79,81,115] required repeated painting and igniting of many small portions of an organic heavy-element solution to produce a given nuclide in suitable chemical form, i.e., an oxide. To achieve solution of the heavy-element sample, the solid in the form of a nitrate was dissolved in a minimum amount of absolute ethyl alcohol. This solution was diluted with an ~1.5% solution of Zapon lacquer (Zaponite adhesive cement, Atlas Powder Company, Chicago, Ill.) in amyl acetate such that the heavy-element concentration was less than 50 mg-ml.

An area of 1 $\frac{1}{2}$-inch diameter on a 1$\frac{7}{8}$-inch diameter x 0.004-inch platinum disc was coated. To help prevent run-off of the organic solution, the area to be coated was defined by means of a circle inscribed with a soft lead pencil and a Zapon ring painted around the circumference of the circle. Once the first few layers of heavy-element oxide were applied, the accurate definition of the painting area was not too difficult to achieve. The organic solution was applied to the platinum foil in thin coats by means of a soft camel's hair brush. The latter was made by binding the hair to a short length of glass rod with platinum wire. In painting, the brush was not allowed to touch for a second time any portion of the painted surface from which the solvent had evaporated. Once painted, the foil was placed beneath a 250-watt heat-reflector bulb to ensure complete evaporation of the solvent. The foil was then fired for 3 to 4 minutes at about 800° C to burn off the Zapon lacquer and to convert the nitrate, essentially quantitatively, into an oxide of known stoichiometry. When the foil had cooled, it was pressed flat between two sheets of cardboard and the coated area rubbed gently with a Kleenex tissue. The above procedure produced a smooth lustrous surface and was repeated until the desired surface density, i.e., 1 mg-cm^2, was reached. Thick foils, weighable for the heavy-element content, were thus prepared.

2. Arrangement of Equipment

The schematic plan view of experimental arrangement is shown in Figure III-7. Both the fission chamber and the collimator-crystal detector were mounted on the axis of the proton beam such that the gamma beam traversed first through the fission chamber and then into the gamma detector. The external beam windows (0.010-inch shim brass) and internal electrodes (Figure III-6) of the fission chamber were such that any attenuation of the gamma beam was negligible. The front surface of the NaI crystal was about 251 cm from the center of the fluorine target and subtended a solid angle (collimated geometry) of 4.53×10^{-5} steradians. The fission chamber was located as close to the rotating CaF_2 target assembly as was feasible; in this arrangement the fissionable sample had a geometry of 4.6 per cent.

3. Procedure

a. Sample Thickness Determination

The areas of all fissionable samples were about 11.40 cm^2. The thickness of each sample was determined both by alpha counting and by weighing. Because of the self-absorption effect in the thick samples, quantitative counting could be achieved only by counting under conditions of reduced geometry. For samples of reasonably high specific alpha activity, i.e., U^{233}, U^{234}, U^{236}, and Np^{237}, low-geometry proportional counting (geometry factors 4.7299×10^{-4} and 8.6329×10^{-4}) was used. The samples of low specific alpha activity, Th^{232}, U^{235}, and U^{238}, were counted in a medium-geometry proportional counter (geometry factor 0.10625). The geometry factors for the spread sources were calculated[80] under the assumption that the sources were uniformly spread and coaxial with the collimator aperture. The counts for replicate sources agreed to within the counting statistics ($\pm$0.1%). All weighings were performed on a semi-micro balance. The agreement between sample masses as determined by both methods employed was quite close, as may be seen in the table that follows.

TABLE III-1

Sample Mass Comparison

Nuclide	mg-Isotope (Weighing)	mg-Isotope (Counting)
Th^{232}	10.60	10.04
U^{233}	9.55_2	9.64_6
U^{234}	9.06_0	9.28_3
U^{235}	9.54	9.5_5
U^{236}	9.00_4	8.95_5
U^{238}	10.26	10.0_5
Np^{237}	9.94	10.0_9

To make this comparison, the heavy-element oxides were assumed to have the following stoichiometries:[38,69,88] ThO_2, U_3O_8, and NpO_2. It can be shown that the presence of trace quantities of other possible oxides, particularly for uranium, would produce a negligible difference in the calculated mass. Further, the alpha pulse-height analyses for the major isotope present in a sample (Th^{232}, U^{235}, U^{236}, U^{238}) and the mass spectrographic analyses (uranium isotopes) were also used in the calculations.

To ascertain the degree of uniformity of the heavy-element samples, a surface mapping of the alpha activity from the U^{234} and Np^{237} was performed. These two were chosen as being representative of

the samples prepared and also were convenient from the point of view of their alpha activities. The uniformity mapping was performed by masking all but a small area of the sample (0.124 cm^2 for Np^{237} and 0.0201 cm^2 for U^{234}) and then counting the alphas from the exposed portion of the sample. The alpha activity was measured with an end window G-M counter placed just above the masked surface of the sample. About 50 locations were mapped in each case to obtain a distribution representative of the entire surface. The alpha activity in both cases was found to be uniform to within about ±4%. All the samples used ranged in thickness from 0.98 to 1.06 mg/cm^2 for the heavy-element oxides.

b. Fission and Gamma Counting

Under usual conditions, the fission chamber was operated as shown in Figure III-6. Four samples, which always included U^{238} as a standard, plus a blank platinum foil were mounted on the multiple-sample holder. The samples were rotated into counting position as desired. For purposes of attaining the best set of operating conditions for the fission chamber, a weightless $Cf^{250,252}$ spontaneous fission source (about 80 f/m) was initially employed. The point chosen for fission counting on the gain plateau was some 600 volts above the knee. The best conditions for alpha-cancellation were established with the aid of the U^{233} sample. It was found that by decreasing the electrode spacing distance A-B from that equivalent to the equal spacing distance, the alpha noise received in the first few channels of the discriminator could be reduced by as much as a factor of 4. Further the alpha noise decreased faster than did the fission rate. The spacing distance, 0.84 cm, was a compromise choice which reduced the alpha pile-up by a factor of two. Optimum conditions for the cancellation voltages on electrodes A and B required that V_A approach a value nearly twice V_B.

The thick samples employed and the alpha discrimination by the fission chamber plus electronic circuitry were such that only short fission plateaus were obtainable. Typically these plateaus had slight slopes beyond which the pulse height dropped off sharply. It was found that with good counting statistics this after-part of the fission pulse-height distribution was perfectly linear over a range of 40 to 50 volts in most cases. Eventually the distribution "tailed" out, presumably due to range straggling of fission fragments in the thick sample. Such straggling arises from the fact that the fragments in passing through homogeneous matter do not all lose their energy in precisely the same way.

As the fission pulse-height distribution covered a range of about 100 volts, the bias levels of the ten-channel discriminator were spaced at about 10-volt intervals, except for the first two channels. These two channels were located such that they received alpha noise from only the most alpha-active samples, i.e., Np^{237}, U^{234}, and U^{233}. Channel one therefore

set a lower bound on the effective length of the fission plateau observed. The total length of the usable plateau (interval from the effective alpha-noise cut-off to the plateau knee) was about 23 volts for U^{238} and under 5 volts for U^{233}. Since the rate of incidence of alpha noise in the first two or three channels was not reproducible, this meant that channel one was lost for the Np^{237} fission counting and channels one, two and sometimes three for the U^{233} and U^{234} counting. Hence, all fission counting was done in the region of the plateau knee. Representative integral fission pulse-height distributions for Th^{232}, at the proton bombarding energies employed, are shown in Figures III-8 and III-9.

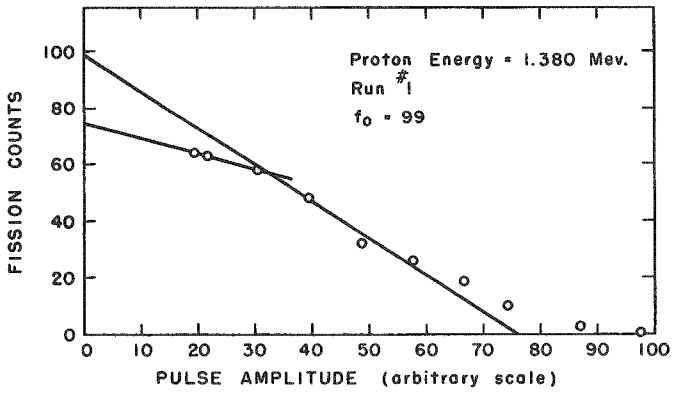

FIGURE III-8
Integral Fission Pulse-Height Distribution Th^{232} (1.380-Mev Protons).

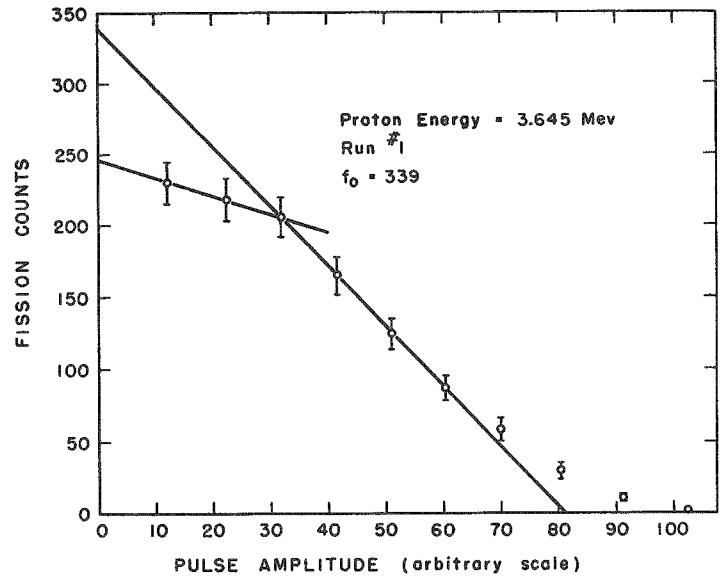

FIGURE III-9
Integral Fission Pulse-Height Distribution for Th^{232}(3.645-Mev Protons).

To monitor the gamma flux experienced by the fissionable sample, the gamma spectrometer was biased to detect only pulse heights exceeding a specified minimum energy loss in the crystal detector. An energy versus pulse-height calibration in the region of interest was obtained using the position of the 6.14-Mev photoline. For the low-energy gamma spectrum (Figure III-10) only energy losses greater than 4.9 Mev were recorded, while with the high-energy spectrum (Figure III-11) an energy loss exceeding 6.3 Mev was required. A higher bias level was chosen in the latter case to bring the integral count rate within reasonable limits.

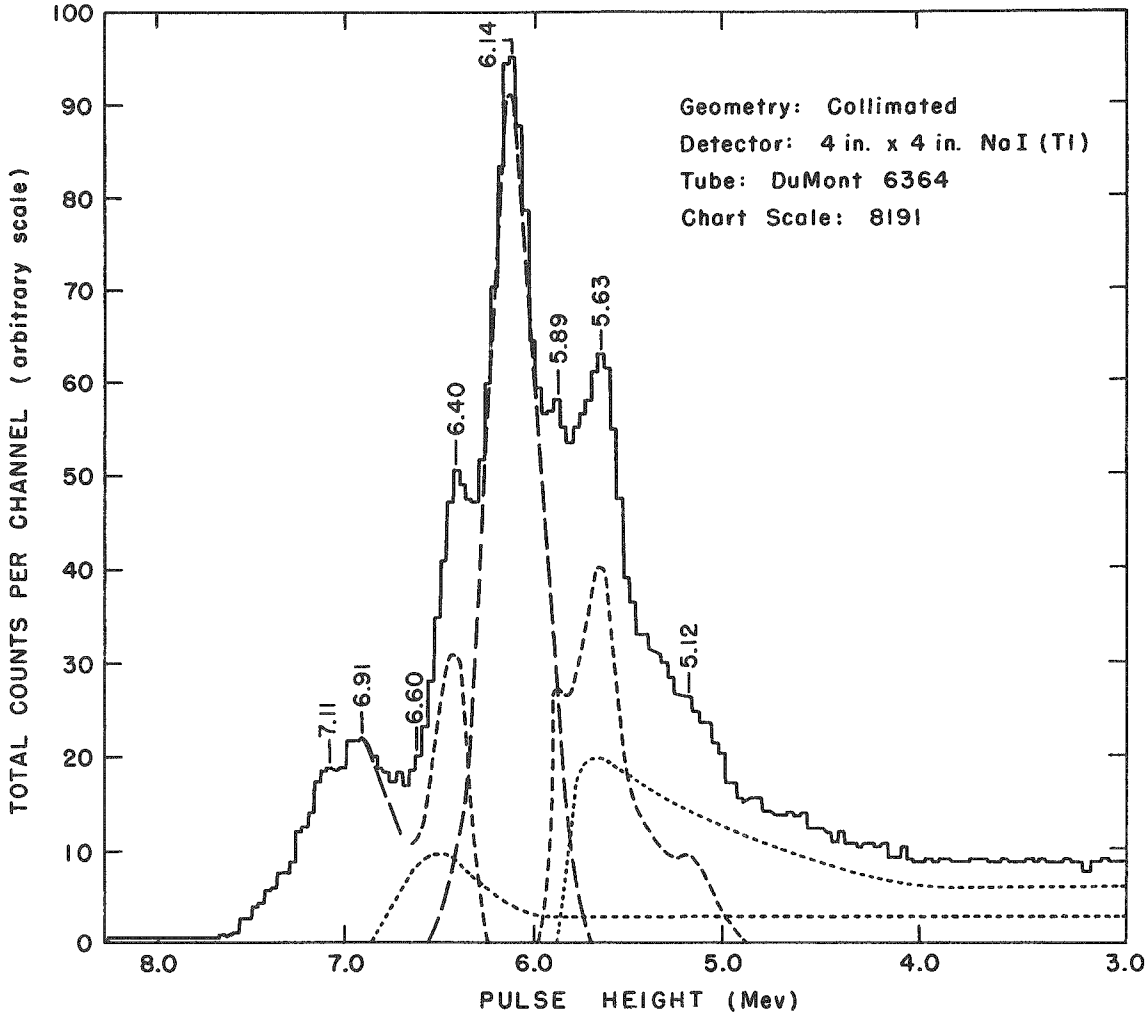

FIGURE III-10

ANALYZED PULSE-HEIGHT DISTRIBUTION FOR THE HIGHER-ENERGY $F^{19}(p, \alpha\gamma)O^{16}$ GAMMA RADIATIONS AT 1.380-Mev PROTON BEAM ENERGY.

Components to the Analyzed Distribution:

——— Observed spectrum

— — Total absorption of the primary γ-ray energy (pair production events with no loss of annihilation radiation)

- - - - - Escape peaks (secondary distribution due to loss of annihilation radiation)

..... Compton electron distribution

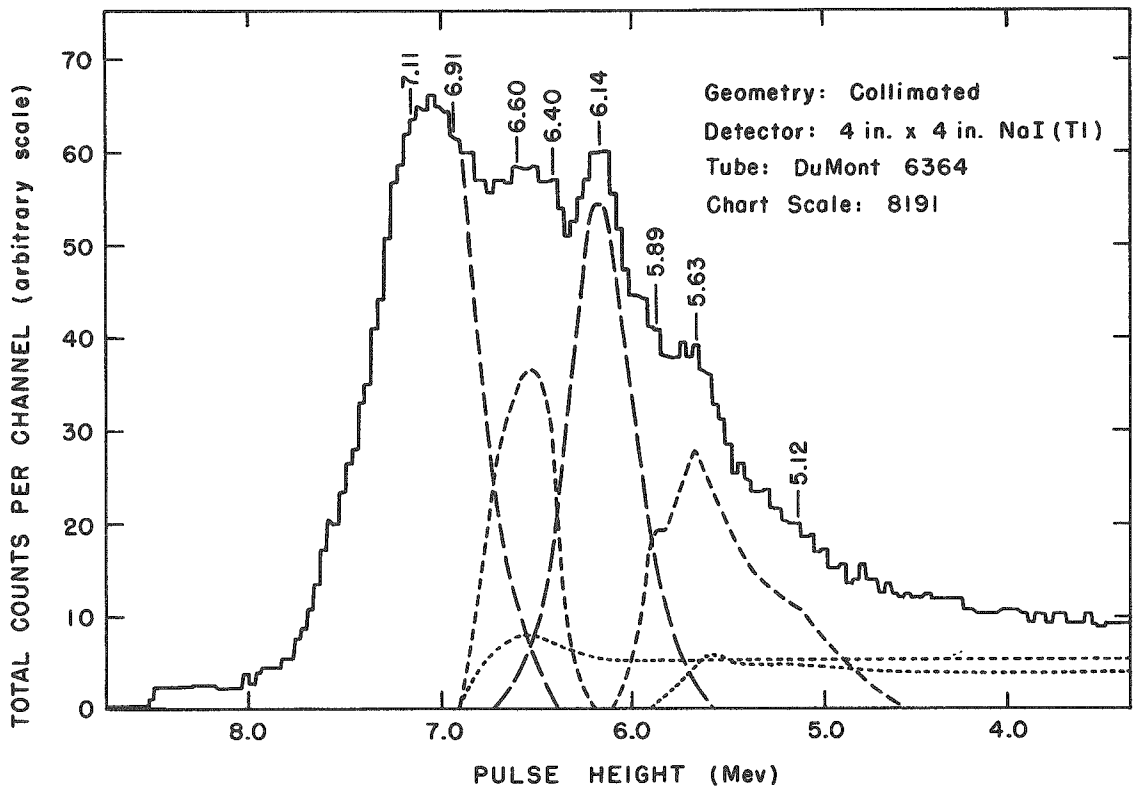

FIGURE III-11

ANALYZED PULSE-HEIGHT DISTRIBUTION FOR THE HIGHER-ENERGY $F^{19}(p, \alpha\gamma)O^{16}$ GAMMA RADIATIONS AT 3.645-Mev PROTON BEAM ENERGY.

Components to the Analyzed Distribution:

——— Observed spectrum

— — Total absorption of primary γ-ray energy (pair production events with no loss of annihilation radiation)

- - - - - Escape peaks (secondary distribution due to loss of annihilation radiation)

..... Compton electron distribution

The normal operating procedure followed was to make a simultaneous fission and gamma count for a specified period. To minimize the effect of unknown "fluctuations," the counting intervals were kept short (15 to 20 minutes) and a new sample counted after each interval. The sample rotation included a blank, U^{238}, plus three other samples taken in order of their mounting. A more rigorous procedure[3] would have specified the counting of the samples in a random manner; however, such a course was not adhered to in the interests of economy of time. The samples were counted until sufficient statistical accuracy had been attained. Ultimately the data of the numerous runs for a given sample were averaged together.

To establish the stability of the electronic circuitry, the bias settings of both the single-channel analyzer and the ten-channel discriminator were checked several times during running periods. This was accomplished with the aid of properly shaped artificial pulses from a precision exponential pulse generator utilized in a manner described previously. The bias level of single-channel analyzer was set to just cut off a pulse of predesignated size. It was found that the bias level drift in each case was less than 0.1%. The bias settings of the discriminator, i.e., channel locations, were established by determining the minimum size pulse necessary to trip a given trigger-pair.

C. Background Measurements

The background detected by the fission chamber, other than alpha noise, might arise from the following sources:

1. Interference from external electrical disturbances, i.e., principally corona associated with the operation of the Van de Graaff;

2. the instantaneous production of large numbers of spurious recoils or secondary electrons by the intense gamma radiation;

3. proton recoils scattered out of the hydrogenous insulators and other structural materials by fast neutrons;

4. natural-background fission rate (spontaneous fission of the heavy-element samples); and

5. neutron-induced fission in the heavy-element target. The primary sources of fast neutrons produced outside the heavy-element sample were those generated in the fluoride target via (p, neutron) reactions on Ca^{46} and Ca^{48} and by (γ,neutron) reactions in the structural materials in the vicinity. Reactions of the latter type might be expected in H^2, C^{13}, O^{17}, and Pt^{195}. Fast neutrons in the heavy-element target would originate from (γ,fission) and (γ,neutron) reactions.

In practice, the electronic circuitry employed in fission counting was insensitive to all but the largest corona discharges. The magnitude of the background arising from factors (2) and (3) above was checked by counting a blank platinum foil. Though small pulses, presumably arising from this source, were occasionally detected, the background contribution was negligible for both the low and high-energy spectrum photons. Likewise, background originating from factor (4) was negligible for the counting periods employed. For U^{238}, the sample with the shortest spontaneous fission half-life, only 4.18×10^{-4} f/m/mg would be expected.

Beam contamination due to neutrons [factor (5) above] was potentially the most serious source of background other than alpha noise. In photonuclear experiments, it is always difficult to establish conclusively that the number of neutron-induced fissions is very small compared to the number of photofissions. An estimate of the number of neutron-induced fissions produced by fast neutrons generated within the heavy-element target by (γ,fission) reactions can be made from: a) the geometry, b) known (n,fission) cross sections, and c) an assumed value for the total number of neutrons produced per photofission. On this basis, the number of (n,fission) events coming from this source was calculated to be negligible. Neutron-induced fissions arising from photo-neutrons generated in the target were also estimated to be unimportant. Since the fission yields produced were sufficiently low as to preclude their radiochemical separation and quantitative assay (see discussion of the peak-to-valley ratio determination for natural uranium), it was not possible to establish the number of neutron captures relative to the number of photofissions that had occurred in the target. A realistic approach to the problem involved attenuation experiments in which the absorption of the fission-producing radiation was measured by interposing various absorbing materials between the photon source and the fission chamber. U^{235} and U^{236} were the heavy-element samples employed. The former isotope has strong resonance neutron-capture cross sections in both the thermal and epithermal regions, while the latter isotope will fission only with fast neutrons (Mev energy range).[72]

The results of the absorption experiments are shown in Figure B-1 and Table B-1 of the Appendix. From Figure B-1 it is apparent that the attenuation of the fission-producing gamma radiation, and hence the fission rate, was similar to that for high-energy quanta. The linear absorption coefficient for lead, as derived from the slope of the appropriate curves, is in fair agreement with previous data.[35] The departure from linearity for U^{235} at 3.645-Mev proton energy, using lead as the absorber, is quite likely due to photoneutron emission in Pb^{207} (natural abundance 21%) whose neutron-binding energy is 6.734 Mev. In iron, whose isotopes all have neutron-binding energies exceeding that of the high-energy gamma quanta, this nonlinearity was not observed. The data presented in Table B-1 also re-enforce this idea. It will be seen that the fission plateau count per transmitted quanta, f_p/C, is essentially constant for the lead and iron absorption results (excepting the

U^{235} case previously noted). On this basis, it was concluded that neutron-induced fission from neutrons in the thermal, epithermal, and "fast" energy regions made no significant contribution to the observed fission count. Further, neglecting the background from this source probably introduced an uncertainty which was much smaller than the statistical errors.

D. Analysis of Data and Results

1. Absolute Gamma-Ray Yield Calculations

A gamma ray of energy 2 Mev or more may interact in two principal ways with a scintillation crystal. The broad distribution of Compton recoil electrons has a high-energy edge[103] at about E_γ-0.25 Mev, where E_γ is the gamma-ray energy. From the pair process, in general, one obtains peaks at E_γ, E_γ-0.51 Mev, and E_γ-1.02 Mev, as none, one, or both annihilation quanta escape the crystal. Because of the complexity of the pulse-height spectra produced in the scintillation detector and the relative insensitivity of the shapes of the full-energy peaks to scattered and other gamma radiation, one can generally use only full-energy peaks in determining the gamma ray yields. It should be noted that the use of a large crystal detector increases the re-absorption, not only of pair-annihilation radiation,[52] but also of bremsstrahlung.[31] At energies exceeding 15 Mev,[90] this latter factor places a serious limitation on the energy resolution attainable with a single-crystal spectrometer.

To relate the intensity of incident radiation to the area under the full-energy peaks, an empirical procedure due to Bell and coworkers[94] was employed. This procedure requires the evaluation of the photopeak efficiency for the geometrical arrangement of source and detector used. The peak efficiency, $\epsilon_p(E)$, is defined as the probability that a gamma ray of energy E impinging on the crystal will cause a pulse that will fall under the full-energy peak. An advantage of the method is that the efficiencies so defined are independent of variations in resolution and surrounding scatterers. Empirically, $\epsilon_p(E)$ was obtained from a measurement of $_p(E)$, the photofraction, and the calculated total efficiency, $\epsilon_t(E)$, of the crystal for a gamma ray of energy E. The photofraction is usually defined[52,93] as the ratio of the area under the full-energy peak of the pulse-height distribution, A(E), which is represented by a Gaussian curve to the area, A_t, under the entire pulse-height distribution. From this one obtains:

$$\epsilon_p(E) = {}_p(E) \cdot \epsilon_t(E) \qquad (1)$$

$${}_p(E) = A(E)/A_t \quad . \qquad (2)$$

The intensity of the incident radiation is then given by:

$$I_e(E) = G\gamma \cdot \epsilon_p(E) \cdot I\gamma(E) \qquad (3)$$

$$I\gamma(E) = \frac{I_e(E)}{G_\gamma \cdot \epsilon_p(E)} \quad , \qquad (3')$$

where I_e = counts under full-energy peak,

I_γ = 4π gamma-ray intensity,

G_γ = geometry of the gamma detector.

Calculations of $p(E)$, and hence of $\epsilon_p(E)$, have been reported[52,91] for radiation incident on the end face of cylindrical crystals from a point source. Because of the high probability for multiple collisions in the crystal, Monte Carlo calculations have been necessary to obtain $p(E)$ directly. Unfortunately, photofractions in the range 6 to 7 Mev for a 4-inch by 4-inch crystal are not available at this time, and the necessary calculations are prohibitively tedious, even with the aid of an automatic computer; hence, it was deemed desirable to determine $\epsilon_p(E)$ empirically.

In the experimental arrangement employed here, the incident beam irradiated a cylinder of small diameter on the axis of the spectrometer crystal. Since the crystal detector was both moderately well-collimated and sufficiently far removed from the source of irradiation, i.e., the fraction of the total solid angle subtended being 3.60×10^{-6}, the radiation was incident essentially perpendicularly on its end face, and the primary gamma-ray interactions were confined to the region of the crystal axis. This "good" geometry is represented by equation (13) of Appendix D, which was used to compute the total crystal efficiencies. To utilize this relationship, "narrow-beam" absorption coefficients are required. Based on a compilation[62] of attenuation coefficients of X rays and gamma rays for the elements sodium, iodine, and thallium, these coefficients were computed for NaI(Tl)-0.1%Tl. The calculated total intrinsic efficiencies are presented below.

TABLE III-2

$\epsilon_t(E)$ for Collimated Radiation Incident Perpendicularly on the Endface of a Cylindrical NaI(Tl) Crystal. Crystal Length = 4.0 Inches

Photon Energy (Mev)	Total Absorption Coefficient (cm^{-1})	$\epsilon_t(E)$
0.50	0.33085	0.9653
6.14	0.12750	0.726_2
6.91	0.12813	0.728_0
7.00	0.12827	0.728_3
7.12	0.12840	0.728_7
12.0	0.139	0.756_3

To obtain $_{p}(E)$ in the energy region of interest it was necessary to analyze the observed low and high-energy gamma spectra (Figures III-10 and III-11) into the constituent gamma rays. Since the 6.91 and 7.12-Mev gamma-ray photolines could not be resolved by the single scintillation detector employed, the photofraction, and hence the photopeak efficiency, was evaluated at 6.14 and 7.0 Mev. The spectrum analysis was performed under the assumption that the peak due to a single gamma ray (6.91 and 7.12-Mev unresolved peaks included) was Gaussian with tails symmetrical on both high and low-energy sides of the observed gamma ray, and a shape for the Compton electron distribution. The observed width of a full-energy peak can be ascribed to: a) photomultiplier statistics, b) difficulties in light collection, c) escape of electron-positron pairs from the crystal, d) bremsstrahlung produced in the crystal by electron-positron pairs, and e) peaking of the tail end of the Compton electron distribution.[103] The width arising from factors (a) and (b) should be small for higher energy gamma rays, while factor (c) probably does not lead to much asymmetry of the peak toward the low-energy edge until energies considerably above 7 Mev are reached.[31,92] Since the primary 6.14-Mev gamma ray produces a single symmetrical photopeak under more idealized experimental conditions,[32] it seems reasonable to ascribe on this basis the asymmetry generally observed on the low-energy side of the full-energy peak ($E_{\gamma} > 2$ Mev) to factors (d) and (e) above. The assumption as to a Gaussian shape for the unresolved peak at 7.0 Mev is not unreasonable in that the relative intensities of the 6.91 and 7.12-Mev lines are not very different.[33,132] The high-energy Compton edge was assumed to occur at $T_{max} = (h\nu_0)\frac{2\alpha_0}{1 + 2\alpha_0}$, where α_0 is the initial photon energy in units of mc^2, corresponding to a photon scattered by 180°. Beyond the peaked tail the distribution was further assumed to be uniform down to zero energy (Figures III-10 and III-11 and reference 103).

Since $\epsilon_{p}(E)$ and $_{p}(E)$ are insensitive to variations in the energy resolution, the full-width at half-maximum was arbitrarily taken as about 6% for the 6.14-Mev full-energy peak[14,137] and a somewhat lesser value for the 7.0-Mev peak.[14] These are probably minimum values, as the energy resolution reaches an optimum value[91] (about 4%) for the 6-Mev electrons in crystals of large dimensions. In the analysis of the gamma-ray pulse-height distributions, the separation of the response of the crystal to the 6.14 and 7.0-Mev gamma rays was achieved with the aid of thick target relative intensity ratios reported in the literature. These data are indicated below and in Figure III-2.

The values of R used in the spectrum analyses were R(1.380 Mev) = 0.48 and R(3.645 Mev) = 1.38. The analyzed distributions are shown in Figures III-10 and III-11. The indicated components add to give the resultant pulse-height distribution. How well the spectrum

decomposition approximated the gamma-intensity ratios is indicated by the area ratios $R(A_{7.0}/A_{6.14}) = 0.466$ and 1.55 for 1.380 and 3.645-Mev proton energies, respectively.

TABLE III-3

Thick Target Relative Gamma-Intensity Ratio vs. Proton Energy. $F^{19}(p,\alpha\gamma)O^{16}$ Reaction

Proton Energy (Mev)	$R = I_{(6.91 + 7.12)}/I_{6.14}$	Reference
0.45	0.043 (±.013)*	137
0.70	0.17 (±.02)	137
1.15	0.38 (±.03)	137
2.6	~1.0	59
3.7	1.4 (±.07)	14
5.0	1.7 ±0.4	111

*Estimated errors in parentheses

To obtain the photofractions, $p(E)$, it was necessary to obtain the peak-to-total areas for a given primary gamma ray. The pertinent areas are tabulated below.

TABLE III-4

Relative Areas of the Components of the Gamma-Ray Pulse-Height Distributions

Component	1.380-Mev Proton Beam Energy		3.645-Mev Proton Beam Energy	
	6.14 Mev γ	(6.91 + 7.12) Mev γ	6.14 Mev γ	(6.91 + 7.12) Mev γ
Total Absorption Line	0.489	0.296[a]	0.384	0.748
Escape Peaks				
a. 1st				0.228
b. 2nd		0.043[b]		0.016[a]
c. Sum	0.230		0.276	0.244
Compton Electron Distribution	0.671	0.308	0.334	0.548
Total Response	1.390	0.647	0.994	1.540
Integral Counting Area	1.437		1.098	
Spectrum Factor[c], F(E)	0.340		0.682	

[a]Includes area due to 1st escape peaks.

[b]Area due to 2nd escape peak corresponding to the 7.12-Mev gamma line not included.

[c]Most intense gamma line.

The calculated photofractions are tabulated below.

TABLE III-5

Photofractions $p(E)$

Proton Beam Energy (Mev)	Photon Energy (Mev)		
	6.14	7.0	Average
1.380	0.352	0.458	0.405 ± 0.53
3.645	0.387	0.486	0.437 ± 0.50
			0.422 ± .036

The values of $p(E)$ derived from a given spectrum were averaged, since it has been shown by Monte Carlo calculations[91] that the photofraction for large crystals goes through a minimum range of values between 5 and 10 Mev. Further, $p(E)$ is essentially constant in the interval 6 to 8 Mev. The best value taken for $p(E)$ in the energy range applicable here is 0.422. This value may be compared with the value estimated from the data of Berger and Doggett[15] of $p(4.45\ \text{Mev}) = 0.42 \pm .01$. For reasons argued above, the agreement was good and well within the standard deviation of the experimental result. From values of $\epsilon_t(E)$ tabulated in Table III-2 and $p(E)$ taken equal to 0.422, the calculated values of the photopeak efficiencies were $\epsilon_p(6.14) = 0.306_5$ and $\epsilon_p(7.0) = 0.307_4$.

Since the gamma photon monitor counted all energy losses in the crystal detector above a specified bias level, it was necessary to relate the response area so determined to that under a full-energy peak. This is expressed in terms of a spectrum factor (Table III-4), $F(E)$, for the most intense gamma-ray line in both the low and high-energy gamma spectra, i.e., the fraction of the total area represented by the full-energy peak. Hence the net observed integral gamma count, C, is related to the counts under the full-energy peak by the relation

$$I_e(E) = F(E) \cdot C \quad . \tag{4}$$

From a knowledge of the geometry of the fissionable sample in the fission chamber with respect to the photon source, G_f, the gamma intensity, $I_0(E)$, experienced by the sample can be expressed by

$$I_0(E) = G_f \cdot I\gamma(E) \quad . \tag{5}$$

Combining equations (3'), (4) and (5) yields

$$I_0(E) = \frac{G \cdot F(E) \cdot C}{\epsilon_p(E)} \tag{6}$$

where $G = G_f/G_\gamma = 1.2_8 \times 10^4$. Using equation (6) plus the thick target gamma-intensity ratio appropriate to a given proton beam energy, the intensities of the 6.14-Mev and the "7.0"-Mev gamma rays incident on the heavy-element samples were calculated. The calculated absolute intensities are tabulated in Appendix A (Table A-1).

A conservative estimate of the total thick target photon yields, normalized with respect to the number of protons incident on the fluorine target, was made using the data of the Th^{232} runs (Appendix A). The calculated yield, Y(1.380), for 1.380-Mev protons on F^{19} was 1.3×10^6 quanta/proton for 4π steradians at zero degrees and may be compared with the reported value[33] of 0.82×10^{-6} quanta/proton for 4π steradians at 90 degrees. The calculated value was based on an assumed average proton current of 14 μa as the integrated charge collected was not recorded in these experiments. Assuming a nominal proton current of 1.5 μa, the yield obtained with 3.645-Mev protons, Y(3.645), was estimated to be 7.7×10^5 quanta/proton equivalent to 0.73×10^9 quanta/sec for 4π steradians at zero degrees. The latter value is in accord, at least as to the order of magnitude, with the result of Swann and Metzger[131] for 3.0-Mev protons. The relative total yield ratio, Y(3.645)/Y(1.380), obtained from the values above was about 61, which is in fair agreement with a similar result of about 33 extrapolated from the early data of Haxby, et al.[66]

2. Fission Counting Yield Calculations

a. Zero Bias Extrapolation of the Integral Fission Pulse-Height Distributions

As indicated previously, the use of thick samples made for abbreviated plateaus in the fission pulse-height distributions. For the samples of high specific alpha activity, an extrapolation along this plateau involved some uncertainty and was indeed impossible for U^{233} and U^{234}. For this reason an empirical procedure was evolved for relating the extrapolated plateau fission count, f_p, with the value f_0 derived by extrapolating along the linear portion of the pulse-height distribution beyond the plateau. As discussed earlier, this latter region was perfectly linear over a sizeable energy interval and was well-defined for all the heavy-element samples investigated. It follows, then, that the slope in this interval is directly proportional to the fissionability of the sample. The method employed involved determining a best value for the ratio (R_p) equal to f_0/f_p. This value was established by obtaining the extrapolated fission counts for samples for which f_p could be realized. In addition, a value was determined for a spontaneous fission sample containing tracer $Cf^{250,252}$ in 1 mg/cm^2 $(U^{238})_3O_8$ for which good statistics in the counting data could be readily obtained (Figure III-12). Typical pulse-height distributions are shown in Figures III-8 and III-9 for Th^{232}. The average values of R_p so evaluated are tabulated in

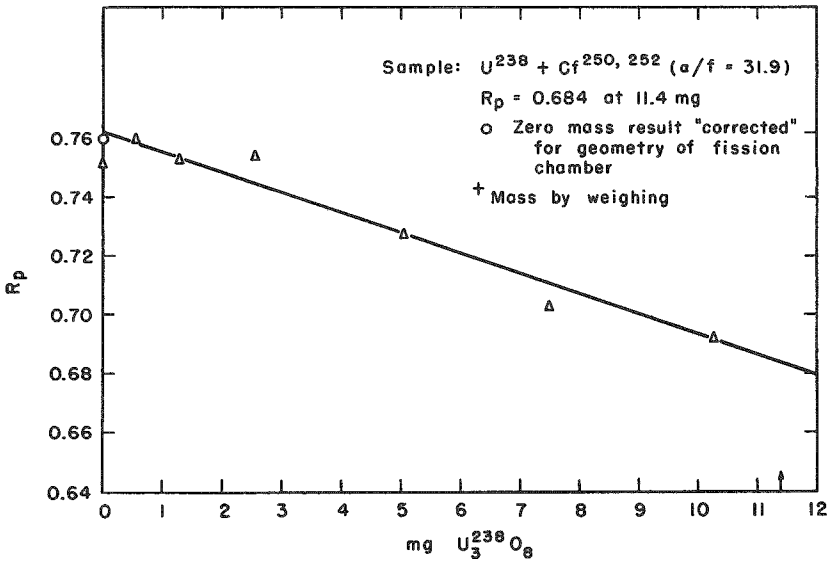

FIGURE III-12

R_p vs. Mass U_3O_8.

Table III-6. The best value for R_p taken was a weighted average[12] of the grand average ($0.710 \pm 0.05_3$) derived from the photofission runs and the $Cf^{250,252}$ result yielding a value, R_p, equal to 0.684. This value multiplied by f_0 derived for each run was taken as the extrapolated plateau fission count.

TABLE III-6

Average Values of R_p

Nuclide	Proton Energy (Mev)	Average R_p (Stand. Dev. Indicated)	Gross Average R_p
Th^{232}	1.380	$0.73_8 \pm 0.02_2$	
U^{238}		$0.67_5 \pm 0.01_4$	
U^{235}		$0.70_6 \pm 0.03_1$	
U^{236}		0.695 ± 0.029	
Np^{237}		0.710 ± 0.011	
All Samples			$0.70_5 \pm 0.05_0$
Th^{232}	3.645	0.726 ± 0.008	
U^{238}		0.707 ± 0.011	
U^{235}		0.706 ± 0.004	
U^{236}		0.713 ± 0.007	
Np^{237}		0.7249 ± 0.0048	
All Samples			0.715 ± 0.016
$Cf^{250,252}$ in U_3O_8		0.684 ± 0.012	

b. Self-Absorption Correction

Since the ranges of fission fragments are so short. i.e., maximum range[118] of gross fission recoils in U_3O_8 being approximately 10.0 mg/cm^2, self-absorption corrections to the fission counting of thick samples are important. This correction was obtained by plotting the extrapolated plateau fission rate per unit mass of sample, $(f/m)_p$/mg oxide, versus mass of sample (Figure III-13) for spontaneous fission sources containing tracer $Cf^{250,252}$ in $(U^{238})_3O_8$. The ratio of $(f/m)_p$/mg oxide, corresponding to the mass thickness of the photofission sample, to the extrapolated value obtained for zero sample mass, at which sample self-absorption vanishes, is then a direct measure of the sample self-absorption. From Figure III-13, it may be seen that the detection factor, ϵ, for a total sample mass of 11.40 mg (i.e., 1 mg/cm^2/mass thickness) is 0.908. A similar determination of this factor using neutron-induced fission of U^{235} with a Ra-Be source yielded a value for ϵ equal to 0.854. The average of these two results is $\epsilon = 0.881 \pm 0.027$. Since the mass spread of the samples (11.22 to 12.01 mg) caused a negligible dispersion in ϵ, the detection factor was assumed constant for all samples and equal to the value of 0.881. It may be noted here that the method employed in determining ϵ is, in principle, self-correcting for any angular asymmetry in the fission-fragment distribution. Unfortunately, it was not convenient to obtain ϵ from photofission measurements. For those two cases where a strong anisotropy[145] is known to exist at the photon excitation energies employed in this investigation, i.e., Th^{232} and U^{238}, ϵ may actually be somewhat different from the value 0.881. In this instance, the uncertainty in the detection factor is estimated to be very small in comparison with errors arising from other sources and hence it was neglected.

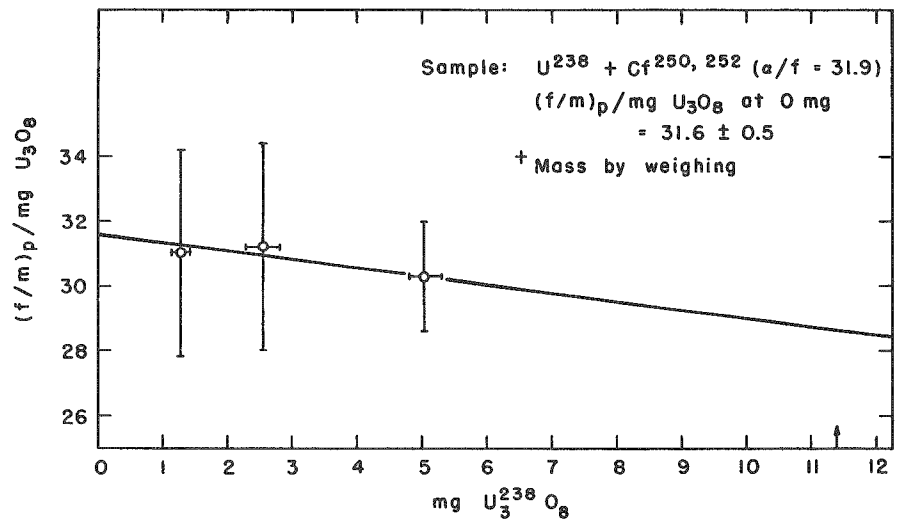

FIGURE III-13
Extrapolated Fission Rate Per Unit Mass U_3O_8 vs. Mass U_3O_8.

c. Ionization Chamber Geometry of Sample

The geometry of the chamber was evaluated by counting a weightless spontaneous fission source ($Cf^{250,252}$) in both the fission chamber and a larger pulse ionization chamber of a 2π geometry. The cut-off point for alpha noise was established quite accurately in the latter chamber and a bias plateau was determined. The sample was identical in every respect with the heavier photofission samples. From the extrapolated plateau fission rate at zero bias established in both chambers, it was estimated that the effective geometry was $(100 \pm < 1)$ % of 2π steradians.

d. Fission Counting Yields

From considerations already developed in this section, the zero mass fission counts, f, were obtained using the relations

$$f_p = \bar{R}_p f_0 \tag{7}$$

$$f = f_p/\epsilon \tag{8}$$

$$f = (R_p)_0 \cdot f_0 \quad , \tag{8'}$$

where $(R_p)_0 = \bar{R}_p/\epsilon = 0.776 \pm 0.038$. This value corresponds to a self-absorption correction at zero bias to $f_\circ$, as can be seen from Figure III-12. The fission counting yields as well as yields per total fission-producing quanta are tabulated in Table A-2 (Appendix A).

3. Photofission Cross-Sectional Calculations

Under the reasonable assumption of negligible beam attenuation in the sample, the cross section for photofission is defined by the equation

$$f = \bar{n} \cdot \sigma_E \cdot I_0(E) \quad , \tag{9}$$

where f is the number of fissions occurring in the sample, $\bar{n} \cong n_0$ is the effective number of target nuclei per cm^2 of target, σ_E is the $(\gamma, \text{fission})$ cross section for nuclear excitation energy E expressed in cm^2, and $I_\circ(E)$ is the number of quanta of energy E incident on the target. Absolute cross sections as a function of energy were obtained by solving two simultaneous equations of the form:

$$f_{1.380} = \bar{n}\,\sigma_{(6.14)} \cdot I_0\,(6.14) + \bar{n}\,\sigma_{(7.0)} \cdot I_0(7.0) \tag{10}$$

$$f_{3.645} = \bar{n}\,\sigma_{(6.14)} \cdot I_0'\,(6.14) + \bar{n}\,\sigma_{(7.0)} \cdot I_0'(7.0) \quad , \tag{10a}$$

where the numbers refer to energies. Equation (10) refers to the low-energy gamma-ray spectrum while (10a) refers to the high-energy spectrum. The fission counting yields and absolute gamma-ray intensities used for the calculations are tabulated in Appendix A. The data of all runs for a given proton beam energy and sample were averaged together to obtain a set of cross sections.

The effective number of target nuclei per cm^2 (see Appendix E), $\bar{n}$, was obtained from the relation

$$\bar{n} \cong n_0 = (\text{elemental mass - mg}) \cdot \frac{6.025 \times 10^{20}}{11._{40} M} , \qquad (11)$$

where M is the isotopic mass (physical atomic weight scale). To arrive at the elemental masses, the heavy-element oxide masses (as determined by weighing), the mass spectrographic analyses (Table III-8), and calculated gravimetric factors of the form $nX/(X_nO_m)$, where X = heavy element and O = oxygen, were used. The calculated atom thicknesses are tabulated below.

TABLE III-7

Heavy-Element Atom Thicknesses

Sample	Isotopes Present	Elemental Mass (mg)	$\bar{n}$ (atoms/cm^2)
Th^{232}		10.60	$2.5_{40} \times 10^{18}$
U^{235}		9.54	$2.2_{56} \times 10^{18}$
U^{238}		10.26	$2.3_{96} \times 10^{18}$
Np^{237}		9.94	$2.3_{31} \times 10^{18}$
U^{234}	U^{234}	9.060	$2.1_{52} \times 10^{18}$
	U^{235}	0.472	$1.1_{2} \times 10^{17}$
	U^{238}	0.165	$3.8_{5} \times 10^{16}$
U^{233}	U^{233}	9.552	$2.2_{78} \times 10^{18}$
	U^{234}	0.0124	$2.9_{5} \times 10^{15}$
	U^{235}	0.000990	$2.3_{4} \times 10^{14}$
	U^{238}	0.149	$3.4_{8} \times 10^{16}$
U^{236}	U^{234}	0.007	$1._{7} \times 10^{15}$
	U^{235}	0.438	$1.0_{4} \times 10^{17}$
	U^{236}	9.004	$2.1_{20} \times 10^{18}$
	U^{238}	0.052	1.2×10^{16}

As shown in Table III-8 following, three samples deviated considerably from isotopic purity.

TABLE III-8

Heavy-Element Samples

Sample	Isotopes Present	Mass%
Th^{232}	232	100
U^{233}	233	98.33
	234	0.127
	235	0.0102
	238	1.53
U^{234}	234	93.44
	235	4.87
	236	-
	238	1.69
U^{235}	234	0.022
	235	99.94
	238	0.038
U^{236}	234	0.07
	235	4.62
	236	94.77
	238	0.54
U^{238} (depleted)*	238	99.96
Np^{237}	237	100

*U^{238}/U^{235} = 2245.

Before the (γ,fission) cross sections for U^{233}, U^{234}, and U^{236} could be calculated, the fission counting yields had to be corrected for the contribution due to other uranium isotopes present. This was accomplished by assuming (with negligible error) that the cross sections, $\sigma_{6.14}$ and $\sigma_{7.0}$, calculated for U^{235} and U^{238} were due only to the isotope in question. Using these cross sections, data pertinent to the U^{234} sample, and equations (10) and (10a), the corrections for U^{234} fission counting yields were obtained. Repeating the same procedure, this time using the cross sections $\sigma_{6.14}$ and $\sigma_{7.0}$ for U^{234}, U^{235}, and U^{238}, the corrections to the fission counting yields for U^{233} and U^{236} were obtained. These corrections to the gross observed fission count at 1.380 and 3.645-Mev proton beam energies, respectively, were: U^{233}, 0.98% and 0.72%; U^{234}, 6.8% and 4.8%; U^{236}, 3.1% and 5.1%. The absolute photofission cross sections derived are listed in Table III-9.

To ascertain how well the computed cross sections compare with previous measurements,[64,66] average cross sections were computed using equation (9). Since I_0 was taken as the total gamma flux incident on the target, $I_0(6.14 + 7.0)$, the cross sections obtained in this manner

TABLE III-9

Photofission Cross Sections

Nuclide	$\sigma_{6.14}(\gamma,f)$ $(10^{-27}\ cm^2)$	$\sigma_{7.0}(\gamma,f)$ $(10^{-27}\ cm^2)$
$_{90}Th^{232}$	$6.1_3 \pm 1.0_6$*	$1\ .4_2 \pm 1.5_5$*
$_{92}U^{233}$	$8._5 \pm 3._9$	$1_{8.9} \pm 7._4$
U^{234}	$3._0 \pm 3._7$	$1_{9.9} \pm 7._0$
U^{235}	$8._7 \pm 2._8$	$1_{1.6} \pm 5._0$
U^{236}	$23._8 \pm 3.7$	$0\ _{.34} \pm 4.89$
U^{238}	$8._6 \pm 1._6$	$3\ _{.5} \pm 2._5$
$_{93}Np^{237}$	$1_{9.3} \pm 3._9$	$9\ _{.7} \pm 6._2$

*Probable errors indicated.

directly reflect the thick target gamma-intensity ratio, $R = I(6.91 + 7.12)/I(6.14)$, corresponding to the proton beam energy employed. These cross sections then are weighted with the relative intensities of the O^{16} gamma-ray lines. The average cross section values are tabulated in Table III-10.

TABLE III-10

Weighted Average Photofission Cross Sections

R	0.48	1.38	0.12	0.91
Nuclide	$\sigma_{av}(\gamma,f)^a$ $(E_p = 1.380\ Mev)$	$\sigma_{av}(\gamma,f)^a$ $(E_p = 3.645\ Mev)$	$\sigma_{av}(\gamma,f)^b$ $(E_p = 0.580\ Mev)$	$\sigma_{av}(\gamma,f)^c$ $(\bar{E}_p = 2.5\ Mev)$
$_{90}Th^{232}$	$4.6_0 \pm 0.46$*mb	$3.4_0 \pm 0.32$*mb	4.4 ± 1.5 mb	1.7 ± 0.5 mb
$_{92}U^{233}$	$11._8 \pm 1.1$	$14._5 \pm 1.5$		
U^{234}	$8.5_2 \pm 0.88$	$12._8 \pm 1.3$		
U^{235}	$9.6_3 \pm 0.82$	$10._4 \pm 1.1$		
U^{236}	$16._3 \pm 1.6$	$10._2 \pm 1.0$		
U^{238}	$6.9_1 \pm 0.68$	$5.6_1 \pm 0.55$	8.7 ± 3.0**	3.5 ± 1.0**
$_{93}Np^{237}$	$16._2 \pm 1.6$	$13._8 \pm 1.4$		

[a]Results of this investigation.

[b]W. J. Hartley, Ph. D. Thesis, University of Pennsylvania, 1955 (unpublished). $\sigma(\gamma,f)$ obtained from measured neutron yields.

[c]Haxby, Shoupp, Stephens & Wells, Phys. Rev. 59, 57 (1941).

*Probable error indicated.

**Naturally occurring isotopes.

4. Peak-to-Valley Ratio for Natural Uranium

On the assumption that observed fission-yield curves are composites of two idealized curves,[134] one for asymmetric fission and the other for symmetric fission, an investigation of the shape of the excitation function connected with each fission mode is of some interest. For a given energy, a useful measure of the relative excitation functions is the peak-to-valley yield ratio of the yield-mass curve. This ratio was evaluated for U^{238} at about 7.0 Mev by irradiating a two-inch diameter foil (7.46 grams) of natural uranium with a total gamma-ray flux of about 10^{12}, obtained using the high-energy spectrum.

Radiochemical analyses[113] were performed for silver and molybdenum. The procedures followed, with slight modifications, were the same as those employed on the Plutonium Project.[37] The activities isolated were 7.5-day Ag^{111} (sufficient time having been allowed for the shorter lived Ag^{112} and Ag^{113} activities to decay away) and 67-hour Mo^{99}, yielding initial counting rates of 0.45 c/m (an upper limit) and 18 c/m, respectively, From these results, a lower limit on the peak-to-valley ratio (fission yield of Mo/fission yield of Ag) of >145 is indicated. This value is in reasonably good agreement with the limit $\geq$ 300 set by Schmitt and Sugarman[117] from betatron studies at 7 Mev. This result therefore substantiates the idea that asymmetric fission is the predominant mode for low nuclear excitation energies[86,116,117] near the fission "threshold."

E. Discussion of Errors

The errors ascribed to this experiment are of two categories[12], namely, random errors and systematic errors. The types of errors in each category and an estimate of their magnitude are indicated below.

1. Determinate Random Errors

a. Standard deviations due to couting statistics: fission counting, ±1.2 to ± 5.4%; gamma counting, less than ±0.1%.

b. Bias level setting for integral counting: <±0.1%.

2. Systematic Errors

a. Determination of sample mass: ±1.3%.

b. Mass thickness uniformity of fissionable samples (enters as a second order error in the sample spread correction): ±3.4%.

c. Correction for sample self-absorption of fission fragments: ±3.1%.

d. Extrapolation of fission counting data to zero pulse-height bias, i.e., standard deviation of the intercept[147], ±4.5%.

e. Physical geometry of the fission chamber and gamm-ray monitor with respect to the gamma-ray source: G_f ±7.6%; G ±8.4%.

f. Spectrum analysis: distribution with 1.380 Mev protons, ±11.1%; distribution with 3.645 Mev protons, ±14.4%.

The accuracies of the cross-sectional calculations (Tables III-9 and III-10) were estimated by compounding the systematic errors with the random errors, as they are independent of one another.[12] The usual technique for doing this is by taking the square root of the sum of the squares.

IV. DISCUSSION AND THEORETICAL INTERPRETATION OF RESULTS

A. Introduction

The results of the previous section indicate that excitation curves for photofission near threshold are, in general, non-monotonic functions of energy. In the energy interval 6.14 to 7.0 Mev, the occurrence of structure seems strongly dependent on the initial type of nucleus. Because of the relatively large errors in the absolute cross-sectional values, the results, at worst, represent order of magnitude estimates of the true photofission cross sections. These cross sections, nevertheless, conclusively demonstrate the existence of structure at low nuclear excitation energies for several heavy nuclides.

A measure of the reliability of the data reported here is seen by comparing the weighted average cross sections with the earlier results shown in Table III-10. It is evident that the results of this investigation are in excellent agreement with values previously reported by Hartley(64,65) as based on measurements of neutron yields. Since the absolute (γ,fission) cross sections for Th^{232} and U^{238} increase with decreasing excitation energy (Table III-9), and the relative gamma-ray intensity ratio I(6.91 + 7.12)/ I(6.14) decreases linearly with decreasing proton energy (Figure III-2), the average cross sections of Hartley should be somewhat larger that the results presented for 1.380-Mev proton energy. Within the experimental errors, this expectation is fulfilled. The agreement with the measurements of Haxby, et al.,(66) is not nearly as good, which probably reflects the poorer sensitivity of these earlier experiments.

The question of nuclear excitation by gamma photons of energies exceeding 7.0 Mev was the cause of some concern in connection with the structure observed in the excitation curves. For the proton bombarding energies employed, only the 12-Mev capture radiation arising from the reaction $F^{19}(p,\gamma)Ne^{20}$ might conceivably contribute to the (γ,fission) yield. From the gamma pulse-height distributions recorded in these experiments, the following upper limits were set on the relative gamma-ray intensity ratio $I_{12}/I_{6.14}$: <0.04% and <1%, for 1.380 and 3.645-Mev protons, respectively. The value at 1.380 Mev is in fair agreement with the data of Farney, et al.,(51) for the intensity ratio $I_{12}/I(6.14 + 7.0)$ equal to (0.08 ± 0.01%). At the higher proton energy, Bent, et al.,(14) reported seeing no lines between 7.5 and 11.0 Mev with an intensity >10% of the 7.0 Mev peak. From these data, equations (10) and (10a), and Tables III-9 and III-10 of the preceding section, it is clear that the giant resonance cross section, σ_{12}, calculated, assuming all fissions are due to the 12-Mev radiation, are in disagreement with the actual values. The peak giant resonance (γ,fission) cross sections for the nuclides examined here are estimated to be in the range 50 to 300 mb.(9) Further, the intensity of the 12-Mev capture radiation should increase with increasing proton energy and hence so should

the weighted average (γ,fission) cross sections of Table III-10. Again no appreciable contribution from this source was apparent. From these considerations, it is concluded that capture radiation makes little contribution to the experimental cross sections and further is not connected with the structure observed.

The general behavior of the excitation functions for photofission is illustrated in Figures IV-1 and IV-2 for the energy interval from the (γ, fission) "threshold" to 7.0 Mev. In addition to the experimental points at 6.14 and 7.0 Mev, the thresholds for fission and neutron emission are indicated.

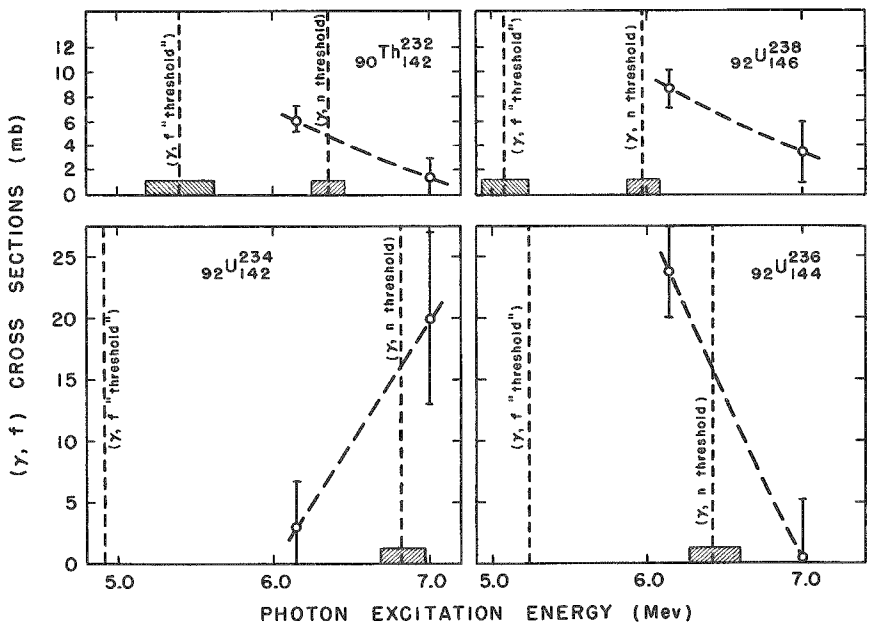

FIGURE IV-1

The Photofission Cross Sections of the Even-Even Nuclides.

The fission "thresholds" are experimental values,(30,90) with the exception of the values for U^{234} and U^{236}. These latter values were calculated from the empirical (γ, fission) threshold equation due to Swiatecki.(133) In this formulation, the height of the fission barrier is referred to the ground state mass predicted by the liquid drop model. Except for Th^{232} and U^{238} (see references 75 and 76), the (γ, neutron) thresholds, i.e., binding energy of the last neutron of the compound nuclear system, were calculated from the mass tables of Huizenga.(73) The (γ,neutron) thresholds are then in effect thermodynamic thresholds. The predicted and experimental thresholds for photofission and photoneutron emission are tabulated in Table IV-1. Though it is conceivable that the two experimental points may straddle a higher cross-sectional value, for want of more complete data and for reasons of simplicity the excitation curve is assumed to vary monotonically between

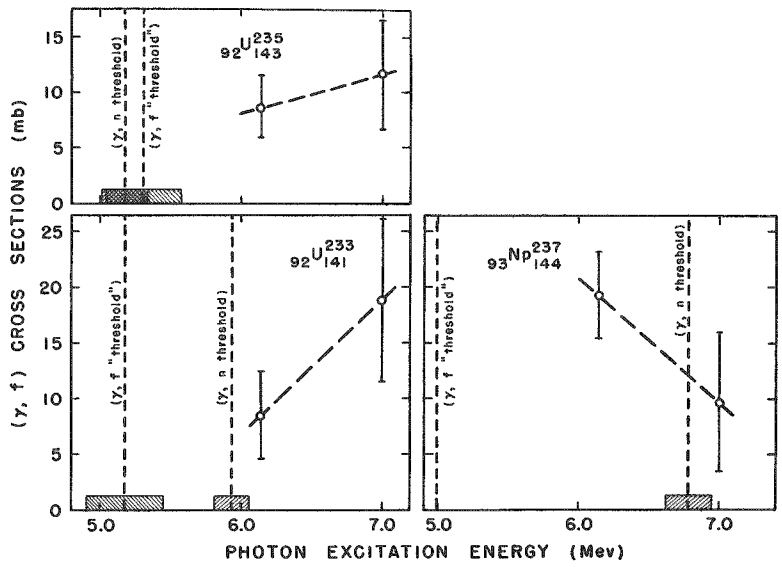

FIGURE IV-2

The Photofission Cross Sections of the Odd-A Nuclides.

TABLE IV-1

Predicted and Experimental Thresholds for Photofission and Photoneutron Emission

Compound Nucleus	Predicted (γ,f)[a]-Mev	Experimental (γ,f)[b]-Mev	"Observed" (γ,f)[c]-Mev	Neutron Binding Energy[d] (Mev)	Experimental (γ,n)-Mev
$_{90}Th^{232}$	5.63	5.40 ± 0.22	5.45	6.33 ± 0.13	6.35 ± 0.10[e]
$_{92}U^{233}$	5.47	5.18 ± 0.27	4.99	5.94 ± 0.12	
U^{234}	(4.91)			6.81 ± 0.14	
U^{235}	5.49	5.31 ± 0.27	(5.53)	5.18 ± 0.16	
U^{236}	(5.24)			6.42 ± 0.16	
U^{238}	5.03	5.08 ± 0.15	5.30	6.07 ± 0.17	5.97 ± 0.10[f]
$_{93}Np^{237}$	(5.18)		4.99	6.78 ± 0.16	

[a] W. J. Swiatecki, Phys. Rev. 101, 97 (1956).
[b] Koch, McElhinney, and Gasteiger, Phys. Rev. 77, 329 (1950).
[c] A. G. W. Cameron, AECL No. 329, July 1956, p. 189
[d] J. R. Huizenga, Physica 21, 410 (1955).
[e] Magnusson, Huizenga, Fields, Studier, and Duffield, Phys. Rev. 84, 166 (1951).
[f] Huizenga, Magnusson, Fields, Studier, and Duffield, Phys. Rev. 82, 561 (1951).

the experimental points. In the subsequent analysis of the results of this investigation, the behavior of the observed (γ,fission) cross sections as a function of energy will be interpreted in terms of the photonuclear capture cross section, $\sigma_c(\gamma)$, and the relative probability for photofission, G_f. Earlier considerations bearing on these two factors were discussed in section II-B (see equation 2').

B. Photonuclear Absorption Cross Section

From the discussion developed in section II (see equation 3'), it follows that the (γ,fission) cross section at 6.14 Mev (except for U^{235}) closely approximates the total photon absorption or capture cross section. It is evident from Figures IV-1 and IV-2 that the capture cross section is, in general, not independent of mass number. Further, if one identifies the thermodynamic (γ,neutron) threshold in U^{234} with the effective threshold for single neutron emission, it is clear that neutron competition with fission cannot be the explanation for the presence of the bump in the excitation curves for Th^{232}, U^{236}, U^{238}, and possibly Np^{237}. Comparing Figures IV-1, IV-2, and II-2 for Th^{232}, U^{235}, and U^{238}, a correspondence between the occurrence or non-occurrence of fission angular anisotropy and a bump in the excitation curve is apparent. Barring neutron competition, the available facts would seem to argue for structure in the total photon absorption cross-section[16] curve around 6 Mev and hence resonance absorption by nuclear levels of the parent nucleus. It is now well-established that, for energies exceeding the (γ,neutron) threshold, the branching probability for photofission is roughly constant over a wide energy range (8 to 22 Mev).[45,74,95] This means that structure in the (γ,fission) excitation curve in this energy region, i.e., the giant resonance, is due essentially to structure in the photon capture cross section. Such a strong energy dependence is apparently unique to the photonuclear excitation process.[16]

On the basis of available evidence a possible mechanism of photoexcitation suggested is that of electric quadrupole absorption. Taking into account the shape possessed by spheroidal nuclei,[63,119] such a mechanism seems quite plausible. The idea of the predominance of electric quadrupole transitions at low energies is discussed in reference 18. The most important evidence to date to support this picture is the Russian angular fission-fragment distribution experiments[11,96] at 9.4 Mev, which indicate (with some uncertainty) that electric quadrupole absorption is at least as important as electric dipole absorption at this energy. Moreover, the indications are that quadrupole absorption is increasing with decreasing energy (energy interval 12 to 9.4 Mev). These results would seem to indicate the necessity for a re-evaluation of the earlier results of Winhold and Halpern[8] who assumed a distribution due only to electric dipole absorption. To explain the bumps in the excitation curves at or around 6 Mev in terms of quadrupole excitation would require that quadrupole absorption

win out strongly over dipole absorption. Such a proposal has been suggested(116) to account for the increase in the probability for symmetric fission in U^{238} from 8 Mev down to 6 Mev and the subsequent decrease below 6 Mev.

From Figure IV-2 it appears that the excitation curves for the odd-A uranium isotopes vary monotonically with energy. Within the limits set by the indicated experimental error, the same statement might be made provisionally for Np^{237}. The fact that the odd-A nuclides differ from the even-even nuclides in this respect (excepting U^{234}) is not too surprising, since in the former cases either a neutron or proton spin is unpaired. If the picture of resonance photon absorption at about 6 Mev via electric quadrupole excitation is accepted, it might not be unreasonable to look for a mass number dependence in the location of the peak (γ,fission) cross section for the even-even nuclides to explain the absence of the bump for U^{234}. According to this picture, at 6.14 Mev the excitation energy of the maximum (γ,fission) cross section will have been exceeded for U^{234}, just reached in the case of U^{236}, and just passed for U^{238}. Since the compound nucleus can exist only for sharply defined energy levels, a large formation cross section, $\sigma_c(\gamma)$, for U^{236} necessarily indicates a correspondence between the excitation energy of the incident photon and one of the levels of the compound system.

C. Relative Probability for Photofission

The gross behavior of the (γ,fission) cross section in the region 6.14 to 7.0 Mev might find an alternative explanation in terms of the branching probability for photofission, $G_f = \overline{\Gamma}_f/(\overline{\Gamma}_f + \overline{\Gamma}_n)$, since the binding energy of the last neutron was exceeded in all cases at 7.0 Mev. To make this analysis, it is assumed that the photon absorption cross section, $\sigma_c(\gamma)$, is varying monotonically with energy. From equation (2) of section II-B, it follows that any structure in the photofission excitation curve could be explained by the occurrence of a sharp discontinuity in the branching probability, G_f. The energy behavior of the average fission width, $\overline{\Gamma}_f(E)$, close to "threshold"(106) is expected to be non-monotonic with some degree of smoothing due to barrier penetration because levels with the same angular momentum should be far apart in this energy region. Such behavior should influence the (γ,fission) cross section, $\sigma_{\gamma,f}(E)$, in like manner. As the excitation energy is increased, this non-monotonic behavior becomes more or less attenuated due to increasing level density and, when the excitation energy is of the order of several Mev above "threshold," the curve is expected to be essentially smooth. However, $\sigma_{\gamma,f}(E)$ might still fall off sharply even with a monotonic dependence of $\overline{\Gamma}_f(E)$ on energy because of the fact that the average total width, $\overline{\Gamma}$, increases sharply at an energy equal to that for (γ,neutron) emission. Thus a discontinuity in G_f could arise only from the competition of neutron emission with fission.

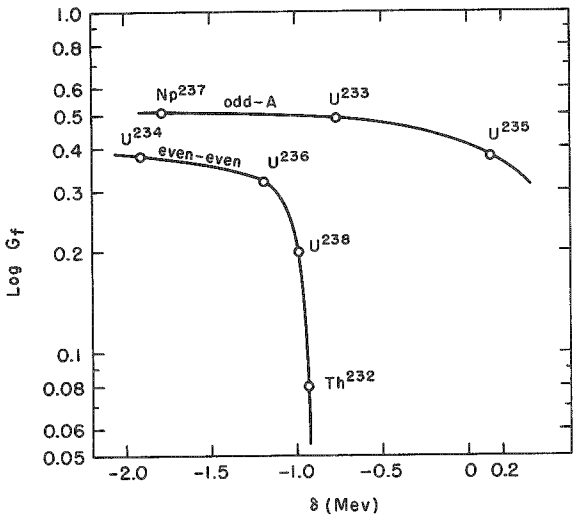

FIGURE IV-3

Relative Probability for Photofission from 8 to 12 Mev vs. Characteristic Threshold Energy Difference δ.

The behavior of the relative probability for photofission G_f, from 8 to 12 Mev, is illustrated in Figure IV-3 for the nuclides investigated. To arrive at the correlation indicated, the data of Huizenga(74) were plotted versus the parameter δ representing a characteristic threshold energy difference. Here δ is taken as the difference between the activation energy for fission, E_a, and the binding energy of the last neutron, $E_b(n)$, of the compound nuclear system. Explicit theoretical expressions have been obtained by Fujimoto and Yamaguchi,(57) which indicate an exponential dependence of Γ_f and Γ_n on δ. Applying statistical arguments with the assumption that level densities in all fissionable nuclei are the same, Jackson(78) has shown further that G_f should be a universal function of the δ. With due regard to the even-odd effect, such a quantitative correlation seems to hold quite well. It will be noted from Figure IV-3 that, with increasing Z^2/A, the even-even nuclides appear to be asymptotically approaching the essentially constant value of $G_f \cong 0.5$ attained by the odd-A nuclides. In this respect, G_f for U^{234} is more nearly like the odd-A values than for the other even-even nuclides, indicating that in this case neutron emission does not compete as successfully with fission one Mev or more above the (γ,neutron) threshold. Qualitatively the parameter δ can be interpreted as an indicator of the level densities existing in the compound nucleus at excitation energies equal to or exceeding the (γ, neutron) threshold. At these energies an exponential level density dependence governs the level widths,(18) $\overline{\Gamma}_f$ and $\overline{\Gamma}_n$, and hence the fission-to-total width ratio G_f.

It is fair to point out that the branching probability data(74) used in Figure IV-3 were computed under the assumption that the photon absorption cross sections were equal, i.e., independent of mass number. As can be seen from the 6.14-Mev cross sections, this is probably not a perfectly valid assumption at higher energies. As observed earlier, the odd-A uranium isotopes appear to show monotonically increasing (γ,fission) cross sections with energy. Such a smooth energy dependence of the cross sections is in keeping with expectation, typical of closely spaced and/or overlapping levels at the saddle point. Further, since the experimental points are well above the (γ,neutron) thresholds, it is not unreasonable to

expect the fission cross sections to increase smoothly with energy. For the other cases, the onset of neutron emission might serve to explain , for all but the U^{234} result, the drop in the (γ,fission) cross section once the (γ,neutron) threshold had been exceeded. Neutron competition might conceivably still be the answer in U^{234}, if account is taken of the uncertainty in the (γ, neutron) threshold and the relative probability for photofission. As indicated in Table IV-1, the actual thermodynamic threshold may be as high as 6.95 Mev, making neutron emission just as feasible energetically at 7.0 Mev. As noted earlier (Figure IV-3), neutron competition with fission is less effective in U^{234} than in the other even-even uranium isotopes, and close to the (γ,neutron) threshold the relative probability for photofission may not change appreciably. The available evidence on the energy dependence of $\overline{\Gamma}_n$, and hence of G_f, near the threshold for neutron emission (an endothermic reaction) indicates[18,108] that Γ_n should vary as the square root of the energy difference $E - E_b(n)$, where E is the excitation energy. This means that neutron competition should come in rather sharply within 0.5 Mev of the (γ, neutron) threshold.[95]

From the above considerations, it appears that neutron competition with fission cannot be clearly refuted nor supported as the explanation for the structure observed in some (γ,fission) excitation curves. Aside from the U^{234} result of this investigation, however, there is other evidence to lend support to the view that irregularities may exist in the region of the (γ,neutron) threshold. Photoneutron measurements on Th^{232} and U^{238} on the high-energy side of (γ,neutron) thresholds indicate[87] that the neutron yields decrease faster than can be accounted for by the presence of neutron competition with fission. Further, from the even-odd systematics of the neutron binding energies in the uranium isotopes,[73,135] a discrepancy in the general trend is apparent in the region of U^{236} and U^{237}. This behavior might be connected with the pronounced structure observed for U^{236}. Thus it is suggested from this evidence that neutron competition with fission is probably the least likely of the two explanations proposed here for structure in the (γ,fission) excitation curves.

D. Collective Model and Photofission Near "Threshold"

In the introductory section of this treatise, it was indicated that odd-parity states of the (1-) type might be connected with the behavior of the (γ,fission) cross sections near "threshold." If it is accepted that neutron emission in competition with fission is not explanation for the structure observed in some (γ,fission) excitation curves, than the data of this investigation are in qualitative agreement with the Bohr proposal.[19] In the Bohr hypothesis, dipole photofission assumes the major role close to the fission "threshold." Quadrupole photofission is neglected despite the fact that the 2+ collective excitations generally lie at least as close to the 0+ state as the corresponding (1-) excitations. A quadrupole hypothesis, however, requiring strong quadropole absorption at low excitation energies, suggests that

the 2+ states are at least as important as the (1-) excitations. Moreover, since the properties of the states leading either to quadrupole or dipole photofission are not identical, one might expect a difference in mass and angular distributions for the two fission modes. While the odd-parity states lead only to asymmetric fission,[19,61] an even-parity collective excitation of the 2+ type might lead, perhaps, to a symmetrical mass distribution.[116] The latter expectation, however, does not seem fully compatible with the occurrence of predominantly asymmetric fission (peak-to-valley ratio >145) indicated by this and other research. To decide these points, in retrospect, a more detailed knowledge of the process of photoexcitation at low excitation energies is required.

V. SUMMARY

The present work is an effort to furnish pertinent data to assist in the theoretical interpretation of the fission process. The answer to the question of how the photofission cross section changes with parent nucleus when excited by photons at two discrete energies near "threshold" was examined for seven spheroidal nuclei in the region of atomic numbers 90, 92 and 93. The ideas which motivated pursuing this problem had their origin in the qualitative proposals of A. Bohr and the results of betatron studies at low energies on the very heavy elements. In the proposal of Bohr, (γ, fission) cross sections for even-even nuclei near "threshold" may be significantly correlated with the spin state of the excited nucleus at the saddle point configuration.

In this investigation, nuclear excitation was achieved using gamma rays obtained by the nuclear capture of protons on fluorine. The 6.14 and 7.0-Mev gamma rays (the 7.0-Mev group being composed of 6.91 and 7.12-Mev gamma rays) represent well-known ground state transitions in O^{16} whose relative intensities change with proton bombarding energy. Protons of 1.380 and 3.645-Mev energy impinged on a thick CaF_2 target. Employing the known thick target relative gamma-ray intensity ratios, $I(6.91 + 7.12)/I(6.14)$, and the measured gamma-ray flux, the absolute yields of the 6.14 and 7.0-Mev gamma-ray components were established. The fission counting was done in a cancellation-type ionization chamber of 2π geometry. The heavy-element targets were nearly uniform oxide deposits on platinum of about one mg/cm^2. From the suitably corrected fission counting data and the absolute gamma intensities, the absolute (γ, fission) cross sections at 6.14 and 7.0 Mev were calculated.

The (γ, fission) cross sections for Th^{232} and U^{238} are greater at 6.0 Mev than at 7.0 Mev, as indicated by earlier betatron results. U^{236} also exhibits a strong resonance at about 6.0 Mev. However, the other even-even uranium isotope investigated, U^{234}, does not show this behavior. Its (γ, fission) cross section appears to be increasing monotonically with energy between 6.0 and 7.0 Mev in spite of the fact that at 7.0 Mev the (γ, neutron) threshold has been exceeded. The odd-A uranium isotopes, U^{233} and U^{235}, also do not exhibit any unusual behavior in this energy interval. The (γ, fission) cross section for U^{235} appears to be essentially constant, which again is a confirmation of earlier betatron studies. For U^{233}, the cross section increases with energy. The one odd-proton nuclide examined, Np^{237}, appears also to exhibit a resonance behavior at about 6.0 Mev. However, because of the fairly large experimental uncertainty in this case, an appreciable difference in the 6.0 and 7.0-Mev (γ, fission) cross sections may not be real.

In correlating these data with existing information of low-energy photofission, two tentative explanations are proposed for the presence of the small bump or resonance in the excitation curves of some nuclides at about 6.0 Mev. The structure observed is attributed to a discontinuity in either the total photon absorption cross section or the fission-to-total width ratio (Γ_f/Γ). Acceptance of the U^{234} results at face value necessitates ruling out neutron competition with fission as a reasonable explanation. In this circumstance, a direct correlation can be made between the angular fission distribution results for low-energy photofission and the results of this investigation. Based on recent Russian angular distribution experiments, it is argued that quadrupole absorption may be the important mode of nuclear photoexcitation at low energies. The alternative explanation suggested allows neutron competition with fission as the explanation for a drop in the (γ, fission) cross section between 6.0 and 7.0 Mev. For U^{234} the proximity of the experimental (γ, fission) cross section to the (γ, neutron) threshold and less serious competition of neutron emission with fission might conceivably explain the failure of the (γ, fission) cross section at 7.0 Mev to decrease. The existence of certain irregularities in the (γ, neutron) threshold region is cited as evidence that this latter explanation is probably on less secure ground.

In conclusion, it should be emphasized that the arguments and interpretation presented here are far from being unique. A complete explanation that is more than speculation requires a more profound understanding of the fission process. For this reason, further research to investigate in detail the excitation curves and angular distributions of different nuclides at low excitation energies is important. Of fundamental importance would be angular distribution experiments in the energy region of 5.0 to 8.0 Mev with photons of discrete energy. Such experiments might conclusively decide the role of quadrupole absorption at these energies. Further work on the excitation curves near "threshold" of the following actinide and transuranium nuclides would be worthwhile: even-even Th^{230}, Pu^{240}, and Pu^{242}; also the following odd-A nuclides: even proton - Pu^{239} and Pu^{241}; odd proton - Pa^{231}, Am^{241} and Am^{243}. Thus far no photofission investigations have been carried out in the heavy-element region between the closed shell plus one at 83 protons and the actinide elements, i.e., between bismuth and thorium. In this region of the nuclear periodic table, two nuclides of interest, Ra^{226} and Ac^{227}, have half-lives which might make them suitable for such study. The activation energies for fission in this region are still not very different from the binding energy of the last neutrons,[136] and from the standpoint of ease of fissionability these nuclides are certainly worth investigating. Also, Ac^{227} is the only heavy nuclide known beyond the closed shell at 82 protons which has an oblate-spheroidal shape.

ACKNOWLEDGEMENTS

The author wishes to express his sincere appreciation to Dr. John R. Huizenga for originally suggesting this problem and for his continuous counsel, advice, and assistance during the course of this work.

I am indebted to Professor Warren W. Miller for his guidance and continued interest throughout the course of this program and to Professor Converse H. Blanchard for illuminating discussions and critically reading early drafts of this manuscript.

I am pleased to acknowledge the technical assistance, many helpful discussions and suggestions of Mr. Willaim C. Bentley on problems relating to the electronic circuitry and counting techniques.

I would like to express my appreciation to the entire Van de Graaff crew under the direction of Mr. Jack R. Wallace for their helpful assistance and smooth operation of the accelerator.

I am indebted to Dr. Donald W. Engelkemeir for consenting to trade away his 4 inch x 4 inch NaI crystal and for many helpful discussions.

I wish to thank Dr. F. Paul Mooring and Dr. Robert E. Holland of the Physics Division for the use of the wobble-target assembly and the 256-channel analyzer, respectively.

I am grateful also to the many unidentified people of the Argonne National Laboratory who gave invaluable advice and assistance.

Lastly, it is a pleasure to acknowledge the continued interest in this program of Dr. Winston M. Manning.

This work was performed under the auspices of the U.S. Atomic Energy Commission.

BIBLIOGRAPHY

A1. Aaron, Hoffman, and Williams, Range-Energy Curves, AECU-663, May 28, 1951.

A2. F. Ajenberg and T. Lauritsen, Rev. Mod. Phys. 27, 77 (1955).

A3. D. E. Alburger, Chapter 24 in Beta- and Gamma Ray Spectroscopy, K. Siegbahn, Editor, Interscience Publishers, New York, 1955, pp. 775-8.

A4. Alder, Bohr, Huus, Mottelson, and Winther, Rev. Mod. Phys. 28, 432 (1956).

A5. Arakatu, Nemura, Sonada, Shimizu, Kimura, and Muraoka, Proc. Phys. Math. Soc. Japan 25, 440 (1941).

A6. J. M. Araujo, Nuovo cim. 12, 780 (1954).

A7. F. Asaro, University of California Radiation Laboratory (personal communication, 1957).

A8. Asaro, Stephens, and Perlman, Phys. Rev. 92, 1495 (1953).

B9. A. P. Baerg, Proceedings of the Symposium on the Physics of Fission Held at Chalk River, Ontario, May 14-18, 1956. AECL No. 329, Paper B5.

B10. G. G. Baldwin and G. S. Klaiber, Phys. Rev. 71, 3 (1947).

B11. Bannik, Kulikova, Lazareva, and Yakovlev, Physics 22, 1186A (1956).

B12. Y. Beers, Introduction to the Theory of Error, Addison-Wesley Publishing Company, Inc., Reading, Mass., 1957.

B13. P. R. Bell, Chapter 5 in Beta- and Gamma Ray Spectroscopy, K. Siegbahn, Editor, Interscience Publishers, New York, 1955.

B14. Bent, Bonner, and Sippel, Phys. Rev. 98, 1237 (1955).

B15. M. J. Berger and J. Doggett, J. Research NBS 56, 355 (1956).

B16. G. R. Bishop and R. Wilson, Nuclear Photoeffect, Encyclopedia of Physics (Springer-Verlag, Berlin, 1957), Volume XLII.

B17. Bjørnholm, Nathan, Nielsen, and Sheline, Nuclear Phys. 4, 313 (1957).

B18. J. M. Blatt and V. F. Weisskopf, Theoretical Nuclear Physics, John Wiley and Sons, Inc., New York, 1952.

B19. A. Bohr, Proceedings of the International Conference on the Peaceful Uses of Atomic Energy, Geneva, August 1955 (United Nations, New York, 1956), Volume 2, p. 151.

B20. A. Bohr, Kgl. Danske Videnskab. Selskab, Mat.-fys. Medd. 26, No. 14 (1952).

B21. Bohr, Fröman, and Mottelson, Kgl. Danske Videnskab. Selskab, Mat. -fys. Medd. 29, No. 10, 8 (1955).

B22. A. Bohr and B. R. Mottelson, Chapter 17 in Beta- and Gamma Ray Spectroscopy, K. Siegbahn, Editor, Interscience Publishers, New York, 1955, pp. 483-493.

B23. A. Bohr and B. R. Mottelson, Kgl. Danske Videnskab. Selskab, Mat.-fys. Medd. 27, No. 16 (1955).

B24. A. Bohr and B. R. Mottelson, Kgl. Danske Videnskab. Selskab, Mat.-fys. Medd. 30, No. 1 (1955).

B25. A. Bohr and B. R. Mottelson, Nuclear Phys. 4, 529 (1957).

B26. N. Bohr and J. A. Wheeler, Phys. Rev. 56, 426 (1939).

B27. Bortner, Hurst, and Stone, Rev. Sci. Instr. 28, 103 (1957).

B28. W. C. Bright, Report MDDC-91, July 1946.

B29. F. Brown, Atomic Energy of Canada, Ltd., Chalk River, Ontario (personal communication via J. R. Huizenga, 1958).

C30. A. G. W. Cameron, Proceedings of the Symposium on the Physics of Fission Held at Chalk River, Ontario, May 14-18, 1956. AECL No. 329, Paper B6, p. 189.

C31. J. G. Campbell and A. J. F. Boyle, Australian J. Phys. 6, 171 (1953).

C32. Carlson, Geer, and Nelson, Phys. Rev. 94, 1311 (1954).

C33. Chao, Tollestrup, Fowler, and Lauritsen, Phys. Rev. 79, 108 (1950).

C34. K. M. Clarke and J. R. Huizenga, Bull. Am. Phys. Soc., II, 2, 377 A (1957).

C35. S. A. Colgate, Phys. Rev. 87, 592 (1952).

C36. B. C. Cook, Phys. Rev. 106, 300 (1957).

C37. D. C. Coryell and N. Sugarman, Radiochemical Studies; The Fission Products, National Nuclear Energy Series, Plutonium Project Record, Volume 9, Division IV, McGraw-Hill Book Company, Inc., New York, 1951.

C38. B. B. Cunningham and J. C. Hindman, Chapter 12 of The Actinide Elements, National Nuclear Energy Series, Division IV, Volume 14A, McGraw-Hill Book Company, Inc., New York, 1954, p. 475.

D39. M. Danos, Ann. Physik 10, 265 (1952).

D40. M. Danos and H. Steinwedel, Z. Naturforsch. 6A, 217 (1951).

D41. C. M. Davisson, Chapter 2 in Beta- and Gamma Ray Spectroscopy, K. Siegbahn, Editor, Interscience Publishers, New York, 1955.

D42. Day, Chao, Fowler, and Perry, Jr., Phys. Rev. 80, 131 (1950).

D43. Dodson, Graves, Helmholz, Hufford, Potter, and Povelites, Chapter 1 of Miscellaneous Physical and Chemical Techniques of the Los Alamos Project, National Nuclear Energy Series, Division V, Volume 3, McGraw-Hill Book Company, Inc., New York, 1952.

D44. R. B. Duffield and J. E. Gindler (unpublished data).

D45. R. B. Duffield and J. R. Huizenga, Phys. Rev. 89, 1042 (1953).

E46. J. P. Elliott, Proc. Roy. Soc., Ser. A, 242, 57 (1957).

E47. W. C. Elmore and M. Sands, Electronics, McGraw-Hill Book Company, Inc., New York, 1949, p. 78.

E48. D. W. Engelkemeir, Argonne National Laboratory (personal communication, 1957).

E49. W. N. English and G. C. Hanna, Can. J. Phys. 31, 768 (1953).

F50. Fairhall, Halpern, and Winhold, Phys. Rev. 94, 733 (1954).

F51. Farney, Given, Kern, and Hahn, Phys. Rev. 97, 720 (1955).

F52. R. S. Foote and H. W. Koch, Rev. Sci. Instr. 25, 746 (1954).

F53. S. Frankel and N. Metropolis, Phys. Rev. 72, 914 (1947).

F54. J. Frenkel, J. Phys. U.S.S.R. 1, 125 (1939).

F55. G. Friedlander and J. W. Kennedy, Nuclear and Radiochemistry, John Wiley and Sons, Inc., New York, 1956, pp. 190-195.

F56. P. O. Froman, Kg l. Danske Videnskab. Selskab, Mat.-fys. Medd. 1, No. 3 (1957).

F57. Y. Fujimoto and Y. Yamaguchi, Prog. of Theor. Phys. 5, 76 (1950).

G58. Gindler, Huizenga, and Schmidtt, Phys. Rev. 104, 425 (1956).

G59. G. Goldhaber, Phys. Rev. 74, 1725 (1948).

G60. M. Goldhaber and E. Teller, Phys. Rev. 74, 1046 (1948).

G61. H. E. Gove, Proceedings of the Symposium on the Physics of Fission Held at Chalk River, Ontario, May 14-18, 1956. AECL No. 329, Paper D2.

G62 G. W. Grodstein, National Bureau of Standards Circular 583, April 30, 1957.

H63. D. Halliday, Introductory Nuclear Physics, John Wiley and Sons, Inc., New York, 1950, pp. 63 and 193.

H64. W. H. Hartley, Ph. D. Thesis, Photoneutron and Photofission Cross Sections, University of Pennsylvania, 1955 (unpublished).

H65. W. H. Hartley, Proceedings of the Photonuclear Conference at Case Institute of Technology, 1955 (unpublished), pp. 2-3.

H66. Haxby, Shoupp, Stephens, and Wells, Phys. Rev. 59, 57 (1941).

H67. W. A. Higinbotham, Nucleonics 14:4, 61 (1956).

H68. D. L. Hill and J. A. Wheeler, Phys. Rev. 89, 1102 (1953).

H69. H. R. Hoekstra and J. J. Katz, Chapter 6 in The Actinide Elements National Nuclear Energy Series, Division IV, Volume 14A, McGraw-Hill Book Company, Inc., New York, 1954, p. 142.

H70. Hornyak, Lauritsen, Morrison, and Fowler, Rev. Mod. Phys. 22, 356 (1950).

H71. D. J. Hughes, Neutron Cross Sections, Pergamon Press, New York, 1957. p. 111.

H72. D. J. Hughes and J. A. Harvey, Neutron Cross Sections, BNL 325, July 1, 1955. Superintendent of Documents, U. S. Government Printing Office, Washington, D. C.

H73. J. R. Huizenga, Physica 21, 410 (1955).

H74. J. R. Huizenga, Phys. Rev. 109, 484 (1958).

H75. Huizenga, Magnusson, Fields, Studier, and Duffield, Phys. Rev. 82, 561 (1951).

H76. Huizenga, Magnusson, Fields, Studier, and Duffield, Phys. Rev. 84, 166 (1951).

H77. E. K. Hyde, Chapter 15 of The Actinide Elements, National Nuclear Energy Series, Division IV, Volume 14A, McGraw-Hill Book Company, Inc., New York, 1954, pp. 568-70.

J78. J. D. Jackson, Proceedings of the Symposium on the Physics of Fission Held at Chalk River, Ontario, May 14-18. 1956. AECL No. 329, Paper B2, p. 125.

J79. A. H. Jaffey, Chapter 16 of The Actinide Elements, National Nuclear Energy Series, Division IV, Volume 14A, McGraw-Hill Book Company, Inc., New York, 1954.

J80. A. H. Jaffey, Rev. Sci. Instr. 25, 349 (1954).

J81. T. Jorgensen, Report MDDC-467, October 1946.

J82. J. A. Jungerman and H. M. Steiner, Phys. Rev. 106, 585 (1957).

K83. Katcoff, Miskel, and Stanley, Phys. Rev. 74, 631 (1948).

K84. L. Katz and A. G. W. Cameron, Can. J. Phys. 29, 518 (1951).

K85. L. Katz, Supplement for the original photon difference tables from 3- to 8 Mev (unpublished).

K86. Katz, Kavanagh, Cameron, Bailey, and Spinks, Phys. Rev. 99, 98 (1955).

K87. Katz, McNeill, LeBlanc and Brown, Can. J. Phys. 35, 470 (1957).

K88. L. I. Katzin, Chapter 4 of The Actinide Elements, National Nuclear Energy Series, Division IV, Volume 14A, McGraw-Hill Book Company, Inc., New York, 1954, p. 78.

K89. I. K. Khoklov, Soviet Physics JETP 5, 88 (1957).

K90. Koch, McElhinney, and Gasteiger, Phys. Rev. 77, 329 (1950).

K91. H. W. Koch and J. M. Wyckoff, J. Research NBS 56, 319 (1956).

K92. H. W. Koch and J. M. Wyckoff, Response Function of Total-Absorption Spectrometers, Scintillation Counter Symposium, Washington, D. C., January 27-28, 1958.

K93. W. E. Kreger and C. S. Cook, Phys. Rev. 96, 1276 (1954).

L94. Lazar, Davis, and Bell, Nucleonics 14:4, 52 (1956).

L95. Lazareva, Gavrilov, Valuev, Zatsepina, and Stravinsky, Conference of the Academy of Sciences of the U.S.S.R. on the Peaceful Uses of Atomic Energy, July 1-5, 1955, Session of the Division of Physical and Mathematical Sciences (Akademia Nauk, S.S.R., Moscow, 1955). Translation by Consultants Bureau, New York, 1955, pp. 217 and 306.

L96. L. E. Lazareva and N. V. Nikitina, Physics of Fission, Supplement No. 1 to the Soviet Journal of Atomic Energy, Atomic Press, Moscow, 1957 (translation by Consultants Bureau, New York, 1957). p. 125.

L97. K. Lee and D. R. Inglis, Phys. Rev. 108, 774 (1957).

M98. M. G. Mayer and J. H. D. Jensen, Elementary Theory of Nuclear Shell Structure, John Wiley and Sons, Inc., New York, 1955, pp. 11, 81, and 186.

M99. Milford, Shankland, and Finegan, Bull. Am. Phys. Soc., II, 1, 402A (1956).

M100. P. Morrison, Experimental Nuclear Physics, John Wiley and Sons, Inc., New York, 1953, Volume II, Part VI.

M101. G. A. Morton, Proceeding of the International Conference on the Peaceful Uses of Atomic Energy, Geneva. August 1955 (United Nations, New York, 1956), Volume 14, p. 246.

N102. O. Nathan and M. A. Waggoner, Nuclear Phys. 2, 548 (1956/1957)

N103. A. T. Nelms, National Bureau of Standards Circular 542, August 28, 1953.

N104. J. O. Newton, Nuclear Phys. 3, 345 (1957).

N105. J. O. Newton, Nuclear Phys. (to be published).

N106. V. G. Nosov, Physics of Fission, Supplement No. 1 to the Soviet Journal of Atomic Energy, Atomic Press, Moscow 1957 (translation by Consultants Bureau, Inc., New York, 1957), p. 38.

N107. Nuclear Sci. Abstr. 10:24B, 26 (1956).

P108. D. C. Peasley, Phys. Rev. 88, 812 (1952).

P109. I. Perlman and F. Asaro, Ann. Rev. Nuclear Sci. 4, 157 (1954).

P110. I. Perlman and J. O. Rasmussen, Alpha Radioactivity, Encyclopedia of Physics (Springer-Verlag, Berlin, 1957), Volume XLII.

P111. J. A. Phillips and P. G. Kruger, Phys. Rev. 76, 1471 (1949).

R112. J. Rainwater, Phys. Rev. 79,432 (1950).

R113. C. L. Rao, Argonne National Laboratory (unpublished results, 1957).

R114. Reineks, Finegan and Shankland, Technical Report No. 24, Nuclear Physics Laboratory, Case Institute of Technology, 1957.

R115. B. Rossi and H. H. Staub, Ionization Chambers and Counters, National Nuclear Energy Series, Division V, Volume 2, McGraw-Hill Book Company, Inc., New York, 1949, p. 210.

S116. R. A. Schmitt and R. B. Duffield, Phys. Rev. 105, 1277 (1957).

S117. R. A. Schmitt and N. Sugarman, Phys. Rev. 95, 1260 (1954).

S118. E. Segrè and C. Wiegrand, Phys. Rev. 70, 808 (1946).

S119. J. C. Slater and N. H. Frank, Electromagnetism, McGraw-Hill Book Company, Inc., New York, 1947, p. 227.

S120. R. W. Spence and G. P. Ford, Ann. Rev. Nuclear Sci, 2, 399 (1953).

S121. H. M. Steiner and J. A. Jungerman, Phys. Rev. 101, 807 (1956).

S122. W. E. Stephens, Editor, Nuclear Fission and Atomic Energy, The Science Press, Lancaster, Pennsylvania, 1948, Chapter 8.

S123. Stephens, Asaro, and Perlman, Phys. Rev. 96, 1568 (1954).

S124. Stephens, Asaro, and Perlman, Phys. Rev. 100, 1543 (1955).

S125. Stephens, Asaro, and Perlman, Phys. Rev. 107, 1091 (1957).

S126. A. Stolovy and J. A. Harvey, Phys. Rev. 108, 353 (1957).

S127. K. Strauch, Ann. Rev. Nuclear Sci. 2, 105 (1953).

S128. V. M. Strutinsky, Physica 22, 1166A (1956).

S129. V. M. Strutinsky, J. Atomic Energy (U.S.S.R.) 4, 150 (1956).

S130. R. K. Swank and J. S. Moenich, Argonne National Laboratory Report ANL-5239, February 1954.

S131. C. P. Swann and F. R. Metzger, Bull. Am. Phys. Soc., II, 1, 211A (1956).

S132. C. P. Swann and F. R. Metzger, Phys. Rev. 108, 982 (1957).

S133. W. J. Swiatecki, Phys. Rev. 101, 97 (1956).

T134. A. Turkevich and J. B. Niday, Phys. Rev. 84, 52 (1951).

V135. R. Vandenbosch (personal communication, 1958).

V136. R. Vandenbosch and G. T. Seaborg, University of California Radiation Laboratory Report UCRL-8047, November 1957 (unpublished).

W137. R. L. Walker and B. D. McDaniel, Phys. Rev. 74, 315 (1948).

W138. J. A. Wheeler, Proceedings of the International Conference on the Peaceful Uses of Atomic Energy, Geneva, August 1955 (United Nations, New York, 1956), Volume 2, p. 220.

W139. J. A. Wheeler, Physica 22, 1103 (1956).

W140. J. A. Wheeler, The International Conference on the Neutron Interactions with the Nucleus, Columbia University, September 9-13, 1957. Session IIIB, Paper 8 (verbal report).

W141. D. H. Wilkinson, Physica 22, 1039 (1956).

W142. Willard, Bair, Kingston, Halm, Snyder, and Green, Phys. Rev. 85, 849 (1952).

W143. Winhold, Demos, and Halpern, Phys. Rev. 85, 728 (1952).

W144. Winhold, Demos, and Halpern, Phys. Rev. 87, 1139 (1952).

W145. E. J. Winhold and I. Halpern, Phys. Rev. 103, 990 (1956).

W146. Wolichi, Jastrow, and Brooks, Naval Research Laboratory Report 4833, October 5, 1956.

W147. W. J. Youden, Statistical Methods for Chemists, John Wiley and Sons, Inc., New York, 1951, Chapter 5.

APPENDIX A

Complete Experimental Data

Table A-1
ABSOLUTE GAMMA-RAY INTENSITIES

Nuclide	Proton Energy (Mev)	Run	Time (Minutes)	C_0	C*	$I_0(6.14)$	$I_0(7.0)$
Th^{232}	1.380	1	20.00	287,694	283,345	$4.0_5 \times 10^9$	$1.9_4 \times 10^9$
		2	20.00	293,596	289,247	4.1_4	1.9_9
		3	60.00	869,138	856,092	$12._3$	5.8_6
		4	20.00	302,663	298,314	4.2_7	2.0_5
		5	20.00	315,241	310,892	4.4_5	2.1_4
		Total			2,037,890	$2.9_1 \times 10^{10}$	$1.4_0 \times 10^{10}$
	3.645	1	15.00	584,368	581,436	$1.2_0 \times 10^{10}$	$1.6_6 \times 10^{10}$
		2	15.00	570,991	568,059	1.1_8	1.6_2
		3	16.04	667,876	664,741	1.3_8	1.9_0
		4	15.00	630,477	627,545	1.3_0	1.7_9
		5	15.00	665,437	662,505	1.3_7	1.8_9
		Total			3,104,286	$6.4_2 \times 10^{10}$	$8.8_5 \times 10^{10}$
U^{238} Standard	1.380	1	15.00	219,876	216,614	$3.0_9 \times 10^9$	$1.4_8 \times 10^9$
		2	15.00	223,336	220,074	3.1_5	1.5_1
		3	15.00	227,660	224,398	3.2_1	1.5_4
		4	15.00	235,941	232,679	3.3_3	1.6_0
		5	15.00	234,613	231,351	3.3_1	1.5_9
	3.645	6	15.00	217,174	213,912	3.0_6	1.4_7
		7	15.00	211,201	207,939	2.9_7	1.4_3
		8	15.00	198,833	195,571	2.8_0	1.3_4
		9	15.00	222,757	219,495	3.1_4	1.5_1
		Total			1,962,033	$2.8_1 \times 10^{10}$	$1.3_5 \times 10^{10}$
U^{238} (Standard)	3.645	1	15.00	647,474	644,542	$1.3_3 \times 10^{10}$	$1.8_4 \times 10^{10}$
		2	15.00	670,950	668,018	1.3_8	1.9_0
		3	15.00	517,797	514,865	1.0_7	1.4_7
		4	15.00	657,319	654,387	1.3_6	1.8_7
		5	15.00	632,607	629,675	1.3_1	1.8_0
		6	15.00	784,685	781,714	1.6_2	2.2_3
		7	15.00	676,542	673,571	1.3_9	1.9_2
		8	15.00	644,114	641,143	1.3_3	1.8_3
		9	15.00	741,318	738,347	1.5_2	2.1_0
		10	17.00	586,644	583,276	1.2_0	1.6_6
		11	15.00	606,976	604,005	1.2_5	1.7_2
		Total			7,133,543	$1.4_7 \times 10^{11}$	$2.0_3 \times 10^{11}$
U^{235}	1.380	1	15.00	220,961	217,699	$3.1_1 \times 10^9$	$1.4_9 \times 10^9$
		2	15.00	225,398	222,136	3.1_8	1.5_3
		3	15.00	226,494	223,232	3.1_9	1.5_3
		4	15.00	220,558	217,296	3.1_1	1.4_9
		5	15.00	245,758	242,496	3.4_7	1.6_7
		6	15.00	236,331	233,069	3.3_3	1.6_0
		Total			1,355,928	$1.9_4 \times 10^{10}$	$9.3_1 \times 10^9$
	3.645	1	15.00	606,644	603,712	$1.2_5 \times 10^{10}$	$1.7_2 \times 10^{10}$
		2	15.01	632,402	629,468	1.3_0	1.7_9
		3	15.01	704,811	701,879	1.4_5	2.0_0
		4	15.01	537,878	534,946	1.1_1	1.5_3
		5	16.00	702,020	698,893	1.4_4	1.9_9
		Total			3,168,898	$6.5_5 \times 10^{10}$	$9.0_3 \times 10^{10}$
U^{236}	1.380	1	15.00	220,112	216,850	$3.1_0 \times 10^9$	$1.4_9 \times 10^9$
		2	20.00	277,089	272,740	3.9_0	1.8_7
		3	15.00	202,389	199,127	2.8_5	1.3_7
		4	15.00	225,569	222,307	3.1_8	1.5_3
		Total			911,024	$1.3_0 \times 10^{10}$	$6.2_4 \times 10^9$
	3.645	1	15.00	739,647	736,676	$1.5_2 \times 10^{10}$	$2.1_0 \times 10^{10}$
		2	15.00	663,877	660,906	1.3_6	1.8_8
		3	15.00	670,484	667,513	1.3_8	1.9_0
		4	15.00	724,063	721,092	1.4_9	2.0_6
		5	15.00	718,486	715,515	1.4_8	2.0_4
		6	15.00	555,048	552,077	1.1_4	1.5_7
		Total			4,053,779	$8.4_1 \times 10^{10}$	$1.1_6 \times 10^{11}$
Np^{237}	1.380	1	15.00	222,489	219,227	$3.1_4 \times 10^9$	$1.5_1 \times 10^9$
		2	15.00	204,086	200,824	2.8_7	1.3_8
		3	16.00	234,440	230,961	3.3_0	1.5_8
		4	15.00	228,185	224,923	3.2_2	1.5_5
		Total			875,935	$1.2_5 \times 10^{10}$	$6.0_0 \times 10^9$
	3.645	1	15.00	756,965	753,994	$1.5_6 \times 10^{10}$	$2.1_5 \times 10^{10}$
		2	15.00	666,118	663,147	1.3_7	1.8_5
		3	15.00	693,679	690,708	1.4_3	1.9_7
		4	15.00	749,067	746,096	1.5_4	2.1_3
		5	17.00	669,909	666,541	1.3_8	1.9_0
		6	15.00	620,721	617,750	1.2_8	1.7_6
		Total			4,138,236	$8.5_6 \times 10^{10}$	$1.1_8 \times 10^{11}$
U^{234}	1.380	1	15.00	211,764	208,502	$2.9_8 \times 10^9$	$1.4_3 \times 10^9$
		2	15.00	207,780	204,518	2.9_3	1.4_1
		3	15.00	219,443	216,181	3.0_9	1.4_8
		4	15.00	223,443	220,181	3.1_5	1.5_1
		Total			849,382	$1.2_2 \times 10^{10}$	$5.8_6 \times 10^9$
	3.645	1	15.00	662,022	659,051	$1.3_6 \times 10^{10}$	$1.8_8 \times 10^{10}$
		2	15.00	655,936	652,965	1.3_5	1.8_6
		3	15.00	724,460	721,489	1.4_9	2.0_6
		4	15.00	729,165	726,194	1.5_0	2.0_7
		5	15.00	562,337	559,366	1.1_5	1.5_9
		6	15.00	643,042	640,071	1.3_2	1.8_2
		Total			3,959,136	$8.1_9 \times 10^{10}$	$1.1_3 \times 10^{11}$
U^{233}	1.380	1	15.00	221,870	218,608	$3.1_3 \times 10^9$	$1.5_0 \times 10^9$
		2	15.00	213,021	209,759	3.0_0	1.4_5
		3	15.00	224,812	221,550	3.1_7	1.5_2
		4	15.00	244,774	241,512	3.4_5	1.6_4
		5	15.00	234,203	230,941	3.3_0	1.5_8
		Total			1,122,370	$1.6_1 \times 10^{10}$	$7.7_3 \times 10^9$
	3.645	1	15.00	643,677	640,745	$1.3_3 \times 10^{10}$	$1.8_3 \times 10^{10}$
		2	15.00	665,704	662,772	1.3_7	1.8_9
		3	15.00	685,652	682,720	1.4_1	1.9_5
		4	15.00	601,645	598,713	1.2_4	1.7_1
		5	15.00	671,639	668,707	1.3_9	1.9_1
		Total			3,253,657	$6.7_2 \times 10^{10}$	$9.2_7 \times 10^{10}$

*Background Subtracted

Table A-2
FISSION COUNTING RESULTS

Nuclide	Proton Energy (Mev)	Run	f_0	f_ρ	f	$\Sigma I_0(6.14 + 7.0)$	$f/\Sigma I_0(6.14 + 7.0)$ (x 10^8)
Th^{232}	1.380	1	99	69	77	5.9_9 x 10^9	1.2_9
		2	89	62	69	6.1_3	1.1_3
		3	260	182	202	1.8_1	1.1_2
		4	102	71.5	79.3	6.3_2	1.2_6
		5	99	69	77	6.5_9	1.1_7
	Total				504	4.3_1 x 10^{10}	$1.1_7 \pm 0.0_6^*$
	3.645	1	339	238	264	2.8_6 x 10^{10}	0.92_3
		2	316	222	246	2.8_0	0.87_9
		3	364	255	283	3.2_8	0.86_3
		4	339	238	264	3.0_9	0.85_4
		5	337	236	262	3.2_6	0.80_4
	Total				1319	15.2_7 x 10^{10}	$0.864 \pm 0.02_5^*$
U^{238} (Standard)	1.380	1	85	60	67	4.5_7 x 10^9	1.4_7
		2	81	57	63	4.6_6	1.3_5
		3	105	73.6	81.6	4.7_5	1.7_2
		4	108	75.7	83.9	4.9_3	1.7_0
		5	114	79.9	88.6	4.9_0	1.8_1
		6	116	81.3	90.1	4.5_3	1.9_9
		7	97	68	75	4.4_0	1.7_1
		8	79	55	61	4.1_4	1.4_7
		9	102	71.5	79	4.8_5	1.7_0
	Total				689	4.1_6 x 10^{10}	$1.6_6 \pm 0.1_5^*$
	3.645	1	633	444	492	3.1_7 x 10^{10}	1.5_5
		2	611	428	475	3.2_8	1.4_5
		3	514	360	399	2.5_4	1.5_7
		4	543	381	422	3.2_3	1.3_1
		5	483	339	376	3.1_1	1.2_1
		6	559	392	435	3.8_5	1.1_3
		7	534	374	415	3.3_1	1.2_5
		8	509	357	396	3.1_6	1.2_5
		9	551	386	428	3.6_2	1.1_8
		10	538	377	418	2.8_6	1.4_6
		11	574	402	446	2.9_7	1.5_0
	Total				4702	$35._0$ x 10^{10}	$1.3_4 \pm 0.1_4^*$
U^{235}	1.380	1	147	103	113	4.6_9 x 10^9	2.4_6
		2	126	88.3	97.3	4.7_1	2.0_7
		3	113	79.2	87.2	4.7_5	1.8_6
		4	118	82.7	91.1	4.6_0	1.9_8
		5	159	112	123	5.1_4	2.3_9
		6	146	102	112	4.9_3	2.2_7
	Total				624	$28._7$ x 10^9	$2.1_7 \pm 0.2_0^*$
	3.645	1	951	667	735	2.9_7 x 10^{10}	2.4_7
		2	871	611	673	3.0_9	2.1_8
		3	1036	726.2	800	3.4_6	2.3_2
		4	876	614	676	2.6_4	2.5_6
		5	1000	701	772	3.4_3	2.2_6
	Total				3656	15.5_8 x 10^{10}	$2.3_5 \pm 0.1_2^*$
U^{236}	1.380	1	221	155	171	4.5_9 x 10^9	3.7_3
		2	226	158	174	5.7_7	3.0_2
		3	212	149	164	4.2_2	3.8_9
		4	227	159	175	4.7_1	3.7_2
	Total				684	$19._2$ x 10^9	$3.5_6 \pm 0.3_0^*$
	3.645	1	1051	736.8	812	3.8_2 x 10^{10}	2.2_4
		2	1023	717.1	790	3.2_4	2.4_4
		3	977	684.9	754	3.2_8	2.3_0
		4	1061	743.8	819	3.5_5	2.3_1
		5	930	651.9	718	3.5_2	2.0_4
		6	869	609.2	671	2.7_1	2.4_8
	Total				4564	$20._0$ x 10^{10}	$2.2_8 \pm 0.1_0^*$

Nuclide	Proton Energy (Mev)	Run	f_0	f_ρ	f	$\Sigma I_0(6.14 + 7.0)$	$f/\Sigma I_0(6.14 + 7.0)$ (x 10^8)
Np^{237}	1.380	1	239	168	185	4.6_5 x 10^9	3.9_8
		2	213	149	164	4.2_5	3.8_6
		3	211	148	163	4.8_8	3.3_4
		4	241	169	186	4.7_7	3.9_0
	Total				698	$18._5$ x 10^9	$3.7_7 \pm 0.2_2^*$
	3.645	1	1411	989.1	108_9	3.7_1 x 10^{10}	2.9_4
		2	1290	904.3	966	3.2_6	3.0_6
		3	1493	1047	115_3	3.4_0	3.3_9
		4	1431	1003	110_5	3.6_7	3.0_1
		5	1443	1012	111_5	3.2_8	3.4_0
		6	1395	977.9	107_7	3.0_4	3.5_4
	Total				635_6	$20._4$ x 10^{10}	$3.2_1 \pm 0.2_2^*$
U^{234}	1.380	1	97	68	75	4.4_1 x 10^9	1.7_0
		2	104	72.9	80.3	4.3_4	1.8_8
		3	142	99.5	110	4.5_7	2.4_1
		4	116	81.3	89.5	4.6_6	1.9_2
	Total				355	$18._1$ x 10^9	$1.9_7 \pm 0.2_2^*$
	3.645	1	1288	902.9	994	3.2_4 x 10^{10}	3.0_7
		2	1160	813.2	896	3.2_1	2.7_9
		3	1259	882.6	973	3.5_5	2.7_4
		4	1147	804.1	886	3.5_7	2.4_8
		5	1165	816.7	900	2.7_4	3.2_9
		6	1275	893.8	984	3.1_4	3.1_3
	Total				632	$19._5$ x 10^{10}	$2.8_9 \pm 0.2_5^*$
U^{233}	1.380	1	179	126	139	4.6_3 x 10^9	3.0_0
		2	170	119	132	4.4_4	2.9_7
U^{234}	1.380	3	130	90.1	101	4.6_9	2.1_5
		4	184	129	143	5.1_2	2.8_0
		5	173	121	134	4.8_8	2.7_5
	Total				649	$23._8$ x 10^9	$2.7_2 \pm 0.2_4^*$
	3.645	1	1389	973.7	107_6	3.1_6 x 10^{10}	3.4_1
		2	1367	958.3	105_9	3.2_6	3.2_5
		3	1436	100.7	111_3	3.3_6	3.3_1
		4	1335	935.8	103_4	2.9_5	3.5_1
		5	1330	932.3	103_0	3.3_0	3.1_2
	Total				531_2	15.9_9 x 10^{10}	$3.32 \pm 0.1_1^*$

*Average Value (mean deviation indicated).

APPENDIX B

Absorption Measurements on Fission-Producing Radiation

TABLE B-1

Absorption Measurements

Nuclide	Proton Energy (Mev)	Absorber Thickness (Inches)	f_p/C* ($\times 10^4$)
U^{235}	1.380	None	$1.8_5 \pm .2_4$
		0.25 Pb	$2.4_5 \pm .3_4$
		0.25	$2.3_1 \pm .3_2$
		0.5	$2.0_5 \pm .3_3$
		1.0	$2.3_2 \pm .4_5$
		Gross Average	$2.1_6 \pm .14$
U^{236}	1.380	None	$2.1_7 \pm .2_6$
		0.25 Pb	$2.2_2 \pm .2_9$
		0.5	$2.5_2 \pm .3_9$
		1.0	$3.5_7 \pm .6_0$
		1.0	$3.0_1 \pm .5_2$
		Gross Average	$2.49 \pm .17$
U^{235}	3.645	None	$16.71 \pm .47$
		None	$16.75 \pm .36$
		0.25 Pb	$19.94 \pm .61$
		0.5	$19.2 \pm .7$
		0.5	$19.0 \pm .7$
		1.0	23.5 ± 1.0
		Gross Average	$18.22 \pm .22$
U^{236}	3.645	None	$16.41 \pm .47$
		0.25 Pb	$16.4 \pm .6$
		0.5	$16.5 \pm .6$
		1.0	$15.4 \pm .8$
		Gross Average	$16.29 \pm .29$
U^{235}	3.645	None	$16.73 \pm .29$
		0.25 Pb	$15.57 \pm .48$
		0.5	$16.74 \pm .53$
		1.0	$16.8 \pm .6$
		Gross Average	$16.53 \pm .21$
U^{235}	3.645	None	$16.73 \pm .29$
		1.0 Paraffin	$51.95 \pm .87$
		1/32 Cadmium	$16.88 \pm .50$
		Paraffin + Cd	$24.08 \pm .59$

*Standard deviations indicated.

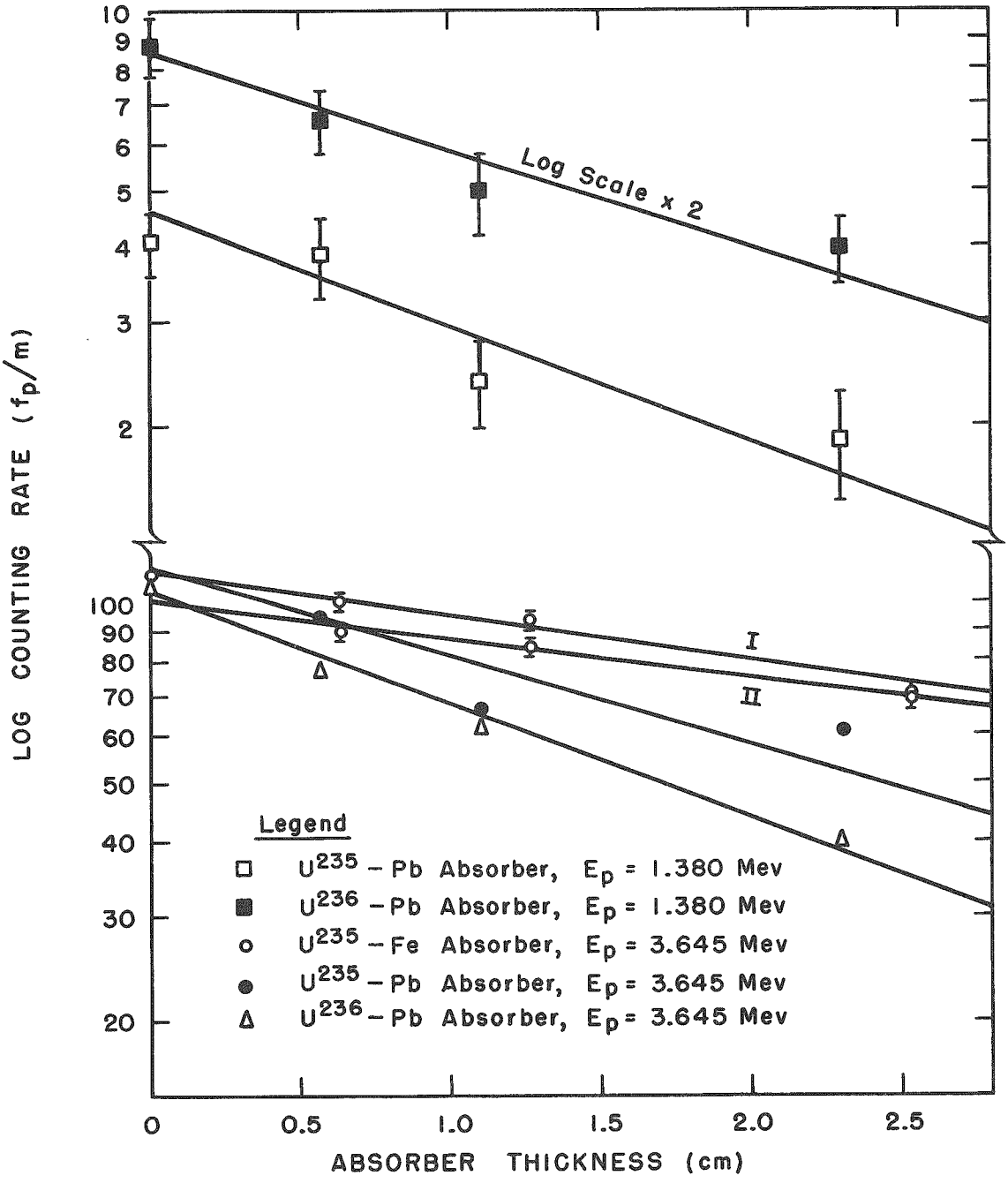

FIGURE B-1.

FISSION YIELD vs. ABSORBER THICKNESS.

APPENDIX C

TABLE C-1

Nuclear Properties of Fissionable Nuclides

Nuclide	Z^2/A	I_o π a-d,h	$t_{1/2}(\alpha)$ (yr) e	$t_{1/2}$(s.f.) (yr) f	$\lvert Q_o \rvert$ c.e. (10^{-24} cm^2) g	Specific Activity (α/m/mg)
$_{90}Th^{232}$	34.90	0 +	1.39×10^{10}	1.4×10^{18}	10	2.47×10^{2}
$_{92}U^{233}$	36.31	5/2+	1.62×10^{5}	$\geq 3 \times 10^{17}$	13.7	2.11×10^{7}
U^{234}	36.16	0 +	2.48×10^{5}	1.6×10^{16}	-	1.37×10^{7}
U^{235}	36.00	7/2-	$7.1_3 \times 10^{8}$	1.8×10^{17}	10.1	$4.7_4 \times 10^{3}$
U^{236}	35.85	0 +	2.39×10^{7}	2×10^{16}	-	1.40×10^{5}
U^{238}	35.55	0 +	4.51×10^{9}	8.0×10^{15}	10.3	7.39×10^{2}
$_{93}Np^{237}$	36.48	5/2+	2.20×10^{6}	$\geq 4 \times 10^{16}$	9.0	1.52×10^{6}

[a]M. G. Mayer and J. H. D. Jensen, Elementary Theory of Nuclear Shell Structure, John Wiley and Sons, Inc., New York, 1955, p. 186.

[b]Nuclear Sci. Abstr., 10:24B, 120 (1956); J. O. Newton, Nuclear Phys. (to be published).

[c]Bleaney, Llewellyn, Pryce, and Hall, Phil. Mag. 45, 992 (1954); D. Strominger and J. O. Rasmussen, Nuclear Phys. 3, 197 (1957); J. O. Newton, Nuclear Phys. (to be published).

[d]Hutchison, Llewellyn, Wong, and Dorain, Phys. Rev. 102, 292 (1956); Huizenga, Rao, and Engelkemeir, Phys. Rev. 107, 319 (1957); F. Asaro and I. Perlman, Phys. Rev. 107, 318 (1957).

[e]W. M. Sullivan, Trilinear Chart of Nuclides, Superintendent of Documents, U. S. Government Printing Office, Washington 25, D. C., January 1957.

[f]M. H. Studier and J. R. Huizenga, Phys. Rev. 96, 545, (1954).

[g]Alder, Bohr, Huus, Mottelson, and Winther, Rev. Mod. Phys. 28, 432 (1956); J. O. Newton, Nuclear Phys. 3, 345 (1957); J. O. Newton, ibid. (to be published).

[h]There is no conclusive evidence for the absolute parity assignments.

APPENDIX D

Total Intrinsic Gamma-Ray Detection Efficiency

A. Interaction of Gamma Radiation with Matter

An analysis of the interaction of gamma radiation with matter shows that the interaction is characterized by the fact that each gamma-ray photon is removed individually from the incident beam in a single event. The attenuation of the intensity, I, as the distance of penetration, x, is increased measures the total probability of the interaction processes. This attenuation, being proportional to x and I, can be formulated as follows:

$$-dI \sim Idx \tag{1}$$

$$-dI = \mu Idx \tag{2}$$

where μ represents the total attenuation coefficient, namely, the probability that a photon be removed from the incident beam per unit thickness of material traversed. This total probability that a process takes place per unit thickness of matter is the sum of the probabilities of occurrence of the various absorption and scattering processes.(41)

$$\frac{dI}{I} = -\mu dx \quad . \tag{3}$$

If the photon intensity is assumed homogeneous in 4π space, then μ is constant. The only other restrictions as to the nature of the radiation lies in the assumptions made concerning the detector efficiency below. Integration of equation (3) yields:

$$\ln \frac{I}{I_0} = -\mu x \tag{4}$$

$$I = I_0 \, e^{-\mu x} \quad . \tag{5}$$

Hence the attenuation of the intensity or the number of interactions produced can be written

$$n = I_0 \, (1-e^{-\mu x}) \quad . \tag{6}$$

B. Absolute Gamma Ray Detection Efficiency

For the case of an effective point-isotropic source coaxial with a right cylindrical crystal detector, the interactions can be formulated generally as follows. Consider a cylindrical NaI crystal of radius R and length t, placed on the polar axis of the coordinate system (r,θ,ϕ). The source S is a distance h from the near crystal face.

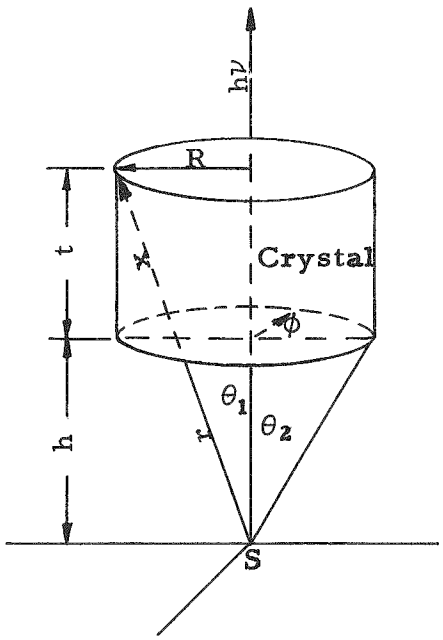

FIGURE D-1

Geometry for NaI Efficiency Calculations.

Notation used:

N_0 = total quanta emitted isotropically from the point source.

N = total primary interactions in the crystal.

Ω = the solid angle (in steradians) subtended by the crystal from the point emitter.

x = the path length in the crystal along an element of solid angle $d\omega$, a function of Ω.

μ = total linear absorption coefficient for NaI(Tl). μ is energy dependent.

The number of quanta striking the crystal in the elementary solid angle $d\omega$ is given by

$$\sum\gamma \; d\omega = N_0 \frac{d\omega}{4\pi} \qquad (1)$$

Then the number of quanta detected by the crystal in the solid angle $d\omega$ will be

$$dN = N_0 \frac{d\omega}{4\pi} (1-e^{-\mu x}) \quad . \qquad (2)$$

This treatment is limited only to first interactions, i.e., no account is taken of second and further interactions such as may exist in the case of multiple scattering. Since the absorption of a scattered photon is essentially simultaneous with the scattering event that produced it and only one pulse is produced, no correction to the counting efficiency need be made for multiple processes. Also

$$dN = \epsilon_t \, N_0 \frac{d\omega}{4\pi} \quad , \tag{3}$$

where $\epsilon_t(E)$ is the total intrinsic efficiency of the crystal for a gamma ray of energy E, i.e., the probability that a photon incident with energy E will have at least one interaction (scattering or absorption) in the crystal. The detector efficiency may vary in an arbitrary way from point to point but for radiation of a given energy it is constant. Except insofar as it is dependent on the position of the detector at which the radiation is received, ϵ_t does not depend on the angle of incidence of the radiation. Equating equations (2) and (3), one obtains

$$\epsilon_t \, d\omega = (1 - e^{-\mu x}) \, d\omega \quad . \tag{4}$$

Integrating over the crystal face, equation (4) yields,

$$\epsilon_t(E) \, \Omega = \int_{x'tal} (1 - e^{-\mu x}) \, d\omega \quad . \tag{5}$$

Alternately integration of equation (2) gives:

$$N = \frac{N_0}{4\pi} \int_{x'tal} (1 - e^{-\mu x}) \, d\omega \tag{6}$$

and

$$\frac{N}{N_0} = \frac{1}{4\pi} \int_{x'tal} (1 - e^{-\mu x}) \, d\omega \tag{6'}$$

Re-defining a new crystal efficiency, $\epsilon(E)$, of the form

$$\epsilon(E) = \frac{N}{N_0} \quad , \tag{7}$$

equations (6') and (7) yield

$$\epsilon(E) = \frac{1}{4\pi} \int_{x'tal} (1 - e^{-\mu x}) \, d\omega \quad . \tag{8}$$

Two limiting geometries are of interest. In one, broad-beam radiation is allowed to fall on the full end face of the crystal detector. The

crystal efficiency for this case can be gotten by suitable evaluation of the integral in equation (8). Referring to the geometry of Figure (D-1), we have:

$$\theta_1 = \tan^{-1}\frac{R}{h+t}$$
$$\theta_2 = \tan^{-1}\frac{R}{h} \qquad (9)$$

for 0 to θ_1 degrees: $x = t \sec\theta$ (10)

for θ_1 to θ_2 degrees: $x = R \csc\theta - h \sec\theta$

$$d\omega = \sin\theta \, d\theta \, d\phi \quad . \qquad (11)$$

Employing the relations of equations (9), (10), and (11), equation (8) becomes

$$\epsilon(E) = 1/2 \left\{ 1 - \cos\theta_2 - \int_0^{\theta_1} \sin\theta \, e^{-\mu t \sec\theta} d\theta \right. \qquad (12)$$
$$\left. - \int_{\theta_1}^{\theta_2} \sin\theta \, e^{-\mu (R \csc\theta - h \sec\theta)} \, d\theta \right\}$$

where $\mu(E)$ is total linear absorption coefficient for NaI(Tl) expressed in cm^{-1}.

t is expressed in cm.

Computations based upon equation (12) have been published[146] to cover a range of standard cylindrical crystals for various values of $\mu(E)$ and h.

The second limiting case pertains to a collimated source of radiation whereby a narrow pencil of radiation is incident along the crystal axis. Here "good" geometry is assumed. This means that the solid angles subtended by the crystal detector from the point source are sufficiently small as to permit the assumption of angular independence of the path length, x, in the crystal. The length of the crystal, t, would then closely approximate the value x. In this case, then, the differential expression of equation (4) for the crystal efficiency reduced to

$$\epsilon_t(E) = (1 - e^{-\mu(E) \cdot t}) \qquad (13)$$

where $\mu(E)$ is the "narrow-beam" linear total absorption coefficient.

APPENDIX E

Spread Correction to the Mass Thickness of the Fissionable Samples

In order to establish whether or not the effective mass and atom thickness for an oblique photon ray is significantly different from that for a normally incident photon ray, the following calculation was performed. Given the following geometry, the problem is to define the effective or average mass thickness seen by photons over the entire surface of the sample.

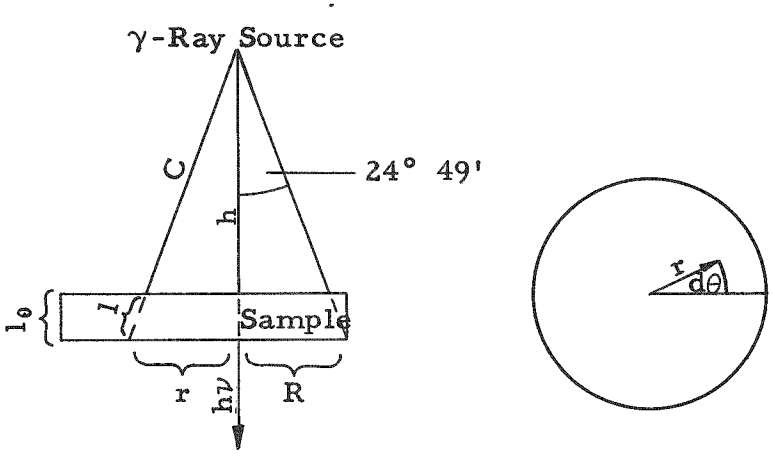

FIGURE E-1
Geometry for Effective Mass Thickness Calculation.

From elementary geometrical considerations, the path length, l, for an oblique ray in the sample can be expressed in the form:

$$l = f \cdot l_0 , \quad f = c/h \tag{1}$$

$$\bar{l} = \bar{f} \cdot l_0 , \tag{1'}$$

where l_0 is assumed constant, i.e., a uniform mass thickness.

Since the mass thickness, n, expressed in mg/cm^2, is related to the sample density ρ by

$$n = \rho \cdot l \quad , \tag{2}$$

it follows then that

$$\bar{n} = \bar{f} \cdot n_0 \tag{3}$$

where n_0 is the mass thickness for a normally incident photon. The evaluation of $\bar{f}$ is arrived at by a straightforward application of the average value problem of integral calculus. Let the average value of the factor f with respect to the sample area be defined by:

$$A\bar{f} = \frac{\int f(A)\, dA}{\int dA} \tag{4}$$

$$f(A) = f(r) = \frac{c}{h} = \frac{1}{h}\sqrt{r^2 + h^2} \tag{5}$$

$$dA = r\, dr\, d\theta \tag{5'}$$

$$f(A)\, dA = \frac{1}{h}\int_0^R \int^{2\pi} r\sqrt{r^2 + h^2}\, dr\, d\theta \tag{6}$$

$$= \frac{2\pi}{3h}\left\{\sqrt{(R^2 + h^2)^3} - h^3\right\}$$

$$\therefore A\bar{f} = \frac{2}{h}\left\{\sqrt{\frac{(R^2 + h^2)^3}{R^4}} - \frac{h^3}{R^2}\right\} .$$

Given the parameters $h = 1.6_2 \pm 0.06$ inch and $R = 0.75_0 \pm 0.016$ inch, $\bar{f}$ is calculated to be $1.0_5 \pm 0.14$. In view of the relatively large uncertainty in this factor, $\bar{f}$ was taken to be not significantly different from unity. Hence $\bar{n} \cong n_o$.

APPENDIX F

Electronic Circuit Diagrams

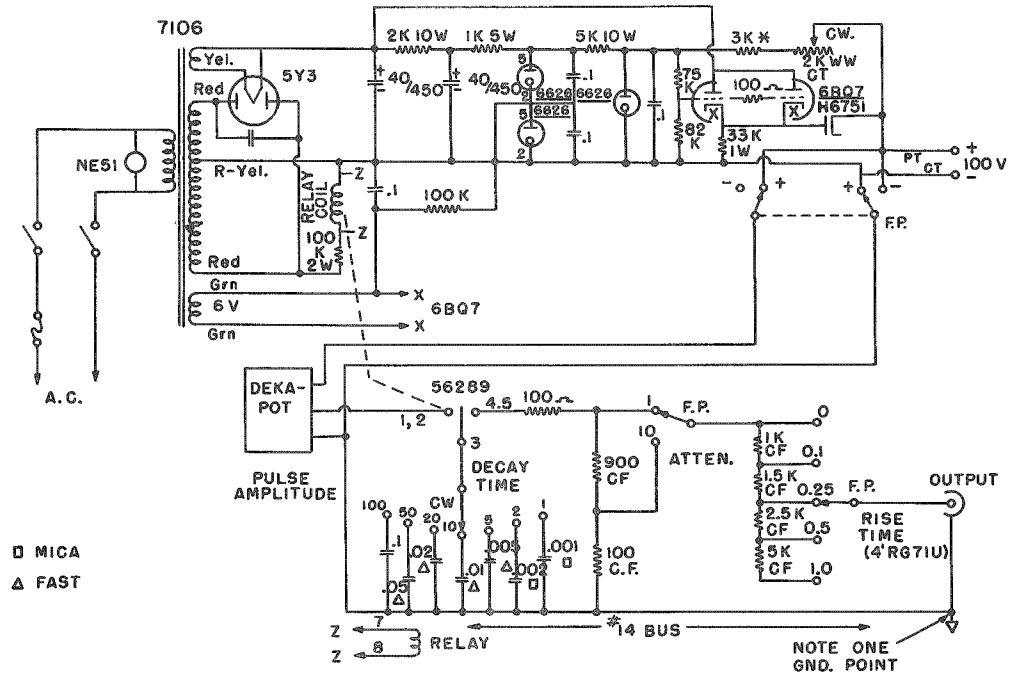

FIGURE F-1
Exponential Pulse Generator.

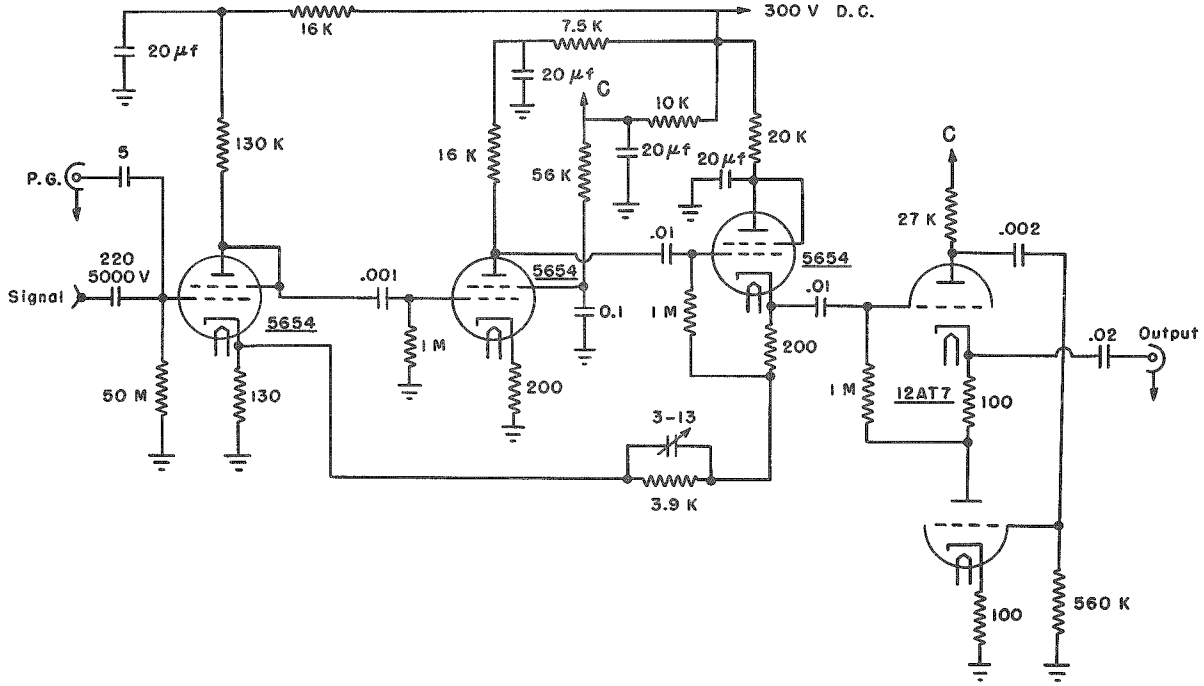

FIGURE F-2
Preamplifier and Stacked Cathode Follower.

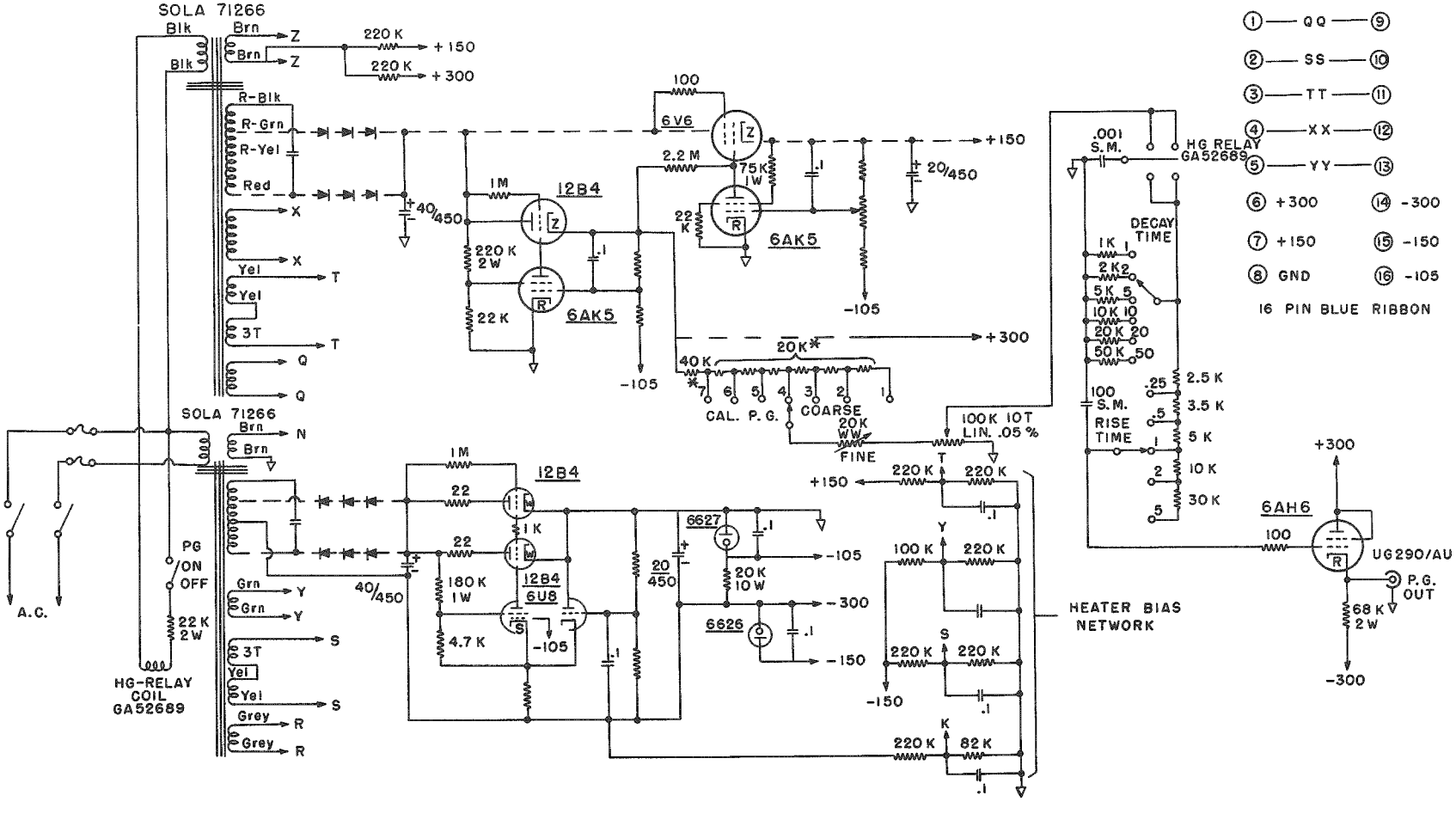

FIGURE F-3
Power Supply and Pulse Generator.

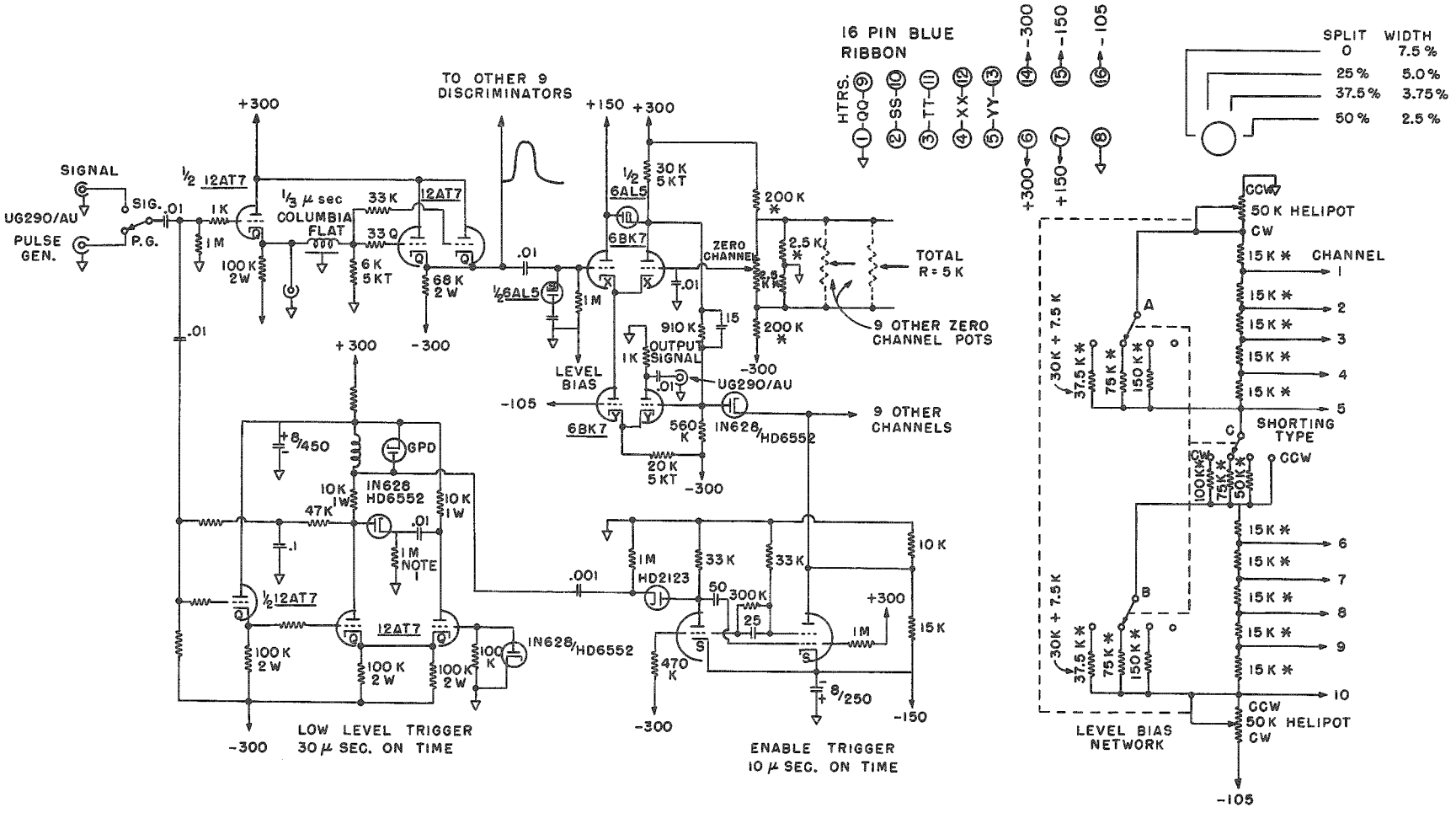

FIGURE F-4
Ten-Channel Discriminator.

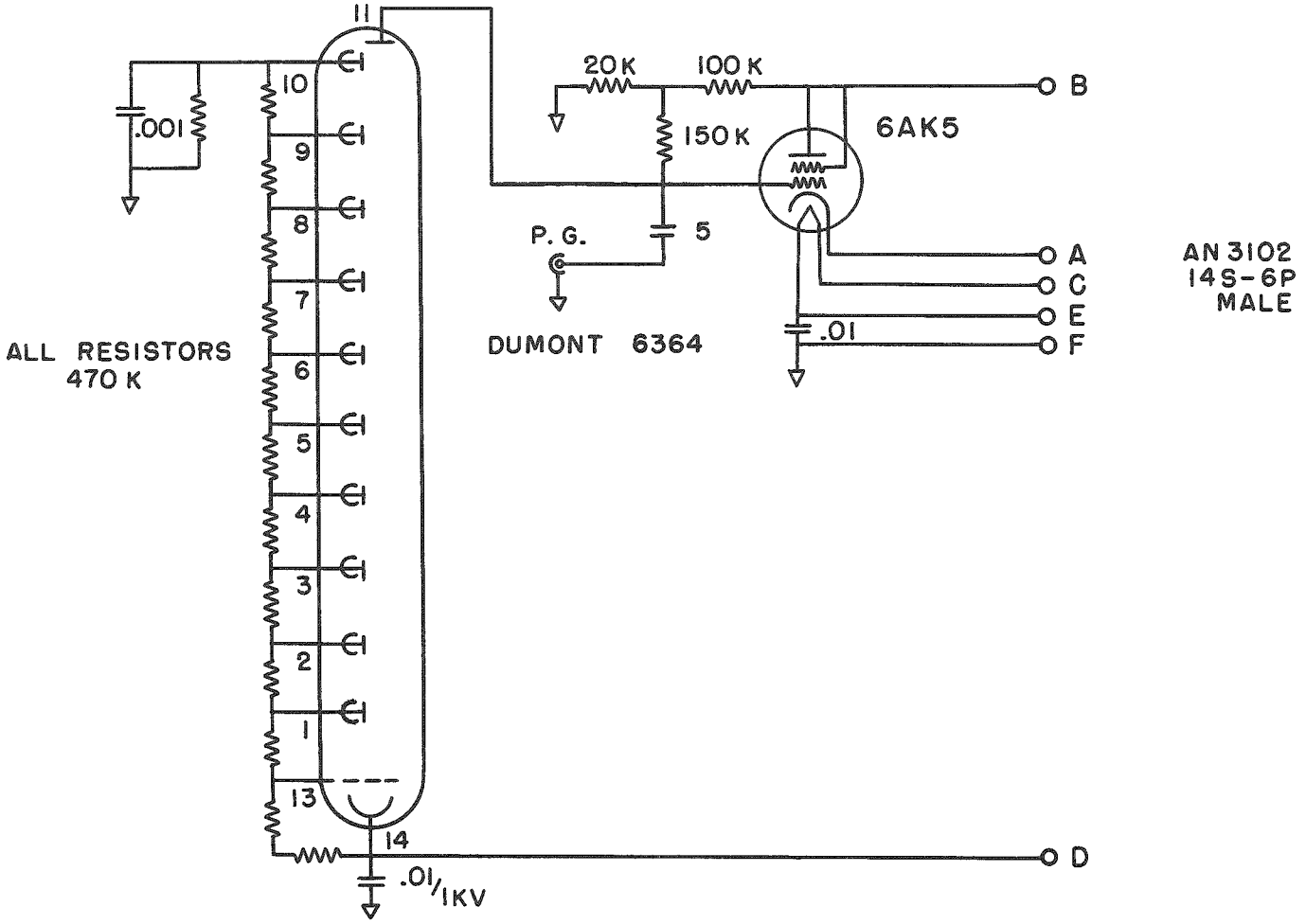

FIGURE F-5
Preamplifier for NaI Scintillation Counter.

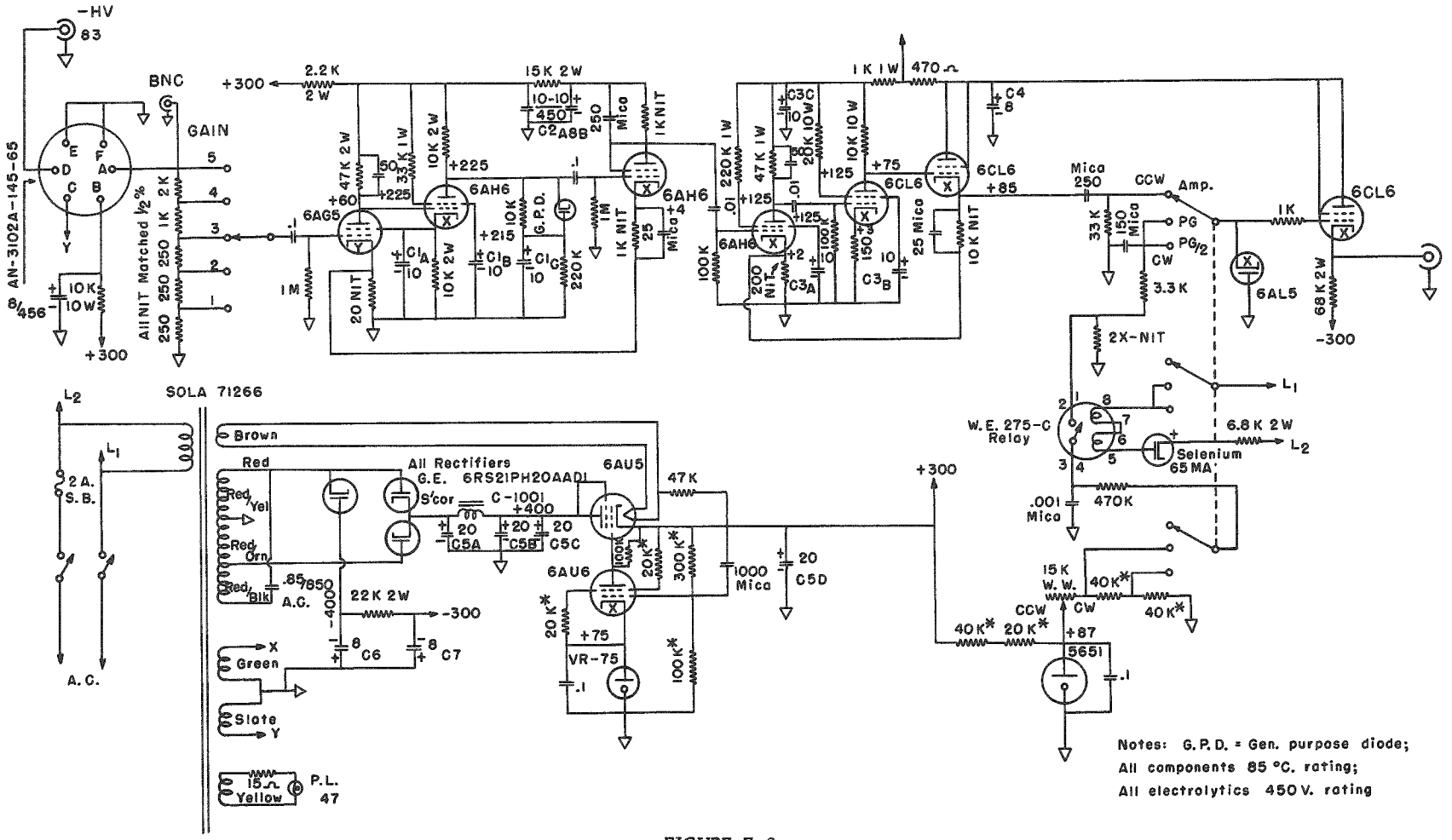

FIGURE F-6
Linear Amplifier.

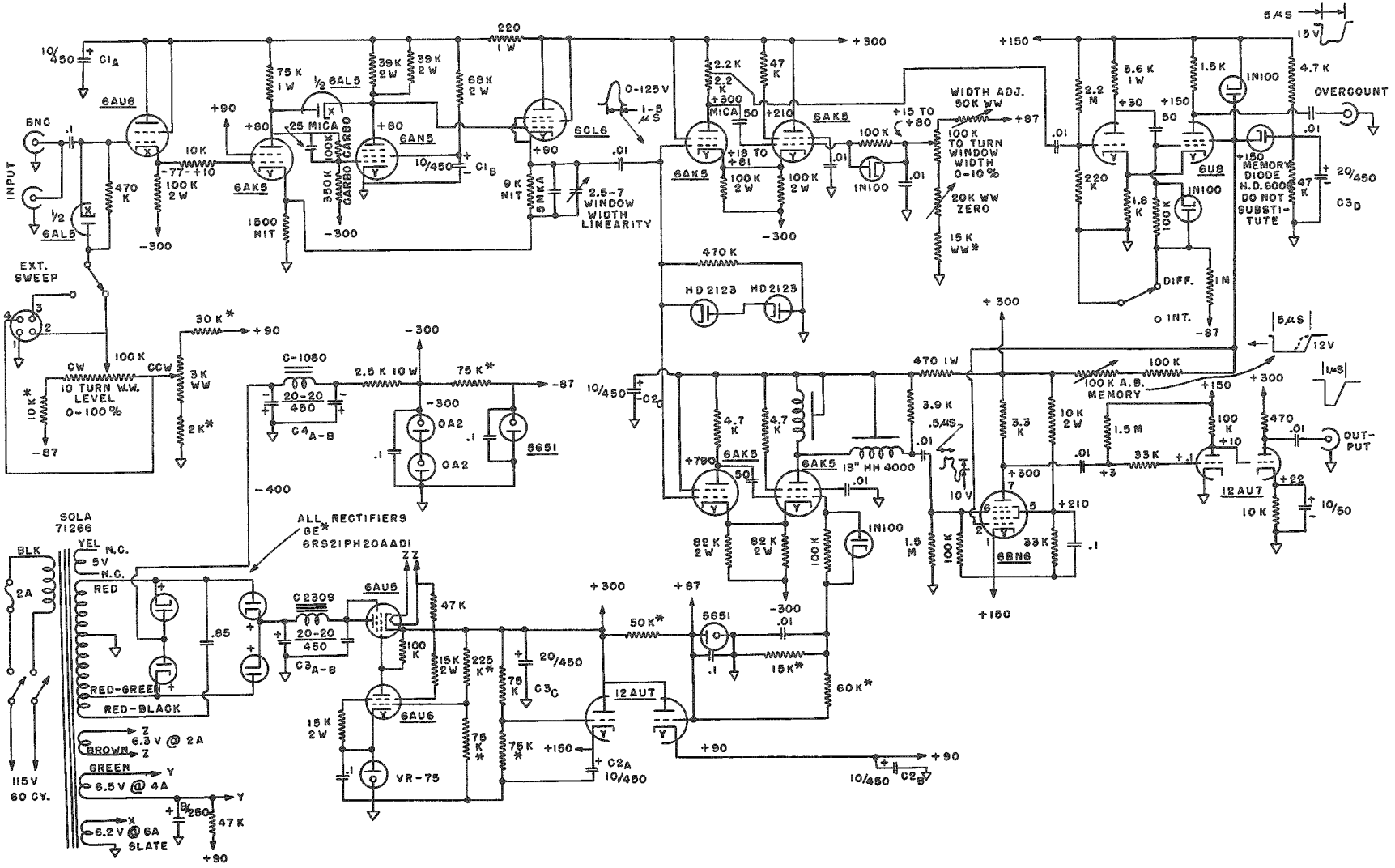

FIGURE F-7
Single-Channel Pulse-Height Anlayzer.

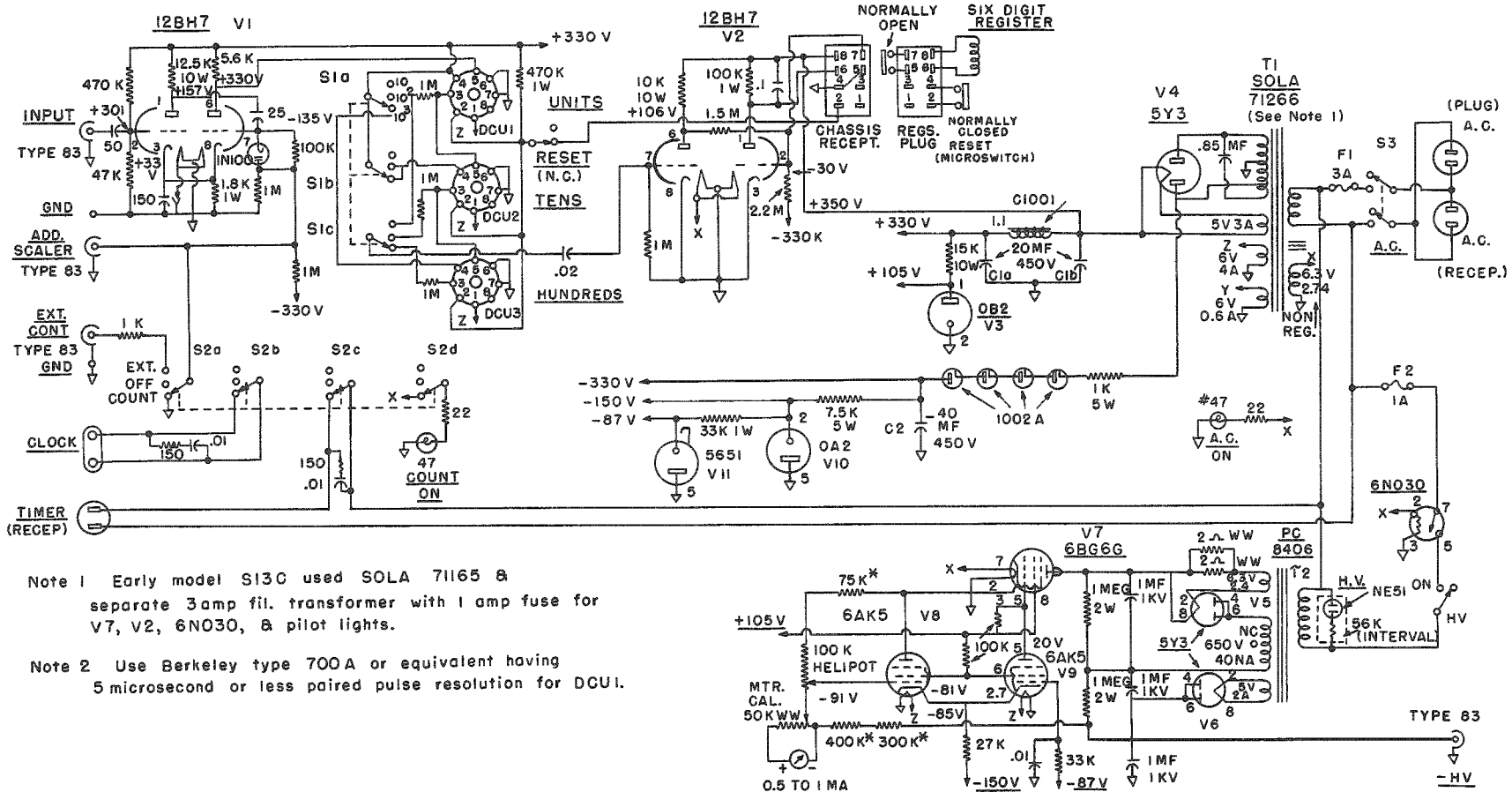

Note 1 Early model S13C used SOLA 71165 & separate 3 amp fil. transformer with 1 amp fuse for V7, V2, 6N030, & pilot lights.

Note 2 Use Berkeley type 700A or equivalent having 5 microsecond or less paired pulse resolution for DCU1.

FIGURE F-8
Scaler and Negative High Voltage Supply.